ABSTRACT

Effects of the Glenohumeral Joint Center on the Role of the Middle Deltoid: Implications for Reverse Total Shoulder Arthroplasty

Jonathan H. Bitter, M.S.B.M.E

Mentor: Brian A. Garner, Ph.D.

For shoulders with rotator cuff damage, the reverse shoulder replacement medializes the center of glenohumeral joint rotation, lending larger moment arms to undamaged muscles like the deltoid. The aim of this thesis was to create and use a computational model of the glenohumeral joint with an adjustable joint center to investigate and quantify the role of its position on middle deltoid moment arms for coronal plane abduction. The model confirmed that muscle moment arms increase as the center of rotation is shifted medially or inferiorly from the anatomical position. Specifically, medial translation of the glenohumeral center increased moment arms at low abduction angles while inferior shifts increased moment arms at high angles. Excursions of the middle deltoid were found to increase linearly as the joint center was moved medially or inferiorly: 1 mm medial translation or 1.33 mm inferior translation caused about 1 mm of increase in muscle excursion.

Effects of Glenohumeral Joint Center on the Role of the Middle Deltoid:
Implications for Reverse Total Shoulder Arthroplasty

by

Jonathan H. Bitter, B.S.M.E

A Thesis

Approved by the Department of Mechanical Engineering

_____

William Jordan, Ph.D., Chairperson

Submitted to the Graduate Faculty of
Baylor University in Partial Fulfillment of the
Requirements for the Degree
of

Master of Science in Biomedical Engineering

Approved by the Thesis Committee

_____

Brian A. Garner, Ph.D., Chairperson

_____

Carolyn T. Skurla, Ph.D.

_____

Jaeho Shim, Ph.D.

Accepted by the Graduate School

August 2013

_____

J. Larry Lyon, Ph.D., Dean

Page bearing signatures is kept on file in the Graduate School.

TABLE OF CONTENTS

LIST OF FIGURES

LIST OF TABLES

ACKNOWLEDGMENTS

I would like to thank the members of my thesis committee, Dr. Garner, Dr. Skurla, and Dr. Shim, for all of your help in getting my thesis perfected and finalized, and for taking the time to serve on the committee. Dr. Garner, thank you for all of your time and effort spent in helping me to understand the biomechanics of the shoulder, and for all of your help in guiding and organizing my research and analysis. Dr. Skurla, thank you for all of your help over the last two years in understanding my role as a graduate student, and in helping me through all of the stages of research that didn't make it into this paper.

I would like to thank Jake Hoffman for his C++ wisdom and assistance. Your help was always given freely and with a smile so that I never felt that my questions were ignorant or irritating, even though they probably were. Also, thank you to Ben Lewis and Josh Weed for helping to bring some life into the lab for lunchtime and Dr. Pepper hours.

I am also grateful for the environment created here at Baylor, by the administration and by the M.E. department. I feel very blessed to have been able to study at a place like Baylor, where high standards and Christian discipleship are commodities that are both commonplace and valued.

Finally, I am grateful to God and my family. I am grateful to God for leading us here and for constantly providing my wife and myself with incredible blessings and opportunities. Sarah, you have been nothing but supportive, loving, and caring. You are the source of motivation and fun that I have relied on in order to achieve any and all of the progress that I've made.

CHAPTER ONE

Introduction

Arthroplasty

Every day humans perform an incredible number of simple movements that require mechanically complex interactions of muscles and joints. When a single muscle or joint is damaged, many of these everyday actions become difficult, painful, or even impossible. Joint damage is not life threatening, but can often be irreparable and can carry life-altering consequences. These consequences can include either pain or loss of function, which can be intermittently inconvenient, or can be constantly painful and can cause a total loss of autonomy.

Millions of people in the United States suffer from some level of joint damage. Arthritis, the leading cause of joint pain, affects one in five American adults [1]. As the effects of arthritis damage the surface of the cartilage, continued use of the joint causes significant wear and tear, further damage, and painful inflammation. Similar effects can be seen in joints that have been damaged by some form of trauma, or other diseases.

For those with severe symptoms, arthroplasty can be a welcome relief. Arthroplasty is an elective orthopedic surgery in which one or more of the articular surfaces of a musculoskeletal joint are replaced. The most popular and effective method of arthroplasty is by prosthetic implant, or joint replacement. Materials and designs for implants are chosen to mimic the shape, size, and function of the anatomical joint. A joint replacement is considered "total" when both articulating surfaces have been replaced.

Those who go through the procedure regain much of their original mobility. Sometimes they regain all their original mobility, but more importantly, there is a significant reduction in pain. However, arthroplasty is not a perfect solution. Our understanding of the human body is growing, but is certainly not complete. As we understand more about the specific joints, bone properties, and muscle functions, we will be able to make joint replacements last longer and act more naturally.

Shoulder Arthroplasty

Of the various joint replacements that are available, the shoulder is arguably the most complex. The shoulder complex consists of the clavicle, scapula, and humerus. This skeletal structure and some of the glenohumeral muscles can be seen in Figure 1. The humerus and scapula are supported in the medial-lateral direction by the clavicle, but the only thing supporting them in the superior-inferior or anterior-posterior directions is a complex interaction of soft tissue. Numerous muscle groups wrap around the joint and around each other to create stabilizing forces. Simple rotations like glenohumeral abduction or humeral rotation require complex force couples that may involve contributions from more than 8 separate muscles working in concert [2–6].

This complexity is of a necessary design. The shoulder could not afford such a large range of motion if it were a typical "ball and socket" joint like the hip. At extreme angles of rotation the enclosing socket would impinge on the neck of the humerus. Instead, the shoulder uses the glenoid, a shallow cup in the scapula, to act as the articulating surface. The rotator cuff (supraspinatus, infraspinatus, teres minor, subscapularis) and other muscles (deltoid, pectoralis major, latissimus dorsi) then provide the tension and stabilization necessary to hold the humerus against the glenoid. The

glenoid, and the rest of the scapula, are finally connected by the clavicle to the thorax and the rest of the body. The rotator cuff is depicted in Figure 1. The clavicle and humerus are also clearly depicted, while the scapula is shown, but is largely obscured by the rotator cuff muscles.

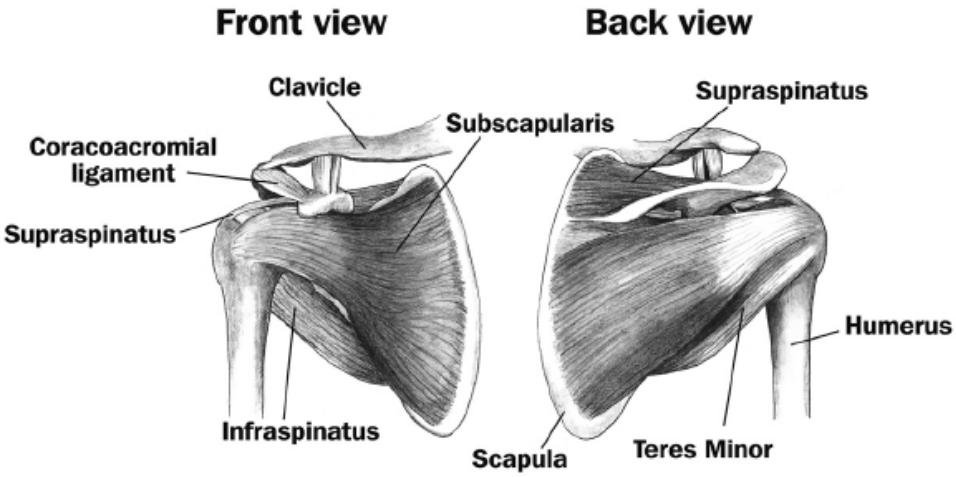

Figure 1: Skeletal anatomy and partial muscular anatomy of the human shoulder [7]

Shoulder replacement surgery became widely available during the 1980's. The process had been studied and revised so that the complexities of the shoulder could be dealt with and the life of the implant had been greatly increased. By the year 2000 the two-year survival rate of an implant was 96%; the five year survival rate was 92%; the ten year survival rate was 88% [8]. These advances in functionality and durability led to an increase in popularity. By 2002 the annual rate of total shoulder replacements had increased by 40% from the rate in 1992 [9]. Of course, widespread utilization of any given surgery will result in equally increased reports of complications.

Some of these complications are not treatable with a revision of total shoulder arthroplasty. The largest cause of prosthesis failure is a tear in the rotator cuff – these

may occur during surgery or during daily activities, especially in the elderly. Rotator cuff tears result in a loss of the stabilizing muscles of the shoulder [10–13]. They create instability and constant risk of dislocation or proximal humeral fracture. Proximal humeral fractures cannot be immobilized in a cast and can also result in rotator cuff tears [14]. They can be treated with arthroplasty or screwed plate fixation but have a high rate of component non-union, tuberosity migration, and often require a lengthy recovery period.

Finally, when shoulder implants do fail, revision surgery has a lower probability of success than did the primary surgery. In revision surgery, the small amount of bone in the glenoid has already been compromised and may not be sufficient to provide a stable fixation of the glenoid keel [8,9,15–17].

Reverse Total Shoulder Arthroplasty

Surgeons developed the Reverse Shoulder Arthroplasty (RSA) in order to alleviate pain and restore function to patients who have suffered a complication that limits the effectiveness of the anatomical prosthesis. The RSA prosthesis inverts the anatomical geometry of the joint. Rather than reinserting the ball-shaped humeral head on the proximal end of the humerus, RSA places an artificial ball component into the glenoid of the scapula.

The humerus is then implanted with an artificial substitute for the glenoid fossa, becoming the “socket” rather than the “ball”. These reverse components are shown in Figure 2. This simple reversal is intended to have several effects that make RSA a viable solution for the aforementioned conditions.

Figure 2: Photograph of the reverse shoulder design. The "ball" is placed into the glenoid of the scapula while the "socket" is integrated into the humeral component. This particular design is the Delta III, by DePuy Orthopaedics [18]

If a proximal humeral head fracture cannot be expected to heal, RSA is used to avoid the loosening of screwed plate osteosynthesis, humeral head necrosis, and tuberosity reduction. By using RSA to solve the problem the humeral head is removed altogether, and less total force is required to pass through the deltoid and the greater tuberosity, which allows it to be strengthened through bone remodeling before any permanent damage, or dislocation can occur [14,19]. When depleted bone stock is a concern in other scenarios, revision surgeries will sometimes utilize RSA rather than repeat implantation of the anatomical design.

Rotator cuff tears are the leading reason a surgeon may turn to RSA rather than the traditional TSA, accounting for almost 50% of all RSA procedures [15]. This is also the condition for which RSA is meant to be most effective. Moving the location of the

ball portion of the ball-and-socket does not alter the position of the humerus or the neighboring geometry of the shoulder's soft and hard tissues. As can be seen in Figure 3, the reverse shoulder implant shifts the glenohumeral center of rotation medially and often inferiorly [13,20]. As the center of rotation shifts without affecting the peripheral geometry, it moves farther from the lines of action of the uncompromised muscles. The orientation and position of the shoulder muscles remain largely unchanged, but the distance from their line of action to the joint center is altered. This creates an increase in the total moment arm of each muscle and its associated torque potential. This shift in the center of rotation also changes the distance the muscle must contract in order to attain any given position. Modern RSA implants are specifically designed to target the moment arm of the deltoid, giving it greater torque capability [13]. If the procedure succeeds in lending greater torque potential to the deltoid and remaining muscles, the patient will have greater strength available to abduct the arm and maintain its stability.

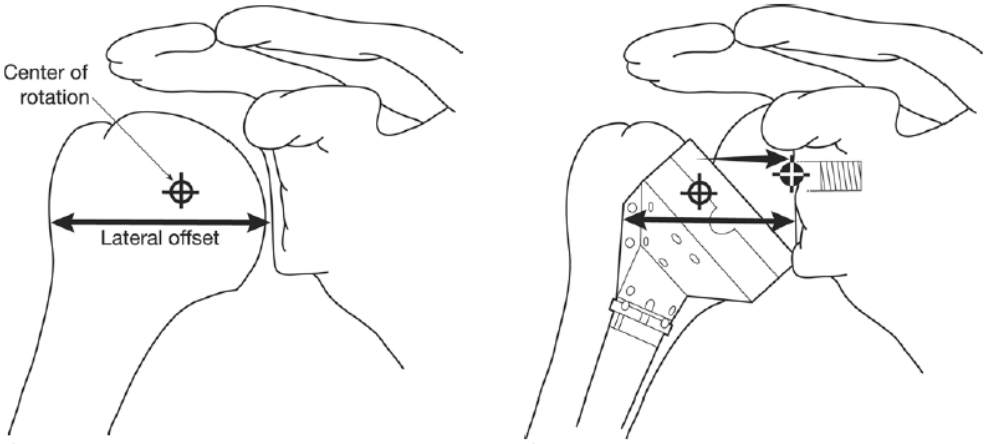

Figure 3: A depiction of the shoulder before and after RSA. Placement of the ball component on the scapula shifts the center of rotation from the center of the humeral head to the face of the glenoid [21]

The RSA concept is theoretically sound and has been shown to be successful in clinical trials and experimental data [2–6,11,12,22]. However, the mechanical advantage is not well understood. This advantage is dependent on the placement of the joint center in the reconstructed shoulder. As shown in Figure 3, the joint center can be significantly changed. However, the position of the joint center is highly variable. It is dependent on available bone stock, patient-specific geometry, implant design, and other factors. To date, there is little to no quantifiable data on these dependencies and no way for a surgeon to tailor the procedure and implant design to ensure that a specific patient gets the musculoskeletal advantage or the range of motion that is needed in order to heal and to operate autonomously.

In order for engineers and surgeons to better design and utilize components for shoulder replacement, it is important to also understand the effects of adjusting surgical and implant related factors. Many RSA components are designed to maximize the increase in muscle moment arms by moving the center of rotation as far medially as possible. However, medialization can result in impingement and scapular notching. To avoid impingement complications, others have mitigated the medial movement of the joint center, but fixing a more lateral center into the glenoid causes greater torque and shear forces to be applied to the scapula [23].

It is important to be able to position the center of rotation based on a knowledge of how it will alter the kinematics, joint loading, range of motion, moment arms and muscle excursion. The success of joint replacement is gauged by decrease in pain and increase in mobility. In the case of RSA, a key metric is also the increase in torque potential of the targeted muscles, specifically the deltoid. The current study is designed

to help increase understanding of how RSA can effect changes in moment arms and muscle excursions, which directly affect the potential torque production of the middle deltoid and the other glenohumeral muscles.

Purpose

The purpose of this study is to analyze the effects of geometric migration of the glenohumeral center of rotation on moment arms and muscle excursion. This study will focus specifically on the muscle most affected by RSA and most active in glenohumeral abduction – the middle deltoid. To achieve the aims of this study, a computational model is constructed and validated to simulate the anatomical and reverse shoulders. The model is first used to recreate experimental studies which provide a basis for model validation. Then, the model is used to explore the space of reasonable glenohumeral joint center locations in a manner that would be difficult to experimentally achieve.

Thesis Overview

This research was accomplished in fulfillment of the requirements for the Master of Science in Biomedical Engineering from Baylor University. Background research that is applicable directly to this thesis is presented in Chapter Two. The methodology used in construction, adaptation, and analysis of the computational shoulder model is described in Chapter Three. The results of analysis are presented in Chapter Four with discussion and suggestions for future research presented in Chapter Five. Chapter Six details the conclusions drawn from these analyses and results.

CHAPTER TWO

Previous Research

Musculoskeletal modeling has become increasingly popular due to the vast amount of data that can be acquired in a short time [24]. Gatti et al. showed that there was good agreement between previously published computational models of the musculoskeletal system and previously published experimental data. The authors gave evidence that computational models can be relied upon to provide information beyond the scope of experimental feasibility [25].

Unfortunately, accuracy in these computational models is limited by complexity and computational power. Increasing complexity requires increased time and effort put into creating the model, but it also necessitates more accurate and more complete data for the model parameters [26,27]. As more data is made available, and as computers become increasingly more powerful, more sophisticated models and methods will be created to help us better understand the human body [28]. For validation and groundwork, this study has relied on previously published data from literature.

Movement of the joint center, whether by means of humeral translation, or by surgery, is the focus of the current study. The effect of the joint center on the moment arms and resulting strength potential of the deltoid and its surrounding muscles is an integral part of their definition.

The following topics are areas of previous research that were useful in understanding the glenohumeral joint center and in developing the model and methodology used to create greater understanding of its effects: range of motion of the

shoulder joint, including healthy and implanted shoulders and their associated complications; glenohumeral translation and its effects on shoulder kinematics; previous research on moment arms of the glenohumeral joint, pre and postoperatively. The following sections describe, in turn, relevant research in each of these categories.

Range of Motion

As previously stated, one of the main goals of arthroplasty is to return mobility to the joint of the patient – in this case the patient's shoulder. Studies have shown that RSA does increase range of motion, but is limited in its possible gains when compared to the anatomical system [29–32]. This is, in part, due to its most common complications: impingement and scapular notching [33]. Radiological evidence of scapular notching has been well documented [14,31,34,35]. Notching occurs because of the unique geometry of the RSA implant. Because the articulating surface is now required to rotate around the glenosphere, the wide surface of the humeral component and the surrounding surface of the transected humerus can impinge on the scapula, just below the inferior rim of the glenoid.

Figure 4 depicts the results of this contact. Because of repeated impact, the bone chips and fractures from fatigue faster than it can be remodeled. After time the resulting "notch" can have serious ramifications, the most common of which is loosening of the glenoid component, and subsequent failure of the implant.

This complication is occasionally reported after implantation of devices that follow the Grammont design, such as the Delta™ series prosthesis from DePuy Orthopaedics [31,34,18].

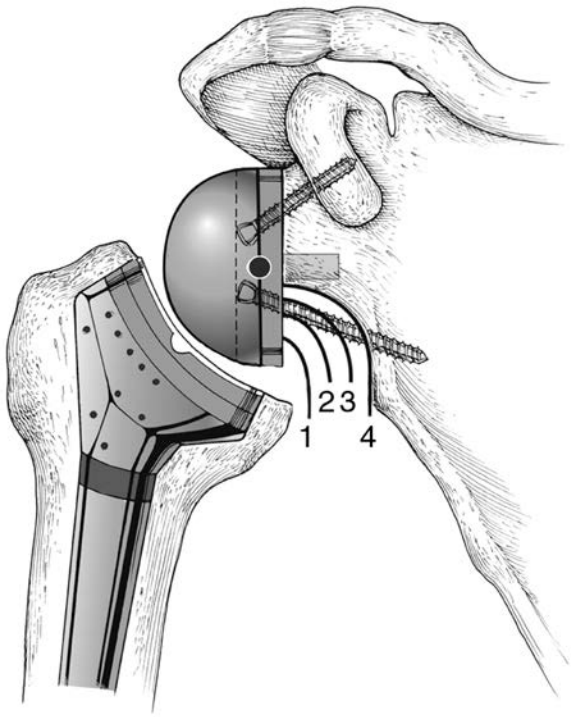

Figure 4: Scapular notching results from impingement of the RSA humeral component on the scapula. The radiographic severity classification is depicted as the scapular bone is eroded to the indicated line [36]

This style of prosthesis medializes the center of rotation to the surface of the glenoid. This requires that the system be designed as depicted in Figure 3, where the arc of the humeral component has the highest risk of impingement into the scapula.

Several designs, such as the ARROW system from FH Orthopedics, were created with the ability to adjust for a less medialized center of rotation. This in turn creates more room for adduction of the humeral component, and mitigates the risk of impingement [31,34]. Research has shown that medialization of the joint center has a negative correlation on possible range of motion, and a positive correlation with impingement risk. Table 1 lists data reported by Virani et al. [37] that shows how the range of motion increases as the implant is moved laterally and distally. The study shows that five millimeters of lateral offset can add approximately 12° to the range of abduction

and 22° to the range of flexion. Looking at these factors alone, the ideal placement of the center of rotation would be 5-8.5mm lateral to the face of the glenoid [31,34,37]. This positioning would increase range of motion and mitigate risk of impingement.

Table 1: Range of motion associated with changes in the glenohumeral joint center, as reported by Virani et al. [37]

Implant/Surgical Factor		Abduction (deg)	Flexion (deg)
Distal Offset	Centered	69.13	131.37
	1 cm	82.19	87.09
Lateral Offset	0 mm	71.44	66.79
	5 mm	83.29	88.68
	10 mm	84.93	114.31

These same benefits, however, may also be achieved by shifting the joint center inferiorly rather than laterally. Distal offset also has a direct effect on the joint center, and the effects on range of motion can also be seen in Table 1. Virani reported that lowering the glenoid component can also help combat impingement and increase range of motion. Manufacturers recommend a central location for the glenoid component drill-hole. However, studies have shown that positioning the drill hole up to 7 mm inferior to the glenoid center, or 11.5 mm above the inferior glenoid rim, can nearly eliminate risk of impingement while increasing range of motion [18,35,37]. It should also be noted that little research has been done with the joint center superior or anterior/posterior to the glenoid center because the loading patterns in postoperative RSA shoulders induce large shear stresses when the glenoid component is thus positioned [18].

In a clinical or operating room setting, the distal offset is a surgical factor, depending upon placement of the drill hole. However, the lateral placement of the joint center is an implant variable which would need to be selected pre-operation based on patient specific data. Implant designers and surgeons must both have access to quality information that allows them to design or implant a device correctly. The engineer seeks to design an implant that works on a broad scale, while the surgeon seeks to choose the method and device that are best suited to the individual.

Shoulder Kinematics

No marked difference in glenohumeral range of motion has been published between shoulders implanted with the typical and reverse shoulder designs [38] (note that this is in reference to glenohumeral range, and not necessarily humerothoracic range). It has also been noted that glenohumeral rotation consistently accounts for at least 2/3 of humeral rotation for all shoulder types [38,39].

However, when comparing shoulders implanted with prostheses to healthy shoulders, one study noted that implanted shoulders consistently rely more on scapular motion than did healthy shoulders [40]. Interestingly, the study showed that this difference did not extend to the comparison of anatomical to reverse implants, as both relied on an increased scapular involvement [40]. It was also observed that the reverse implant did not impede rotation, but that patients were unable to obtain maximal abduction angles without passively rotating the humerus. Bermann *et al*. surmise the difficulties lie in being unable to produce the required muscle force, despite the reduced muscle force requirements, and that this may be caused by the changes in muscle excursion induced by the reverse prosthesis [38].

Glenohumeral Translation

Through the range of abduction, the articular surface of the glenoid moves medially and superiorly as it is rotated by the scapula [41]. As seen in Figure 5, the translation can be significant. Even as the scapular system rotates and translates, the humeral head can shift with respect to the glenoid. In a resting position the humeral head rests on the inferior border of the glenoid rim then migrates superiorly as the humerus abducts [41,42].

During active abduction the humeral head quickly rises from the inferior rim as the abductors are activated and then maintains a position where its center is aligned within a half millimeter of the glenoid center for almost the entire range of motion in abduction. The total effect of this translation can be seen in Figure 6. With respect to the scapula, the joint center of rotation migrates a total magnitude of approximately 3 mm in the superior-inferior direction [4,41,42].

Figure 6 also shows that damage to the supraspinatus of the rotator cuff will allow greater migration of the humeral head. It shows that migration in healthy shoulders follows roughly the same patterns as the migration for shoulders with damage to the supraspinatus.

However damage to the supraspinatus increases the magnitude of the migration distance. The same study also reports that damage to the supraspinatus can lead to erratic translation of the humeral head, rather than the regular translation described in Figure 6 [42].

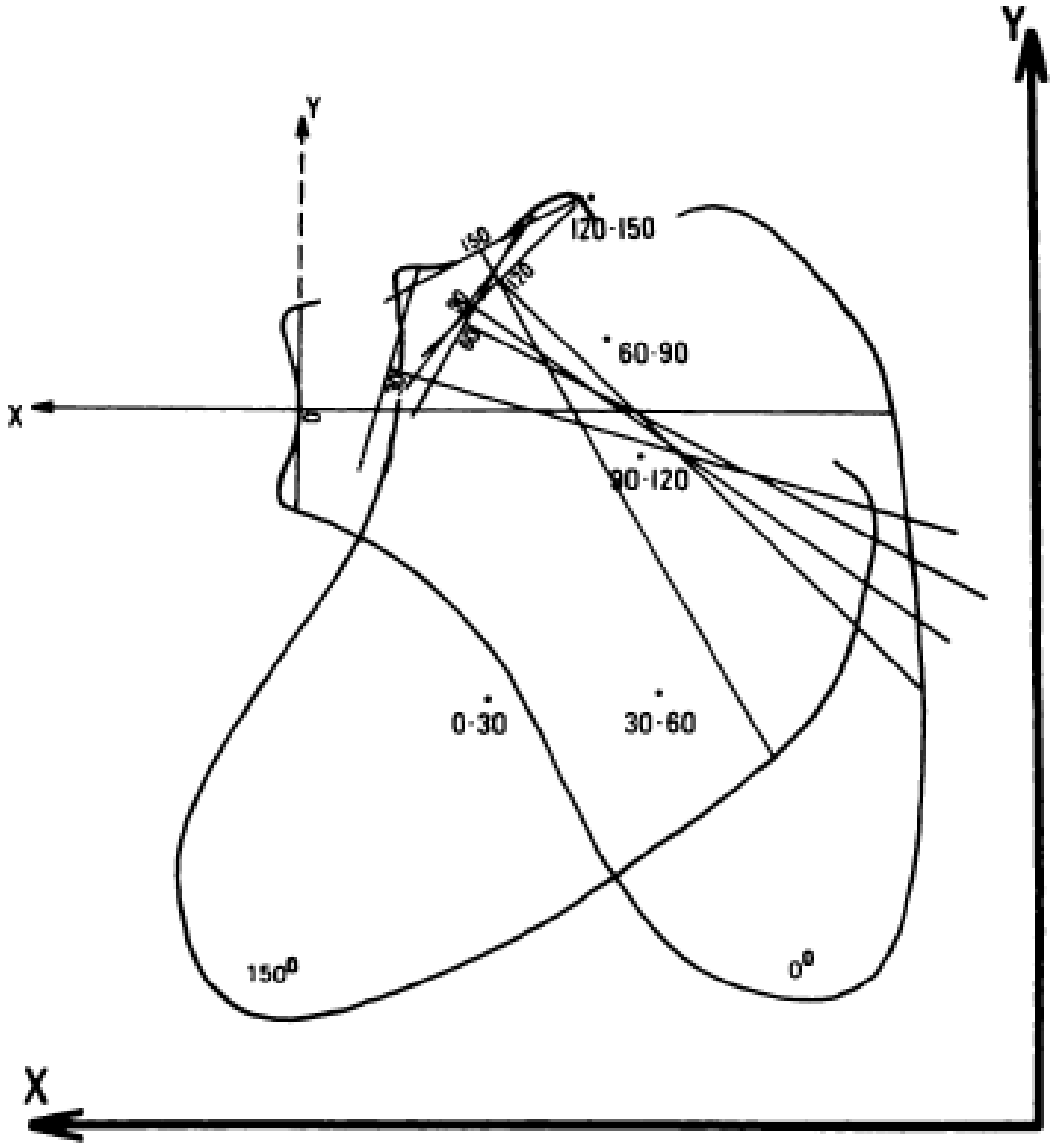

Figure 5: Rotation and translation of the scapula within the scapular frame at various angles of abduction. The two completely drawn scapulas are labeled as 0° and 150°, indicating the positions of the scapula at those degrees of humerothoracic abduction [41]

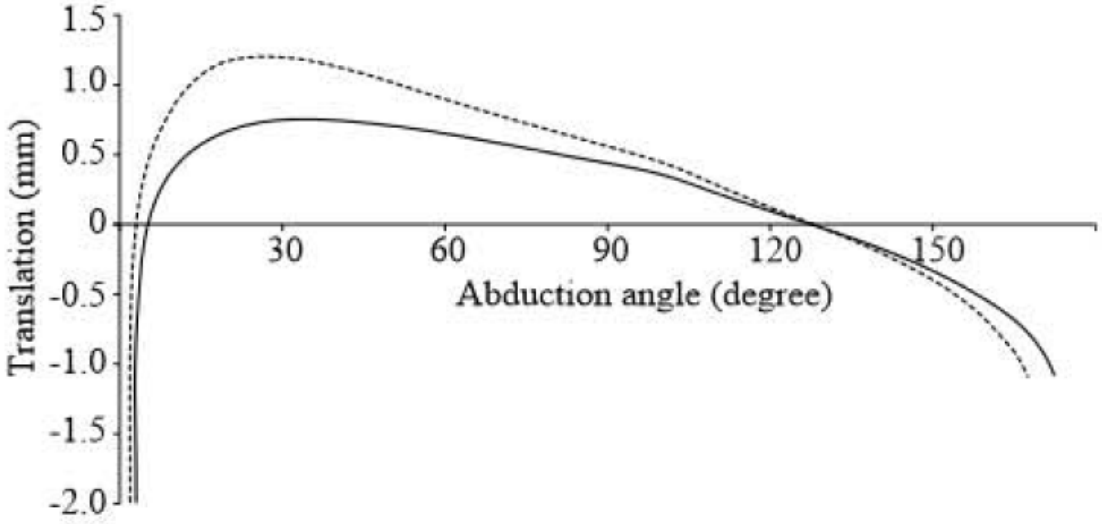

Figure 6: Vertical translation of the humeral head, parallel to the glenoid face, as a function of abduction angle. 0 mm of translation indicates positioning at the glenoid geometric center. The solid line represents translation within a healthy shoulder while the dotted line represents translation with a damaged supraspinatus [42]

Moment Arms

The moment arms and associated torque capabilities of the glenohumeral muscles have a large impact on joint forces, total shoulder torque, and the muscle force length curves. Because of this important role, the moment arms of the various glenohumeral muscles have been the subjects of numerous studies, both experimental and computational in nature. Several of these experimental studies form the basis of validation and calibration for the current model. Studies by Ackland et al. [6,12] are given specific attention because they analyze both the anatomical and reverse configurations using the same experimental protocol.

Anatomical Moment Arm Studies

To date, almost all applicable studies have examined the moment arms of the glenohumeral muscles with the anatomical center of rotation. Because of broad insertion

and origin sites, each muscle may have several different mechanical characteristics depending on the line of action of differing multipennate sections. Thus, only studies that divided the muscles into functionally distinct sub-regions were considered for this study.

A similar consideration is the treatment of the joint center of rotation. Some methodologies for calculating muscle moment arms are dependent on knowing the precise location of the joint center. Meskers et al. [43], and Veeger [44] have both confirmed that this rotation center is located at the geometric center of the glenohumeral head, as expected. Regardless, the tendon excursion method has become popular because it does not require the location of the center of rotation. For the purpose of continuity, only studies that employed the tendon excursion method were considered for this study.

The studies by Ackland et al. [6], Liu et al. [4], Otis et al. [5], and Kuechle et al. [3], report middle deltoid moment arms that are compared in Figure 7. These trends show middle deltoid moment arm generally rising at early abduction angles to a peak at around 60 degrees of GH abduction. Except for Keuchle, the studies report moment arm magnitudes of between 9 and 14 mm at the early abduction angles. These low magnitudes are curious because the average humeral head diameter is 51 mm. The moment arm is the perpendicular distance from the center of rotation to the line of action of the muscle. If the center of glenohumeral rotation is located at the geometric center of the humeral head, then the reported moment arms imply that the line of action of the muscle lies well within the 25.5 mm radius of the humeral head. Interestingly, the Kuechle data does not exhibit the trend of increasingly small moment arm magnitudes at small abduction angles. Instead the data shows fairly sustained magnitudes of about 19 mm at the early abduction angles, though this value is still within the 25.5 mm averaged

humeral head radius. Chapter 3 of this thesis will seek to address this apparent discrepancy.

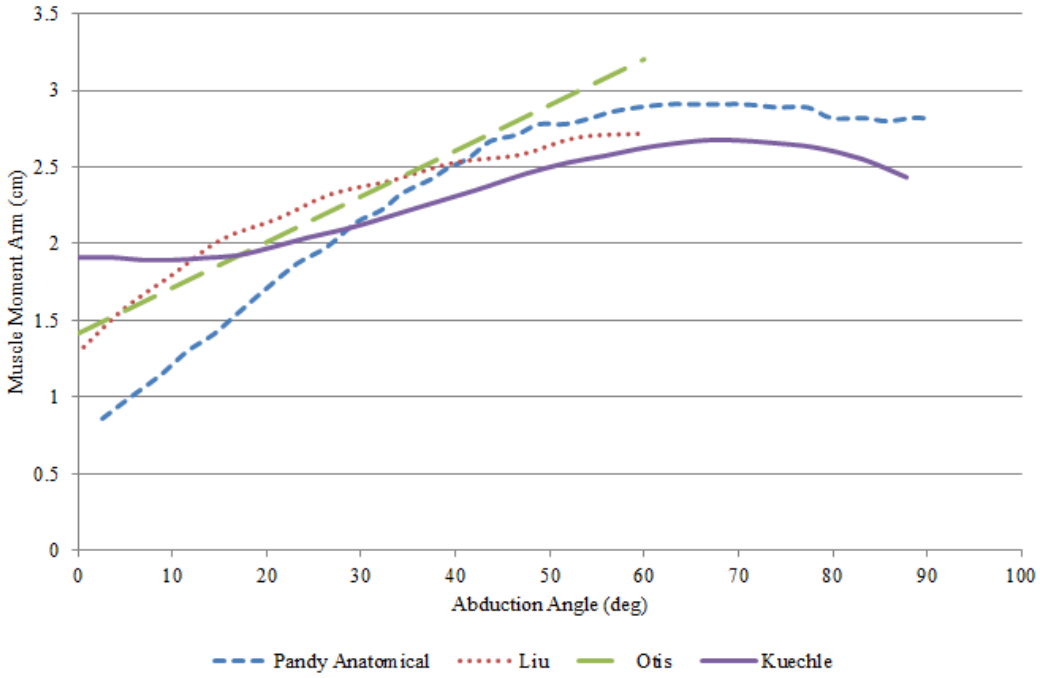

Figure 7: Moment arms, reported in the ALOK studies, of the middle deltoid in a healthy shoulder [3–6]

These four studies on the anatomical shoulder from Ackland, Liu, Otis, and Kuechle will be referenced repeatedly. From this point onward they will be referred to as the ALOK studies, when they are referenced as a group. A second study from Ackland et al. deals with the reverse shoulder [12]. It will also be referenced often. For clarity, the two Ackland papers will be distinguished as the anatomical and RSA Ackland studies.

Reverse Shoulder Moment Arm Studies

Few studies have attempted to quantify the moment arms of the postoperative RSA muscles. The Ackland RSA study [12] is a continuation of the anatomical study, making it valuable because of the continuity in experimental procedures used to obtain

the two data sets. The comparison between the anatomical and RSA moment arms in Figure 8 shows the anticipated difference in moment arm magnitude. The moment arms for reverse shoulders are consistently higher than those of the anatomical shoulder. It is also interesting to note that with the same experimental procedure and apparatus, the results of the RSA study do not show the same decrease in magnitude that the anatomical data shows at low angles of abduction.

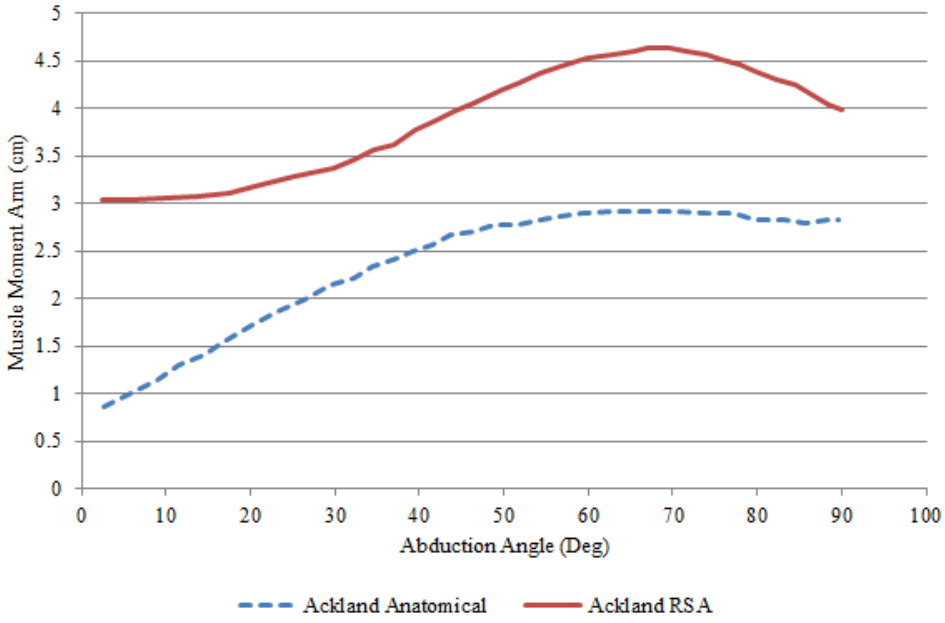

Figure 8: A comparison of anatomical and RSA moment arms from two separate studies by Ackland et al. [6,12]

The Ackland RSA study placed an emphasis on consistent placement of the joint center of rotation. The center of rotation was positioned "in contact with the glenoid surface" in order to reduce shear loading, and was also inferiorly placed in order to increase range of motion. Numerically this shift was described as medial 20.9 ± 3.9mm and distal 9.5 ± 4.1 mm in the scapular plane, when using the anatomical joint center as a reference point. The joint center used in the RSA Ackland study actually occurs inferior

to the range of recommended values, as they were previously summarized [18,35]. Only two other studies were found that referenced the moment arms of the middle deltoid for reverse shoulders [45,46].

Both studies were based on biomechanical models similar to that used in the current study, and both studies focused exclusively on the deltoid. However, neither study explored the effects of the joint center on moment arms or muscle excursion. They focus primarily on glenohumeral forces and scapular rhythm. Each study used moment arm predictions to compare the model to literature.

The moment arm data for all three divisions of the deltoid can be seen in Figure 9 for Terrier et al. and in Figure 10 for Kontaxis, et al. Both figures also display a comparison of the moment arms for the reverse and the anatomical anatomies for their respective models.

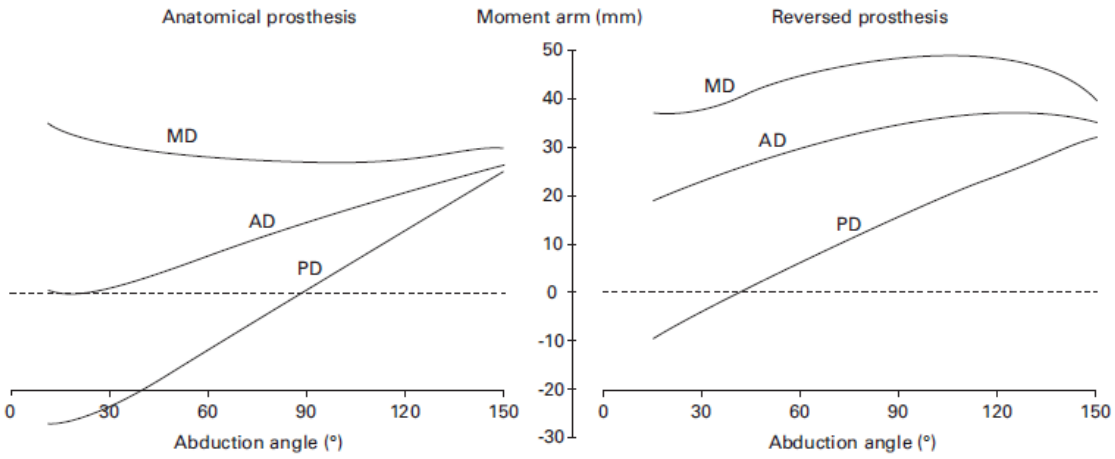

Figure 9: Anatomical and reverse shoulder moment arms as a function of abduction angle. MD represents Middle Deltoid, AD is Anterior Deltoid, PD is Posterior Deltoid. These results were obtained by manipulation of a musculoskeletal model from Terrier et al. [45].

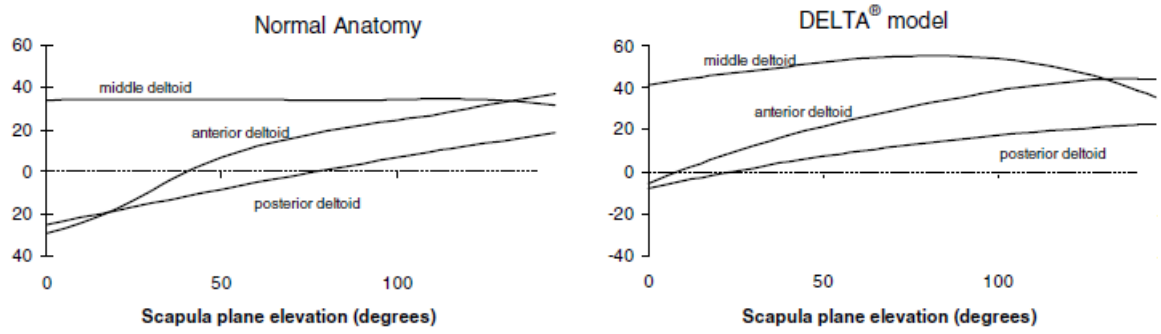

Figure 10: Anatomical and reverse shoulder moment arms as a function of abduction angle, from Kontaxis et al. [45], vertical axis measures moment arms in millimeters.

Neither of the RSA model studies compared the results of their anatomical models to the anatomical data found in literature. The magnitudes of moment arms in both models are far greater than the magnitudes seen in any of the experimental studies. The trendline for the anatomical middle deltoid from the Terrier study is actually inflected opposite of the experimental data with moment arm magnitude decreasing as the abduction angle increases. The anatomical trendline from Kontaxis also deviates from the experimental data in that there is no change in magnitude through the first 90 degrees of abduction.

The RSA model results from these studies [45,46] show better agreement with the experimental data of Ackland *et al*. [12] than did the anatomical results. As shown in Figure 11, the magnitude and general shape of the middle deltoid moment arms are similar across all three studies. Each of the data sets has been scaled to show the moment arms over angles of glenohumeral abduction only. For the Ackland RSA data, the scaling was 2/3 of the rotation for angles above 30°. Terrier *et al.* included scapular rotation over the entire range of data, but with the same ratio of glenohumeral to scapular rotation: 2/3 of the rotation for all angles. Kontaxis *et al.* neglected to report methodology on scapular

rotation, and only mentioned that it was employed. Because the reported ranges of motion for both Terrier and Kontaxis were similar, the Kontaxis data was scaled identically to the Terrier data. Note that the validity of this assumption is directly related to the similarity in treatment of scapular rhythm between the two studies.

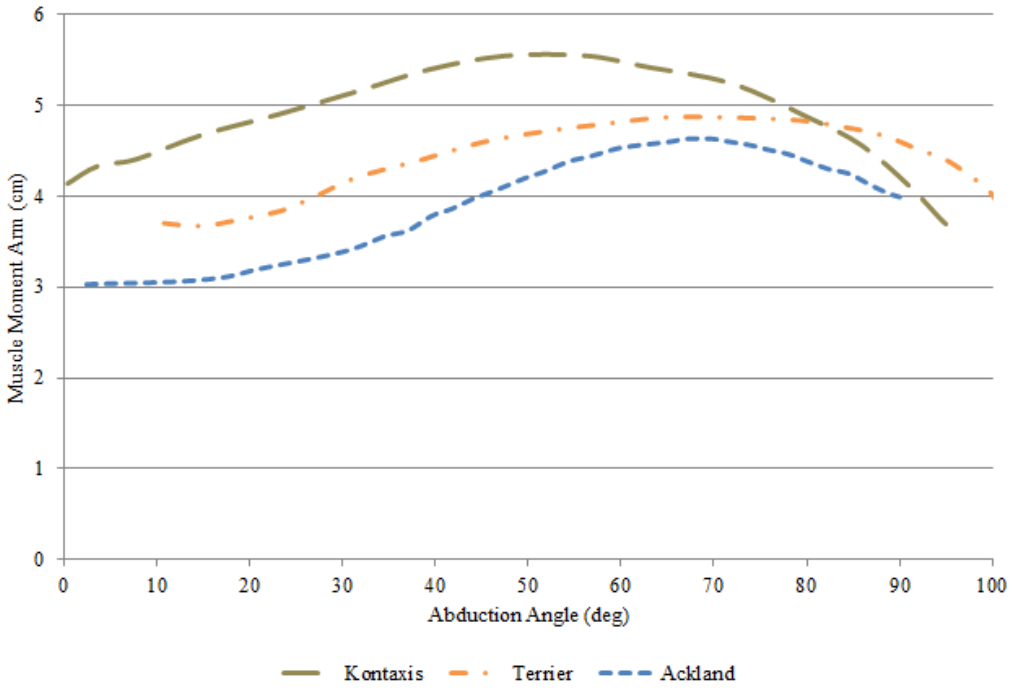

Figure 11: Comparison of computational moment arms of the middle deltoid for an RSA configuration from literature with experimental RSA moment arm data [12,45,46]

Experimental Methods Comparison

It is possible that a methodological difference between Kuechle [3] and the rest of the ALOK studies created the gap seen between their respective results. Table 2 summarizes the most influential points of methodology that may have caused this deviation.

Table 2: Methodology comparison between experimental muscle moment arm studies (GH = glenohumeral) [3–6]

Study	Excursion Tracking Method	Plane of Rotation	Method for Rotation Control	Treatment of Scapular Rhythm	Muscle Preparation	Representation of Muscle Line of Action	Muscle Tensioning Weight
Ackland 2008	Motion Capture	Coronal	Passive	After 30° GH abduction, scapular rotation at 1°/2° GH Rotation	All muscles dissected away	Line sutured into insertion tendons and routed through eyelets at origin centroids	1000g
Liu 1997	Potentiometer	Scapular	Passive	No rhythm, fixed scapula	All muscles dissected away	Line sutured into insertion tendons and routed through eyelets at origin centroids	200g
Otis 1994	Potentiometer	Scapular	Muscle Loading	No rhythm, fixed scapula	Deltoid, supra/infraspinatus, teres minor, subscapularis left intact	Line overlayed on intact muscle.	250g
Kuechle 1997	Potentiometer	Coronal & Scapular	Passive	No rhythm, fixed scapula	Deltoid, supra/infraspinatus, teres major/minor, subscapularis left intact	Line passed through intact muscle.	100g

The main point that separates the methodology of Kuechle from the other ALOK experiments was the treatment of the muscle paths. For all studies except that of Kuechle and Otis the muscles were dissected away and the lines of action were replaced by wire. Kuechle passed a similar wire through the intact muscles. It is possible that this experimental difference helped them to avoid having their data affected in the same way as Ackland *et al.,* Liue *et al.,* and Otis *et al.* Note that Otis *et al.* also left the muscles intact, but still reported the surprisingly low moment arms at low angles of abduction. The difference could have been that Otis overlaid the wire rather than passed it through the muscle, or it could simply be that they had very few data points for analysis, as compared to the other ALOK studies.

Regardless, all four are quality studies that provided the present study with valuable information regarding trends of muscle moment arms, and mechanics of the joint center. Further discussion of their deviations can be found in Chapter 5.

CHAPTER THREE

Methodology

The methodology described in this chapter will be divided into four main sections. The first section is a description of the model used in this study. The following sections include descriptions of several sub-studies that make up the body of work performed by the author. Sub-study 1 describes a parameter sensitivity test, which measured how adjustments to muscle path parameters affect the role of the middle deltoid in glenohumeral abduction. Sub-study 2 describes various ways the model parameters may be tuned to reproduce middle deltoid moment arms that are consistent with the data reported in literature. Sub-study 3 investigates the role of the glenohumeral joint center by testing a range of possible locations for the rotation center that may be obtained by Reverse Shoulder Arthroplasty.

Model Description

The computer model used in this study is a modification of the Garner model [47] which is based on the CT scans from the Visible Human Project [48]. The surface of each bone was mapped on a slice-by-slice basis by using an image threshold algorithm. The resultant contours were then reconstructed to form 3D surface models of the skeletal system.

Reference Frames

As described in Chapter One, humeral rotation may require movement of all three bones that connect it to the thorax. Rotation may occur simultaneously at the

sternoclavicular joint, acromioclavicular joint, and the glenohumeral joint. However, in the simulations for this study, the only necessary rotation was in the glenohumeral joint. Thus the thorax, clavicle, and scapula were treated as a common rigid body. They were collectively held in the ground frame, which was assigned to the scapular coordinate system for this model.

The scapular coordinate system, or frame, has its origin at the rotation center of the acromioclavicular joint. The negative x-axis passes through the medial border of the scapula, while the negative z-axis is oriented to pass inferiorly through the geometric center of the spherically-shaped humeral head. Note that this creates a coordinate system that is out of alignment with most of the camera angles shown in this paper, most of which are aligned with the X-Z plane of the humeral system.

The humeral coordinate system, or frame, has its origin at the geometric center of the humeral head. The negative z-axis is oriented to run parallel with the axis of the humeral shaft. The x-axis aligns parallel to the plane formed by the humeroulnar joint and the z-axis.

In general, the humeral coordinate system is free to move in all three rotational degrees of freedom with respect to the scapular coordinate system. These coordinate systems are visually depicted in Figure 12. Note that the scapular negative Z-axis passes through the origin of the humeral system, which is also the geometric centroid of the humeral head.

The definition of these coordinate systems is based on those described by Garner and Pandy [47]. The reference positions of the limbs as well as planes of rotation were based on descriptions from Ackland and Pandy [6,12].

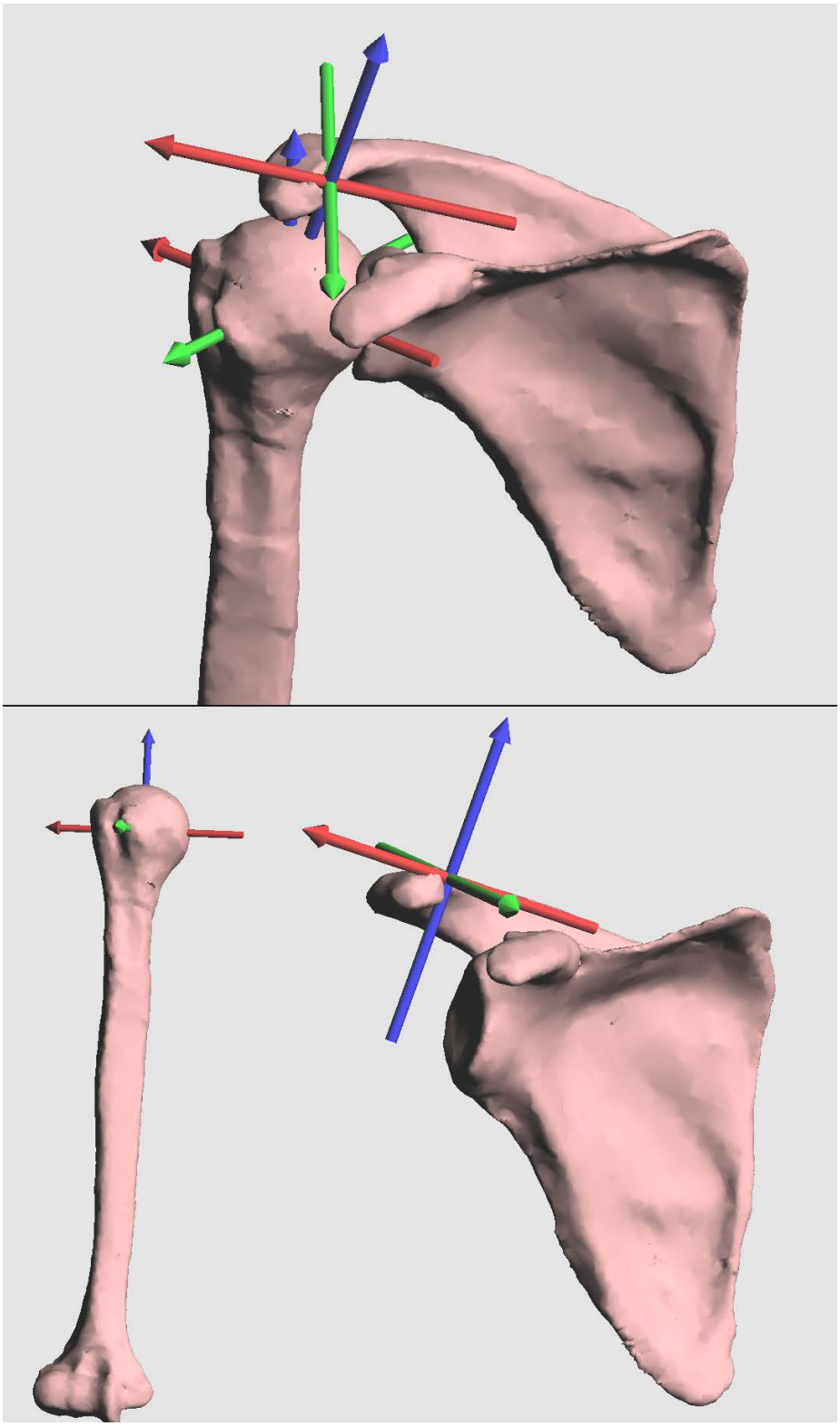

Figure 12: Assembled (top) and separate (bottom) images depicting the reference frames for the scapula and humerus. X, Y, and Z axes are respectively red, green, and blue.

Plane of Rotation

The procedure reported in the Ackland studies [6,12] called for humeral rotation in the coronal plane. The Kuechle study also performed humeral abduction in the coronal plane while the other ALOK studies performed humeral abduction in the scapular plane. The current study was made to simulate the Ackland procedure as closely as possible. This is because none of the other ALOK studies had correlated data for the reverse shoulder.

Based on descriptions found in the literature, the axis of rotation for abduction in the coronal plane was defined as the vector perpendicular to the coronal plane and passing through the glenohumeral joint center.

The coronal plane was defined as 30° posterior to the scapular plane. The scapular plane was defined, in accordance with the Ackland description, to contain the geometric center of the humeral head and two points on the medial border of the scapula. These points were defined as is depicted in Figure 13.

The axis for glenohumeral abduction in the coronal plane was defined such that the it was the vector perpendicular to the coronal plane and passing through the center of the glenohumeral rotation. In the scapular reference frame, the normalized direction vector for the axis of rotation is [0.3097, 0.6500, 0.0403].

For each of the sub-studies that will be described hereafter, this direction vector was used. The direction vector in each study was passed through the joint center being used for the particular sub-study and thus represented the axis for abduction in the coronal plane.

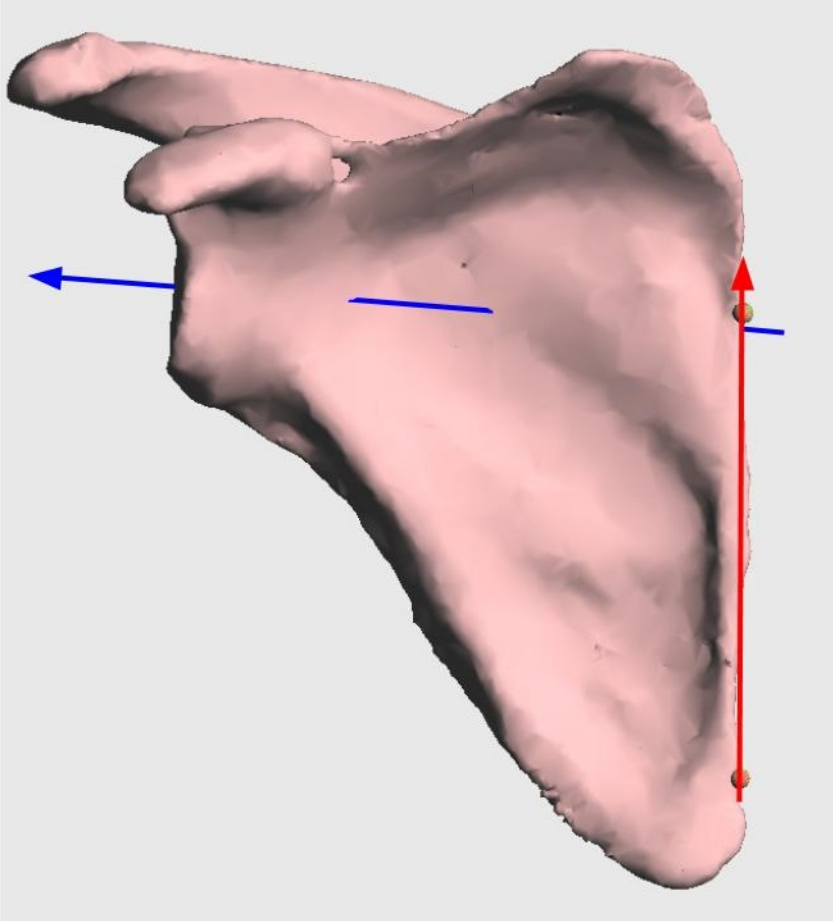

Figure 13: Definition of the scapular plane. Two points were identified on the medial border, to define the red vector, or the scapular vertical. The scapular plane contains these points and the geometric center of the humeral head (blue vector).

Scapular Rotation

As noted in Chapter 2, under *Shoulder Kinematics,* scapulothoracic motion plays a major role in defining the coordinate systems of the scapula and humerus. However, scapulothoracic motion was not included in this study because the origin of the middle deltoid is on the acromion of the scapula while the insertion is on the humerus. Thus scapular rotation will rotate both attachment points of the muscle and will not directly affect its excursion or moment arms.

In order to accurately compare the model prediction (without scapular rotation) to the experimental data, it was necessary to deal with the scapulothoracic rotation that was employed in the experimental studies. The Ackland studies simulated scapulohumeral rhythm for all angles of abduction above 30° by applying 1° of scapular abduction for every 2° of glenohumeral abduction. None of the other studies used to validate the current model applied any scapular rotation [3–5]. In order to accurately compare the data from Ackland et al. with the model and the other ALOK studies [3–5], the change in rotation past 30° was scaled by 2/3. This essentially removed scapular rotation from the data and adjusted the maximum humerothoracic abduction from 120° to 90°. This scaling should not affect the moment arm data for the middle deltoid because changes in length of the middle deltoid should be dependent only on rotation within the glenohumeral joint. Scapular rotation should shift the entire system.

Deltoid Muscle

The scope of this study was limited to the middle deltoid. Focus on the deltoid allows for validation of the various experimental datasets of both the anatomical [3–6] and the reverse [12] shoulder geometries. Because RSA focuses on altering the moment arm of the deltoid, the deltoid also provides the best opportunity for studying the various effects of RSA, including changes in moment arms and glenohumeral forces.

Focusing on the deltoid also makes coronal plane investigation an obvious starting point. As described in Chapter Two, the middle deltoid is most effective in the coronal plane and becomes less effective as the plane of humeral rotation approaches the sagittal [3–6,12]. This contrast is lessened when the role of the deltoid is expanded by RSA.

Calculation of Moment Arms

The model was used to compute moment arm values for a number of joint centers, and muscle parameter configurations, over the range of motion. The mathematical formula used to calculate the moment arms was based on the same kinematic method that is employed in the ALOK studies, which is sometimes referred to as the "virtual work" method. The manner in which the computation is accomplished is based on the work of both the muscle and the joint. If ideal conditions are assumed (e.g. frictionless contraction of the muscle) then the work done by the muscle and joint are as follows:

$$W_m = f * \Delta l_m \qquad \text{Equation 1}$$

$$W_j = \tau * \Delta \qquad \text{Equation 2}$$

where W_m and W_j are, respectively, work done in the muscle and joint, f is the tensile force produced by muscle contraction, l_m is the instantaneous length of the muscle, τ is the torque at the joint, and Θ is the angle of articulation.

Equations 1 and 2 may be combined to obtain:

$$\tau * \Delta\Theta = f * \Delta l_m$$

Rearranging leads to:

$$\frac{\tau}{f} = \frac{\Delta l_m}{\Delta\Theta}$$

Finally, torque is a measure of force multiplied by the perpendicular distance from its line of action to the joint center. As the changes in length and theta approach zero, the right side of the equation becomes:

$$Moment\ Arm = \frac{dl_m}{d\Theta} \qquad \text{Equation 3}$$

Thus, through the "virtual work" method, the model computes the moment arm as a function of rotation and muscle length. This is done by performing a numerical

differentiation over the entire range of motion. The model iterates through the range of motion, and computes the length of the muscle before and after every small perturbation in angular position. The moment arm is then calculated as described in Equation 3, by dividing the perturbation in muscle length by the change in angle.

Normalizing Moment Arms

The computed moment arms were normalized to account for size variations between the model and ALOK moment arm studies [3–6,12]. Normalization was accomplished by scaling the computed moment arm values by 0.923, the ratio of 51.0 mm to 55.0 mm, which are, respectively, the average humeral head diameter of the experimental population, and the humeral head diameter of our model.

Model Parameters

Because of the dependence on muscle length and joint angle, the proscribed muscle path is an important variable in any moment arm simulation. The origin, insertion, and obstacles (neighboring musculoskeletal components) all affect the muscle path, and thus affect the mechanical advantage of a muscle. These parameters can all affect the angle at which the muscle force is applied to the skeleton, and the distance of the force vector from the rotation center (the moment arm).

In this study, a via-cylinder [49] was used to model the muscle path, and to represent the anatomical obstacles that the middle deltoid would normally circumvent. The surface of the cylinder acts as a frictionless guide, forcing the muscle to wrap around it rather than take the shortest straight-line path from point to point.

Figure 14 shows how the cylinder was used in this model: the cylinder acted as an obstacle when it intercepted the straight-line path between the origin and insertion. When the cylinder was placed outside of this path, or once the abduction angle lifted the path above the cylinder, then the cylinder no longer had any effect on the path. The location of the origin, insertion, and cylinder were the parameters that were used to describe the modeled muscle path. When in contact with the cylinder, the muscle path will always extend tangentially from the cylinder as the humerus abducts through its range of motion.

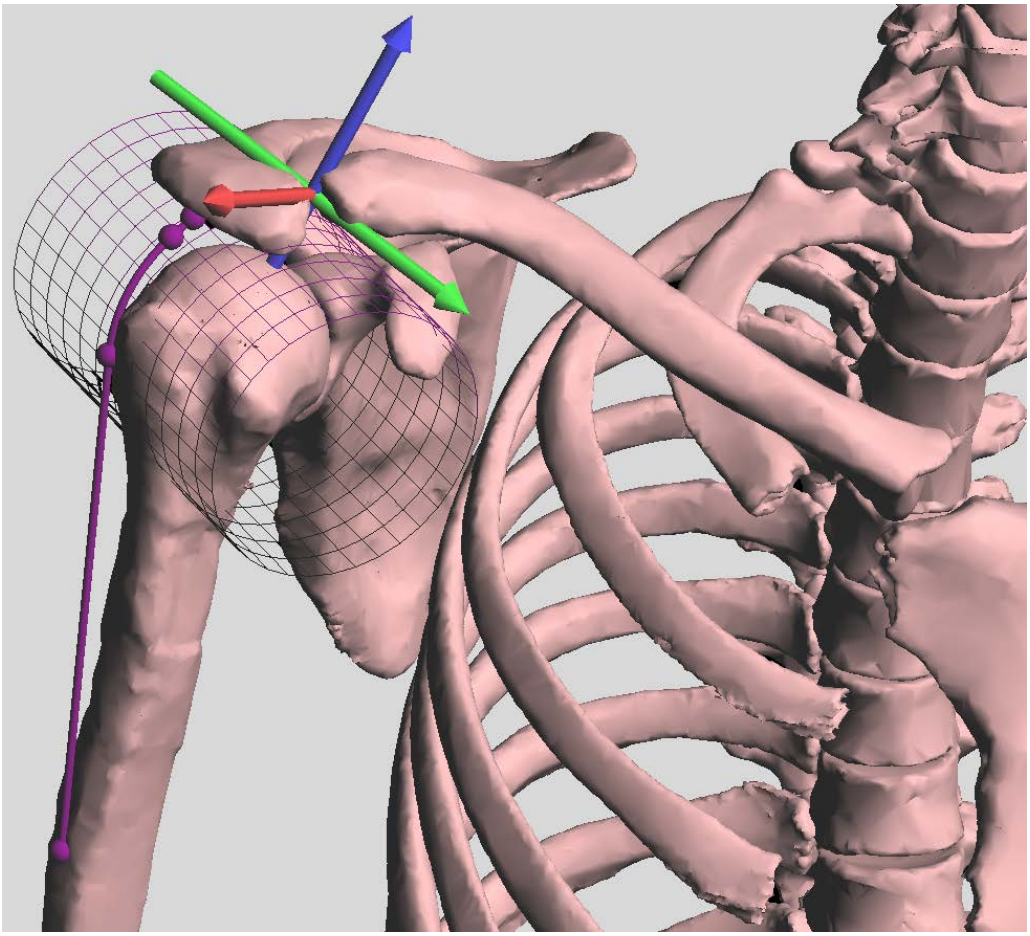

Figure 14: Via-Cylinder model with middle deltoid displaying spherical markers at the origin, insertion, and points of tangential contact with the cylinder. The cylinder has been oriented parallel to the axis of rotation

Sub-Study 1: Parameter Effects

Sub-Study 1 was designed to analyze the effects of the middle deltoid muscle path geometry on moment arms over the range of abduction in the coronal plane. This muscle path geometry is intended to represent the cross-sectional centroid of the muscle belly as it spans between attachment sites and around underlying anatomical structures. This geometry may be different for various individuals, and it can be affected substantially by surgical procedures such as the reverse shoulder replacement.

Sub-Study 1.1: Cylinder Effects

Medial-lateral and superior-inferior translation of the via-cylinder were tested for their separate effects on the curve of the moment arm as a function of joint angle. Radius of the cylinder was also tested to see if the size of a shoulder influences the magnitude of the moment arm, the trends over the range of motion, or both.

Sub-Study 1.2: Origin Effects

As a line, the muscle path attempts to act as an average of the entire volume of the actual middle deltoid. In order to best model the attachment site, the placement of the origin was tested for effect on the moment arm curve. The tested locations were confined to the lie within the area of the anatomical attachment site. For the origin, this is the entire lateral curve of the acromion.

Sub-Study 1.3: Insertion Effects

The position of the insertion point was also tested for its effect on the computed middle deltoid moment arms. The attachment area for the insertion is smaller than that of the origin, and thus positional tests were confined to the deltoid tuberosity.

Sub-Study 2: Experimental Data Replication

Sub-Study 2 was designed create a better understanding of the data and its underlying significance in the ALOK studies. Causes of the surprising data trends were explored by attempting to use the model to replicate the experimental data trends through various methods of manipulation of the model parameters.

Sub-Study 2.1: Fixed Anatomical Joint Center

This simulation was designed to investigate the muscle path geometry that would be necessary to create the muscle moment arms reported in the ALOK studies if the center of rotation were fixed in an anatomical position, with the axis of rotation passing through the geometric center of the humeral head. Such positioning of the anatomical center of rotation is both intuitive and confirmed in literature [43,44].

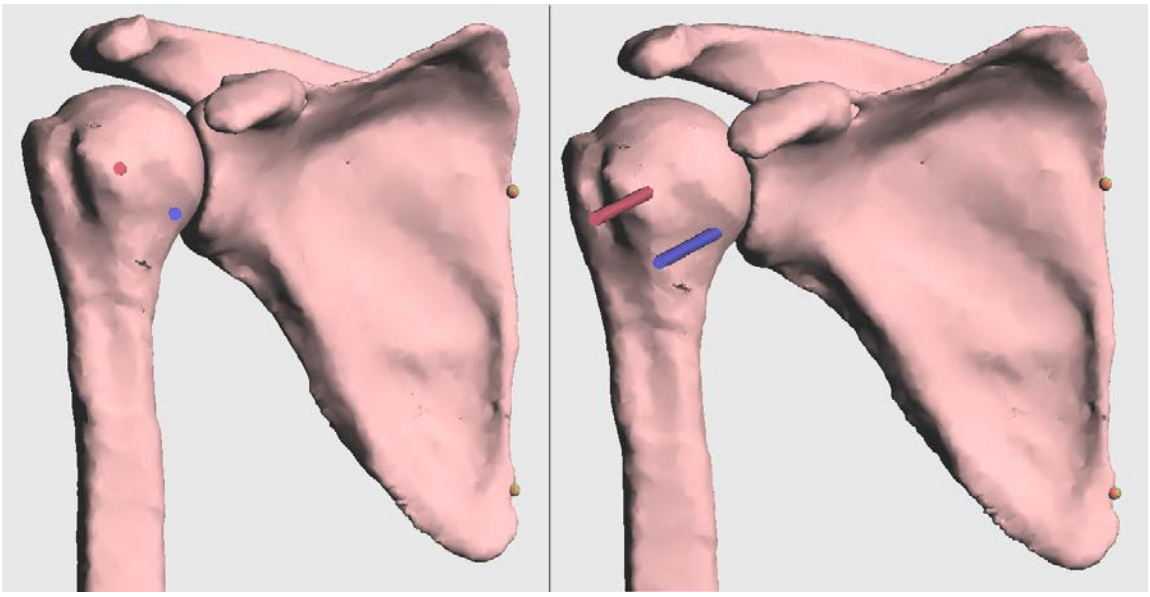

Figure 15: Red axis passes through the anatomical joint center. Blue axis passes through the RSA joint center, as defined by Ackland et al. [6]. Both images are of the same glenohumeral orientation, but taken from different angles. On the left the camera is perpendicular to the coronal plane, where the right is taken perpendicular to the scapular.

In Figure 15, the red center of rotation marks the anatomical center. With the center of rotation fixed, the musculature was manipulated to maximize agreement between the predicted moment arms (as a function of abduction angle) and the ALOK moment arms. The model allowed for the muscle path of the deltoid to be manipulated by adjusting the path parameters: the origin and insertion of the muscle and the size and position of the via-cylinder. Manual adjustments were made to the muscle path in order to fit the computed middle deltoid moment arm data to that of the ALOK studies, without any regard for the feasibility of the resulting muscle path geometry. As explained on page 32, the computed moment arms were scaled by a ratio of 51/55, which normalized the size of the modeled humeral head to the average size of the experimental population.

Sub-Study 2.2: Fixed Anatomical Muscle Parameters

This simulation was performed in order to illustrate what location of the center of glenohumeral abduction would be necessary to create the muscle moment arms seen in the literature if the muscle anatomy were fixed in a feasible anatomical position. The muscle parameters (insertion, origin, and via-cylinder) were defined to represent viable anatomy determined by the author. This definition was representative of an older population with reduced musculature. This was modeled by using a small diameter via-cylinder with the minimum path obstruction necessary to avoid having the muscle path penetrate the humeral head. The insertion point was also adjusted to match the muscle path as described by Ackland *et al*.[6].

Sub-Study 2.2.1 With the muscle parameters fixed in such a way as to satisfy anatomical feasibility, the center of rotation was manually adjusted. Translation of the

joint center was limited to the scapular XZ plane, leaving the y-coordinate in the center of the glenoid. Adjustment of the center of rotation was made such that computed abduction moment arms matched the magnitudes and trends of the data reported in the ALOK studies, and irrespective of geometric feasibility. Because of ambiguity in the optimal placement of the muscle origin, the process was repeated for three different anatomically viable origin sites: superior placement, lateral placement, and inferior placement.

Sub-Study 2.2.2 Because the data from Kuechle *et al*. [3] is more representative of the author's expectations, as well as the Ackland RSA data [11], special interest was paid to the fit of the model to Kuechle's data. This was an effort to fit the model to a unique data trend, as well as an effort to illuminate the causes of the difference between Kuechle's data and the rest of the ALOK . The only methodological differences from 2.2.1 were the emphasis on the Kuechle data, and the placement of the origin on the lateral edge of the acromion – the orientation that was inferred from Kuechle's paper.

Sub-Study 2.3: Migrating Center of Rotation

This simulation was created to expound upon Sub-Study 2.2. If the musculature is fixed in the anatomical position as in Sub-Study 2.2, then the data from the literature might be better explained by a joint center that actively migrates throughout the range of humeral abduction. The goal of this exercise was to match the model to the slope of the experimental data over discreet intervals. Each interval represented a 5° range of abduction. Because this was a precision exercise, it was necessary to follow the curve of

only one data set at a time. This exercise was repeated for the Ackland anatomical data set [6], the Kuechle anatomical data set [3], and the Ackland RSA data set [12].

For each discreet range of abduction angles, the model's center of glenohumeral abduction was altered in order to create agreement between the model prediction and the experimental data. The center of rotation corresponding to each angle was then recorded to track any potential migration of the joint center that may explain the differences between the unexpected moment arm data for the anatomical Ackland study, and the expected trends seen in the Kuechle and RSA Ackland studies.

Sub-Study 2.4: Reverse Shoulder Data Comparison

The joint center position, as described by Ackland's RSA studies [12,50], was also used as a source of comparison. The model's joint center of rotation was positioned as described by Ackland *et al*. This position was 20.9 mm medial to the anatomical joint center, and 9.5 mm inferior, in the scapular plane. Along with the data from the computational moment arms by Kontaxis *et al*. [46], and Terrier *et al*. [45], Ackland's RSA data was used to define an acceptable range of magnitudes and trends. The model was compared to this range when it was given the muscle path parameters used in Sub-Study 2.3, and given the joint center location defined by Ackland.

Sub-Study 3: Joint Center Simulations

Sub-Study 3 was comprised of a set of simulations that were used to understand the trends of moment arms and muscle excursions as a function of the joint center location. The same muscle path parameters that were established in Sub-Study 2.2.1 were used in this sub-study.

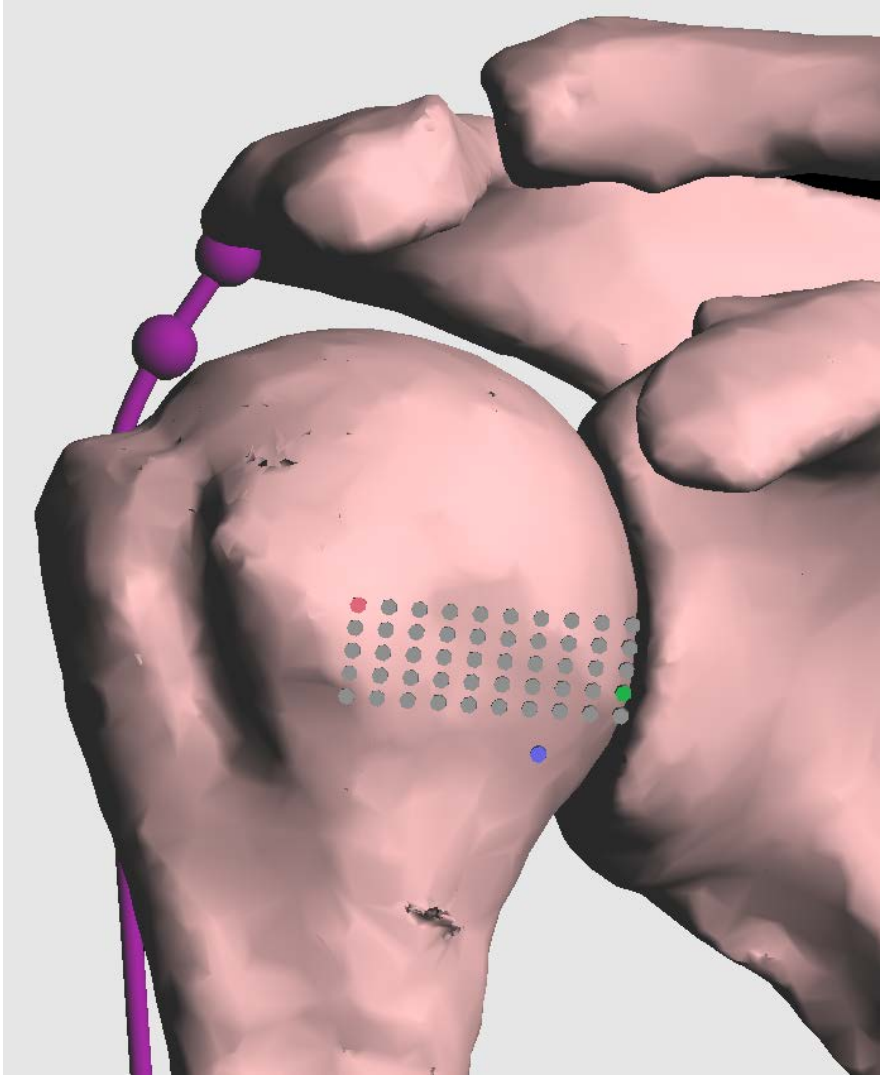

Figure 16: Within the acceptable range of joint centers, the tested locations are shown in gray. The red, green, and blue joint centers respectively describe the anatomical joint center, the RSA center as described by Ackland et al. [12] and the RSA center as defined by the "12 mm Rule" [35]

Figure 16 depicts a grid of the individual joint centers used for a sequence of separate simulations. For each simulation the model computed the mechanical advantage of the shoulder and the total excursion of the middle deltoid through the range of motion.

From previously described data [12,18,31,34,35,37,50], the test locations shown in the grid above were defined in a range composed of five equally spaced rows and ten

perpendicular columns. This range begins at the center of the glenoid face, then extends laterally to the anatomical joint center; for the current model, this was a distance of 27 mm. The range then extends inferiorly to a level 11.5 mm superior to the inferior glenoid rim, which was equal to 6.19 mm below the anatomical center in the current model. However, for the sake of thoroughness, the fifth row was added one layer below this inferior limit, for a vertical range of 8.25 mm. This means that each horizontal shift between columns is 3 mm, and each vertical shift between rows is 2.06 mm.

CHAPTER FOUR

Results

Results from each sub-study will be described, in turn, here in this chapter. The first set of results will be from Sub-Study 1 on effects of the model parameters. This will be followed by the results of Sub-Study 2, on the investigation into the ALOK and RSA data sets, and the model parameters required to fit the model to these data. Sub-Study 3 will conclude the chapter with moment arm and muscle excursion trends that are produced by changes in the joint center.

Sub-Study 1: Parameter Effects

The accuracy of any model is dependent upon the given set of parameters. In the current model, parameters involving skeletal geometry were set according to the Garner model [47], as described in Chapter 3, and according to the humeral dimensions from literature, as described in Chapter 2. Adjustable parameters of this model were the size and position of the via-cylinder, the position of the muscle origin and insertion points, and the glenohumeral center of rotation (which will be discussed in detail in a later section). Each of these parameters affected the curve of the muscle moment-arm as a function of the glenohumeral abduction angle.

Sub-Study 1.1: Via-Cylinder Effects

However, within the realm of anatomically correct positions and sizes, the effects of the via-cylinder can be classified fairly succinctly. When the cylinder obstructs the muscle path, it divides the moment-arm curve into two distinct regions, separated by a

discontinuity in the slope of the curve (Figure 17). The left-hand portion of the curve corresponds to the lower angles of abduction where the muscle path contacts the cylinder. At these angles, the moment arm curve is almost linear. On the right-hand portion of the curve, where the muscle path lifts free of the via-cylinder, the higher-angle data is parabolic in appearance. Figure 17 depicts medial and lateral placements of the via-cylinder, and the resultant degree of muscle-path obstruction. Note that the camera angle is aligned with the axis of the via-cylinder, such that the cylinder appears to be a circle. The image is a close inspection of the glenohumeral joint such that only the proximal portion of the humerus, and the glenoid and acromion portion of the scapula are depicted.

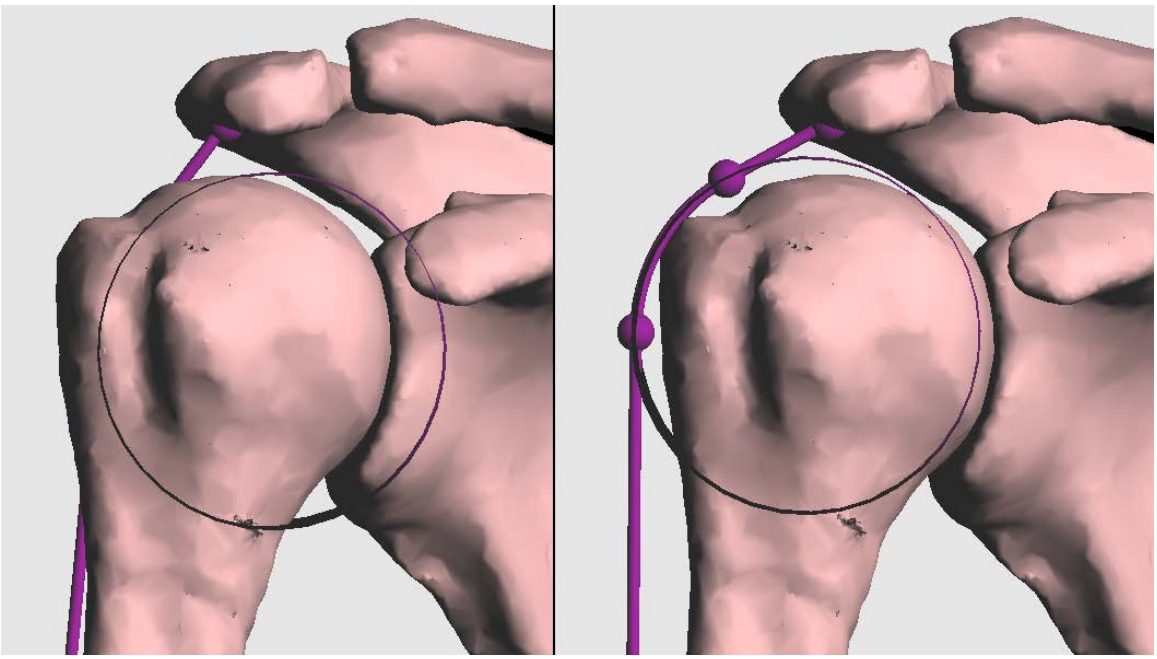

Figure 17: Depiction of the two positions of the via-cylinder used for the results shown in Figure 18. The via-cylinder was moved in the scapular-plane X-direction, simulating more or less lateralization of the anatomical obstacles that the middle deltoid must circumvent (e.g. bone and other muscles) The image on the right depicts a more lateral position of the via-cylinder while the left image is of a medialized obstacle set.

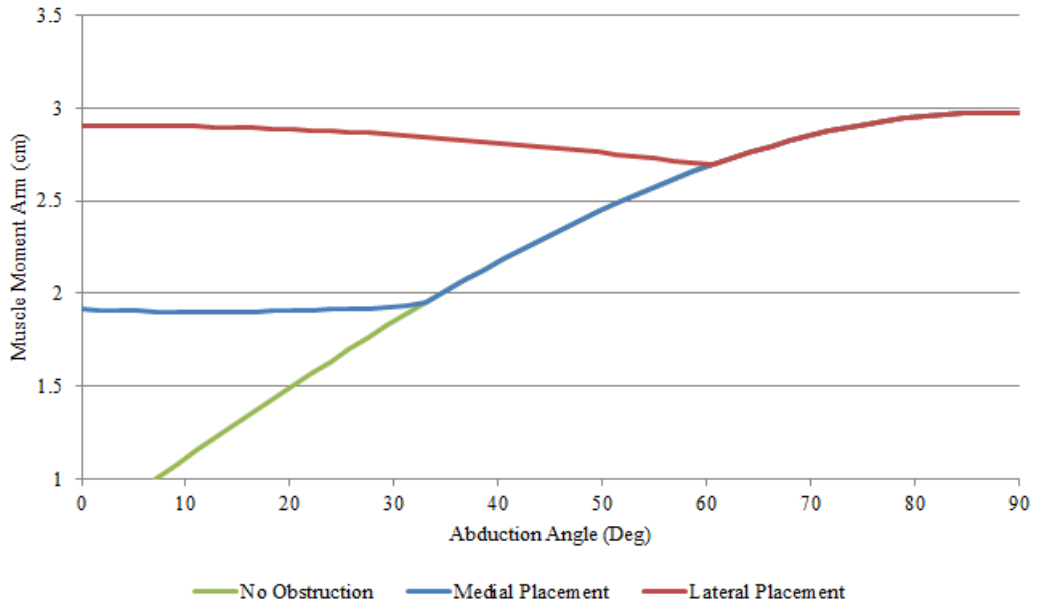

Figure 18: As the-via cylinder is moved medially and laterally, as pictured in Figure 17, it affects the angle at which the muscle path is freed from the obstruction of the cylinder. This point correlates to the divergence in slopes seen near 30° and near 60°. If the via-cylinder is removed from the model completely, then there is no obstruction, as represented by the green curve.

As the cylinder moves medially and laterally in the scapular plane, the division between linear section and the parabolic section shifts. The plot in Figure 18 demonstrates that no change is made to the magnitude or the slope of the parabolic section. However, it does affect the location of the slope discontinuity, and to a lesser extent it also affects the slope curve through the smaller angles of abduction. If the cylinder is removed completely from the muscle path, there is no linear section of data, and the entire curve is parabolic in nature. Medial translation of the cylinder forces the division of linear and parabolic to migrate to the left while lateral translation increases the predominance of the left-hand linear portion, forcing the discontinuity to the right.

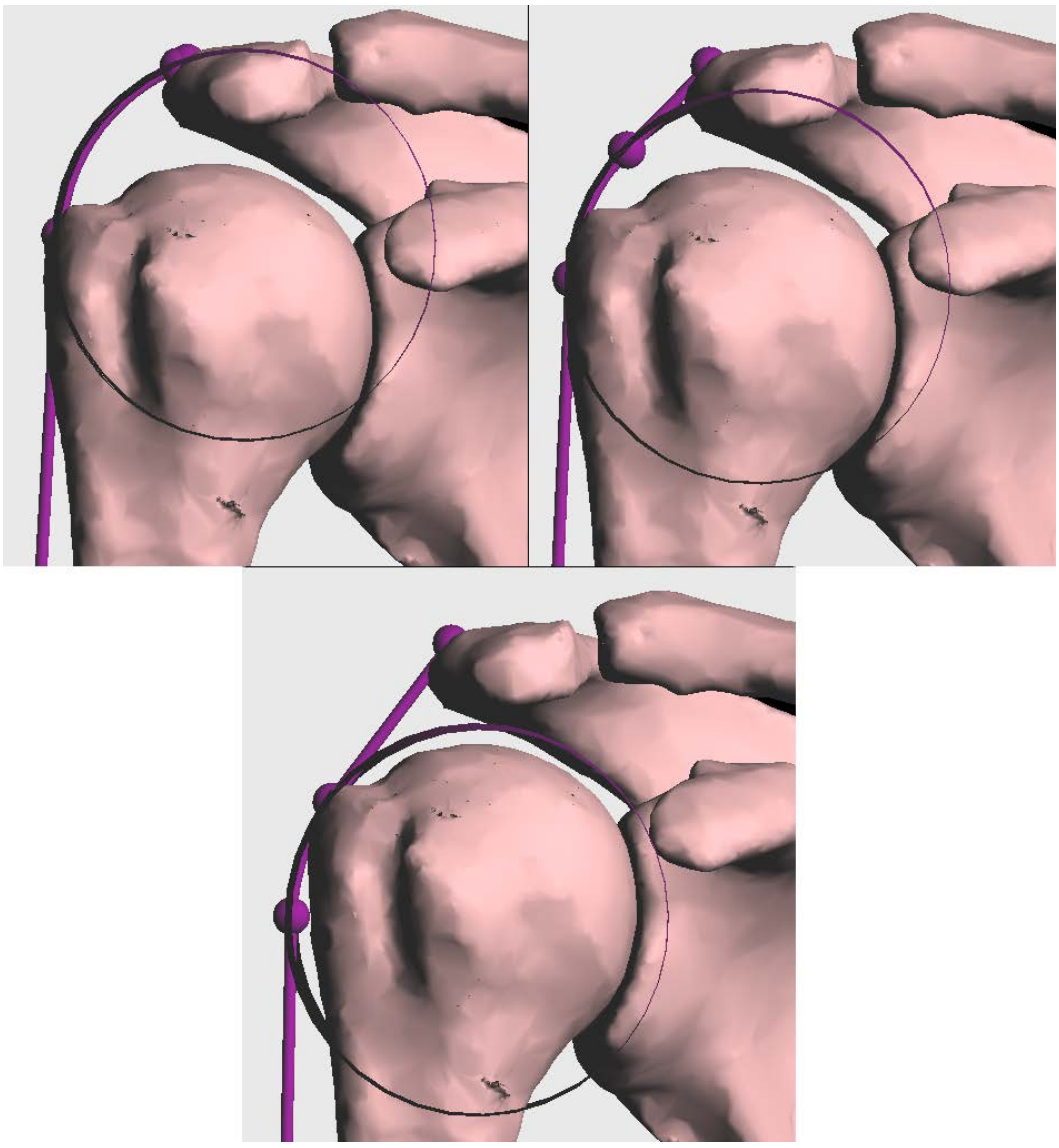

Figure 19: Depiction of vertical via-cylinder translation. The positions depicted correspond to the results in Figure 19. The superior-inferior placement of the cylinder is measured by an inferior offset from the position of the origin (uppermost purple sphere). The 0 mm inferior offset is pictured top-left in this figure, and as a green curve in Figure 20. The top right image depicts a 7 mm inferior offset. Bottom image depicts a 17 mm offset.

Superior-inferior translation of the via-cylinder in the scapular plane, depicted in Figure 19, also affects the position of the slope discontinuity. Also, like medial lateral translation of the cylinder, it does not have any discernible effect on the moment arm curve for angles above the slope discontinuity. However it has a very discernible effect

on the slope of the low-angle portion of the curve, or the linear section. As seen in Figure 20, the difference between the slopes of the high and low angle regions becomes less distinct as the cylinder translates superiorly. If the cylinder moves superiorly enough to touch the origin, as shown in the upper-left image in Figure 19, the slope discontinuity ceases to exist, as shown in the "0.0 mm" curve in Figure 20. Conversely, the other two curves show that the slopes become more disparate as the cylinder is translated distally.

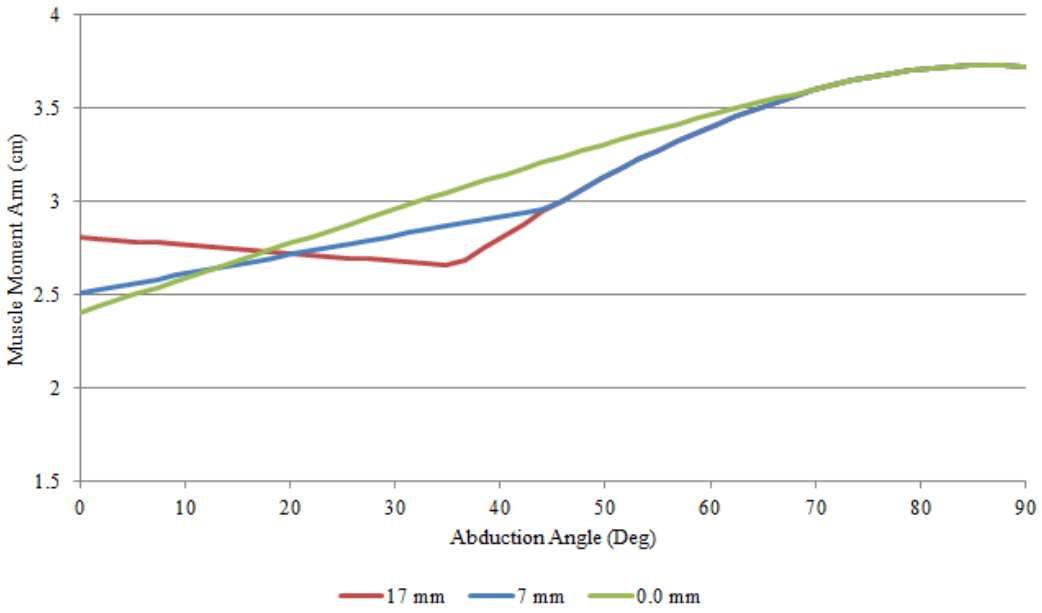

Figure 20: Comparison of effects of vertical of the via-cylinder placements seen in Figure 19. In the legend, each curve is labeled by the inferior distance of each respective via-cylinder from the origin.

The radius of the cylinder does not have any effects that are obviously distinct from the horizontal or vertical translation. As much as an increase in radius causes the cylinder to obstruct the muscle path further laterally or superiorly it has the same effect that a lateral or superior translation would have. Radial adjustments can, however, be useful for obtaining the desired combination of vertical and horizontal effects.

Sub-Study 1.2: Muscle Origin Effects

Small adjustments to the origin of the middle deltoid had a surprisingly large impact on the magnitudes of the moment arms. Medial-lateral movement of the origin affected the moment-arm curve noticeably, but not to the same magnitude as superior-inferior shifts. If all other parameters are held constant while the origin is moved medially, the slope of the curve is largely unaltered. However, because the slope discontinuity occurs earlier, the similar slope achieves a greater maximum moment arm within the range of motion of the glenohumeral joint. This trend is illustrated between Figures 21 and 22, where the placement is depicted, and the resulting trends are plotted, respectively.

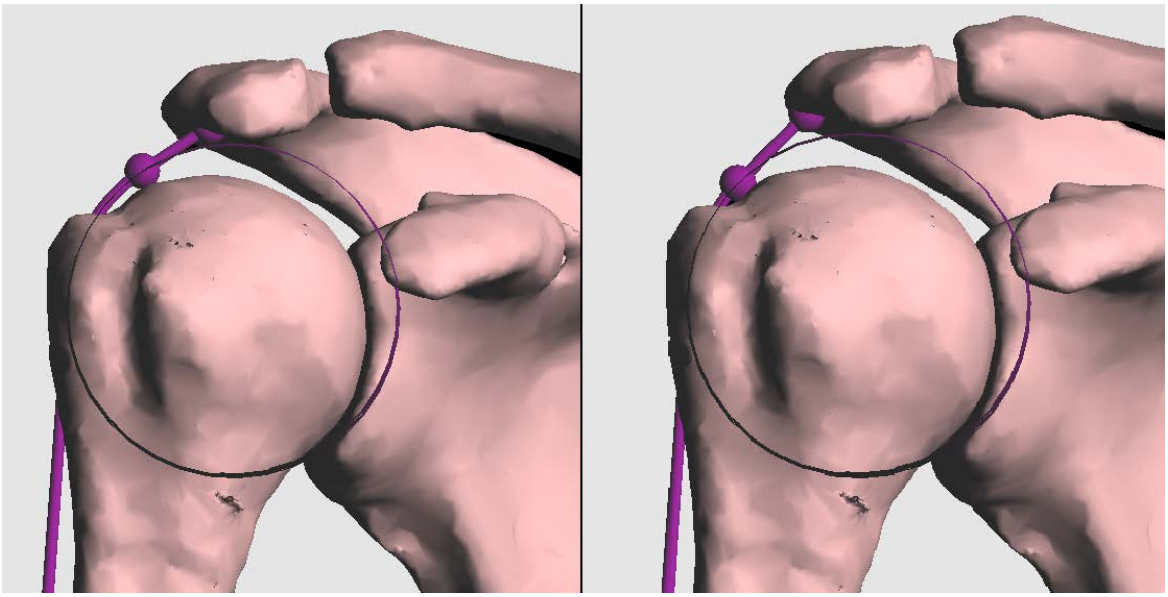

Figure 21: Origin (uppermost purple sphere) positions correspond to the results in Figure 22. Medial origin placement is depicted on the left, and lateral placement of the origin is depicted on the right.

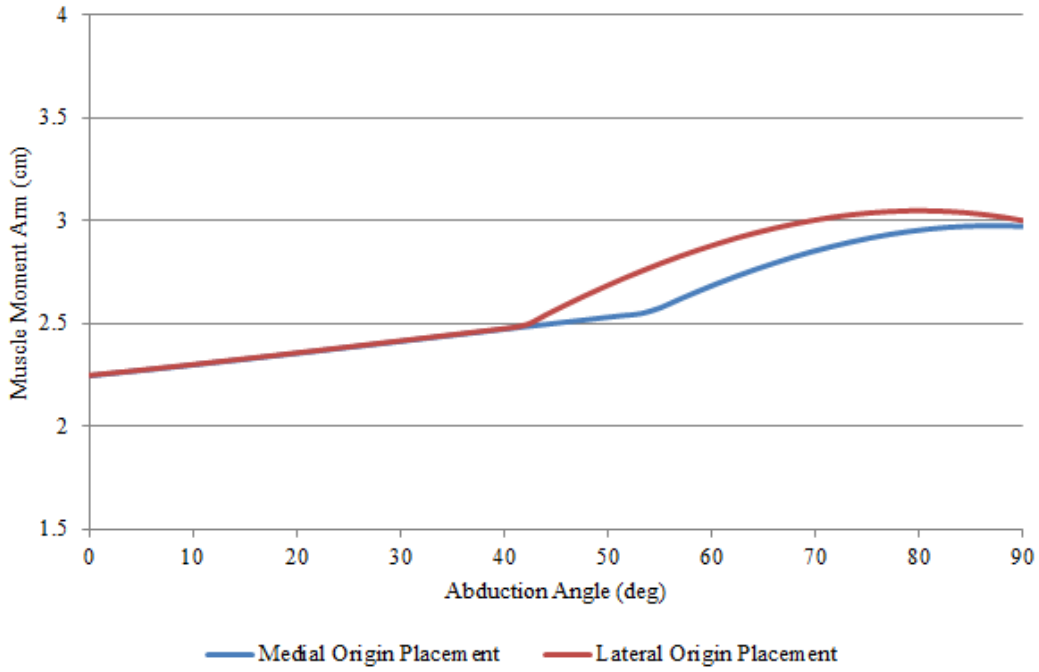

Figure 22: Comparison of model prediction of muscle moment arms corresponding to the anatomical configurations depicted in Figure 21

A more obvious trend is observable in vertical shifts of the muscle origin. If all other parameters are held constant and the point of insertion is moved in the inferior direction, the global maximum, the maximum gradient, and the location of the maximum gradient scales downward. The trends are illustrated in between Figures 23 and 24, where the placement is depicted, and the resulting trends are plotted, respectively.

Sub-Study 1.3: Muscle Insertion Effects

The muscle insertion point has little discernible effect on the muscle excursion or the associated moment arm data. Not only is the best location for the insertion point much less ambiguous than the origin, the effect of insertion adjustment was much smaller than that produced by a similar change in the origin. The insertion point was confined to the deltoid tuberosity, and left unchanged through all subsequent sub-studies.

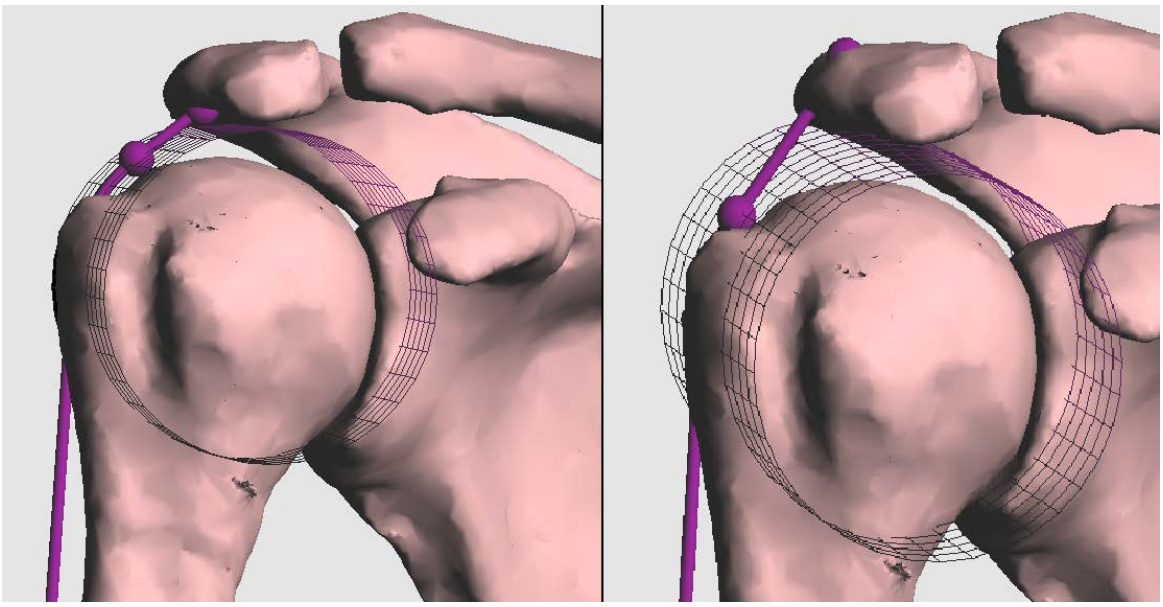

Figure 23: Positioning of origin of the middle deltoid on the inferior surface of the acromion (left) and on the superior surface (right). *In vivo* the middle deltoid origin envelopes both represented locations.

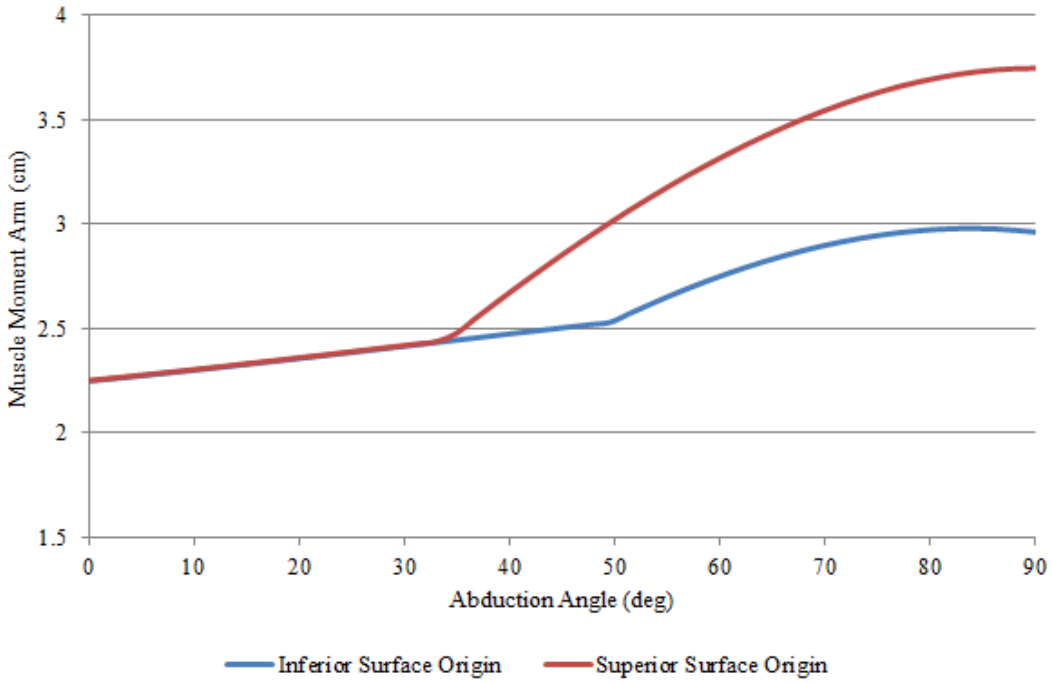

Figure 24: Comparison of model prediction of muscle moment arms with each of the origin locations depicted in Figure 23

Sub-Study 2: Experimental Data Replication

The simulations that follow attempt to justify or understand inconsistencies between expected data trends and the experimental data obtained from the ALOK studies [3–6]. A detailed list of final parameters for each of the following sub-studies can be found in Appendix A.

Sub-Study 2.1: Fixed Anatomical Center of Rotation

In this study the joint center was fixed at the anatomical position (the geometric center of the humeral head), while the muscle parameters were manipulated in an effort to reproduce the ALOK muscle moment arm trends. The model was able to produce magnitudes and trends for the middle deltoid moment arm that were similar to the experimental datasets. However, the muscle path geometry necessary for the model to fit the experimental data was found to be anatomically infeasible. Figure 25 is a visualization of the physiology that resulted in the moment arm curve in Figure 26.

Each of the specified studies apart from that of Kuechle et al. have relatively constant positive slopes from 0° of abduction up until 20-40° of abduction, along with a resting moment arm of less than 15 mm. As shown in Figure 25, in order to imitate these data trends, it was necessary to place the origin of the middle deltoid on the inferior surface of the acromion. This placement is within the viable attachment area of the *in situ* middle deltoid. However, it was also necessary to completely remove the via-cylinder from the muscle path and allow the line of action to assume a straight route from the origin to the insertion. This path takes the line of action well within the radius of the humeral head, indicating that the middle deltoid would have to tunnel through the humerus in order to fit this set of parameters.

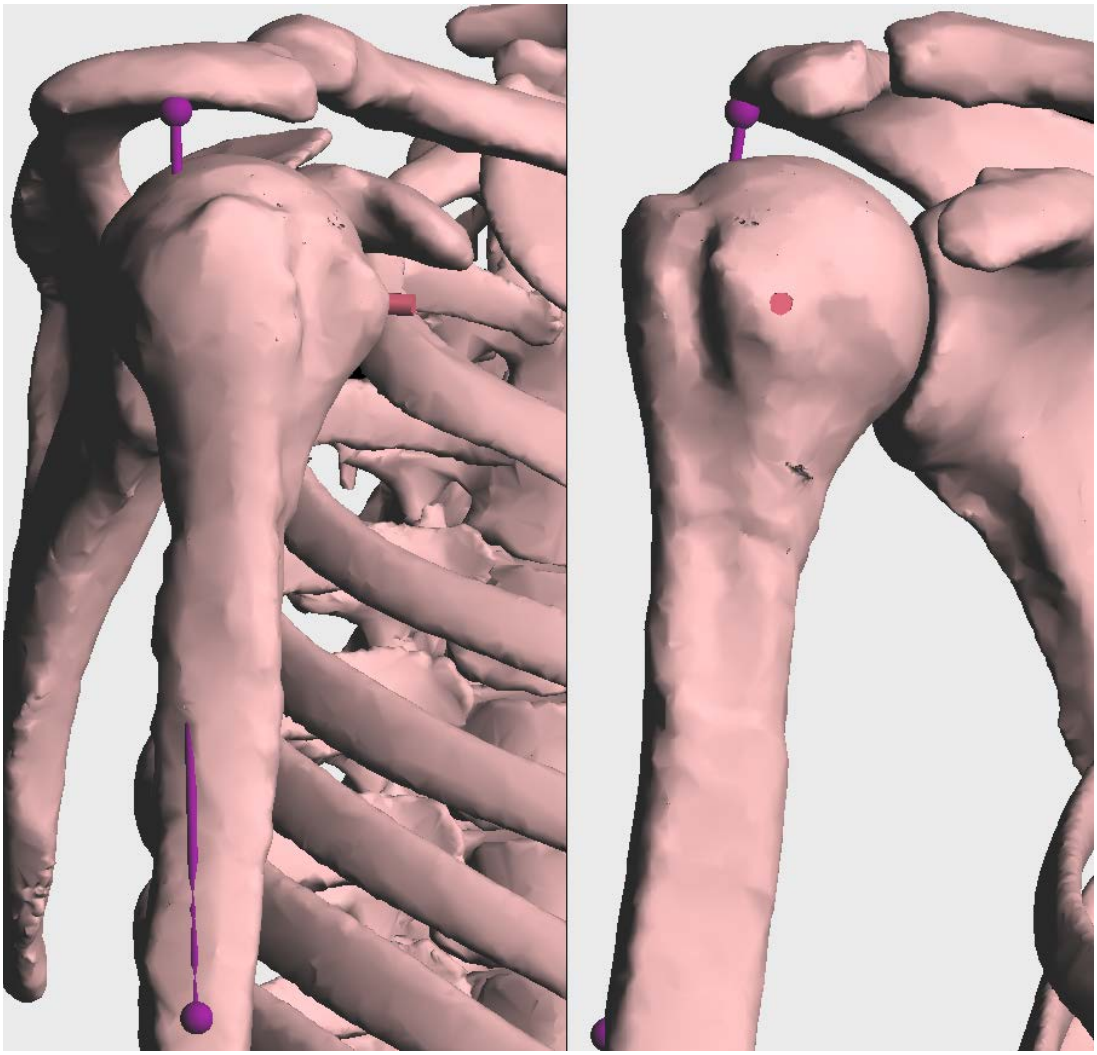

Figure 25: For Sub-Study 2.1, in order to match the model to the experimental data, the muscle origin and insertion (purple spheres) were manipulated, while the via-cylinder was removed entirely. The resultant muscle path is pictured (in purple) from the side and front. The path clearly passes through the humeral head and shaft.

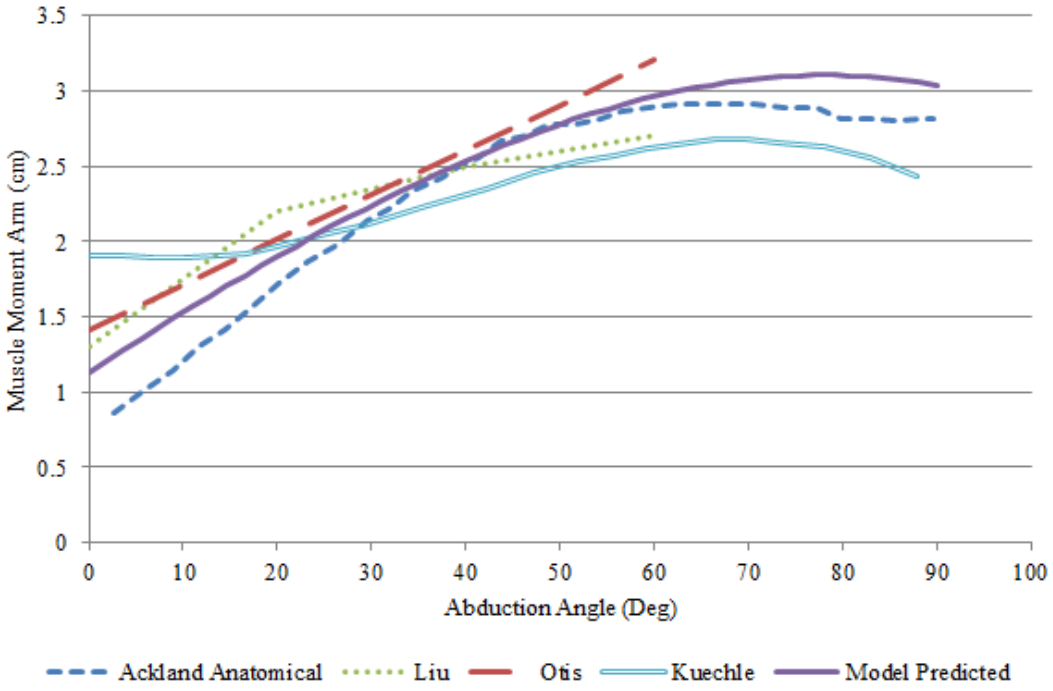

Figure 26: Comparison of experimental middle-deltoid moment arms [3–6] to the modeled curve with the glenohumeral center fixed at the center of the humeral head,

Sub-Study 2.2 – Fixed Anatomical Muscle Parameters

As an alternate means of analyzing the perceived discrepancies in the data taken from the ALOK studies [3–6], this set of sub-studies was designed to satisfy muscle path requirements and dimensions while adjusting the glenohumeral joint center of rotation. Each iteration of this sub-study emulates a unique set of muscle path parameters that were selected to match anatomical descriptions.

Sub-Study 2.2.1. In this sub-study the glenohumeral center was adjusted in an effort of match the modeled moment arms to the data from Ackland et al., Liu et al., and Otis et al. It was unknown if the position of the muscle origin would affect the ability of the model to predict trends similar to that of the experimental data. Thus, Sub-Study 2.2.1 was iterated through three distinct origin positions: centered on the superior surface

of the acromion, centered on the lateral edge of the acromion, and centered on the inferior surface. In the first iteration of this sub-study Figure 28 shows superior positioning of the muscle origin and the associated location of the joint center, while Figure 27 shows the resultant model prediction of the moment arm curve in comparison to the ALOK experimental data. In the second iteration, Figures 29 and 30 then display the same set of information, but for a lateral positioning of the muscle origin. Finally, the third iteration follows the same format of displayed results – for inferior placement of the muscle origin.

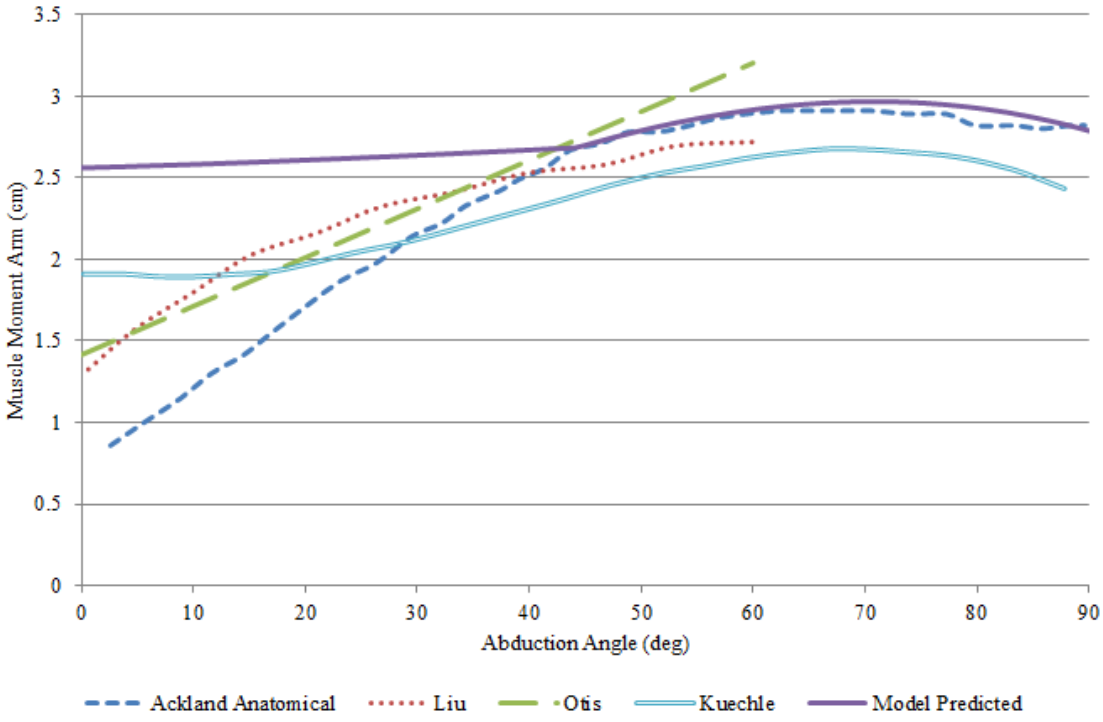

Figure 27: Comparison of model predicted moment-arm curve that resulted from an anatomically correct configuration of muscle parameters. Because there are several anatomically correct positions for the middle deltoid origin, this iteration of the xub-study was performed with a superiorly placed origin. The via-cylinder and center of rotation were accordingly adjusted to gain the depicted agreement to the data from literature, specifically the Ackland anatomical study.

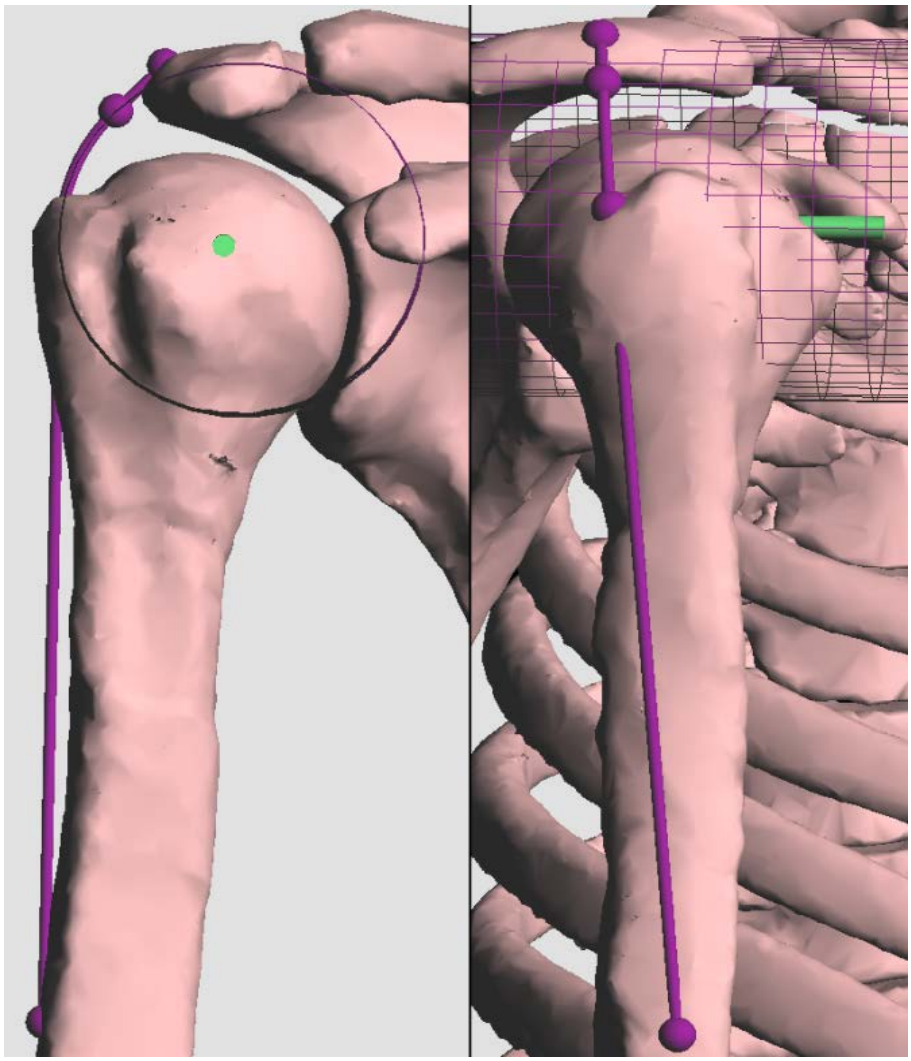

Figure 28: Side and front views of the shoulder configuration that justifies the depicted muscle origin (upper purple sphere). The joint center (green) was chosen to best replicate trends seen in the ALOK data. Resultant model prediction can be seen in Figure 28.

Figure 29 shows that above the slope-discontinuity in the model's prediction, the curve fits extremely well with the trends of the experimental data. With the muscle-path parameters set, the curve was fitted to the data by moving the joint center. With the origin positioned on the superior surface of the acromion, the results of this iteration of Sub-Study 2.2.1 show that the required position of the joint center was 10.5 mm superior to the expected anatomical joint center.

The second iteration of Sub-Study 2.2.1 fixed the origin of the middle deltoid at the lateral edge of the acromion. This orientation can be seen in Figure 29.

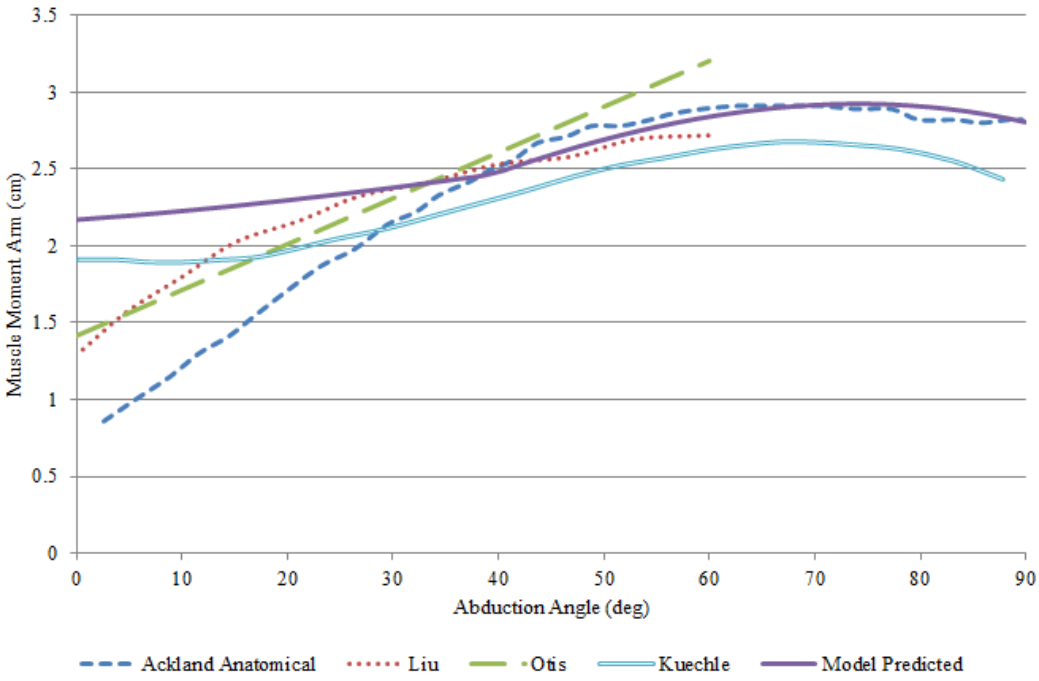

Figure 29: Comparison of model predicted moment-arm curve that resulted from an anatomically correct configuration of muscle parameters. Because there are several anatomically correct positions for the middle deltoid origin, this iteration of the sub-study was performed with a laterally placed origin. The via-cylinder and center of rotation were accordingly adjusted to gain the depicted agreement to the data from literature, specifically the Ackland anatomical study.

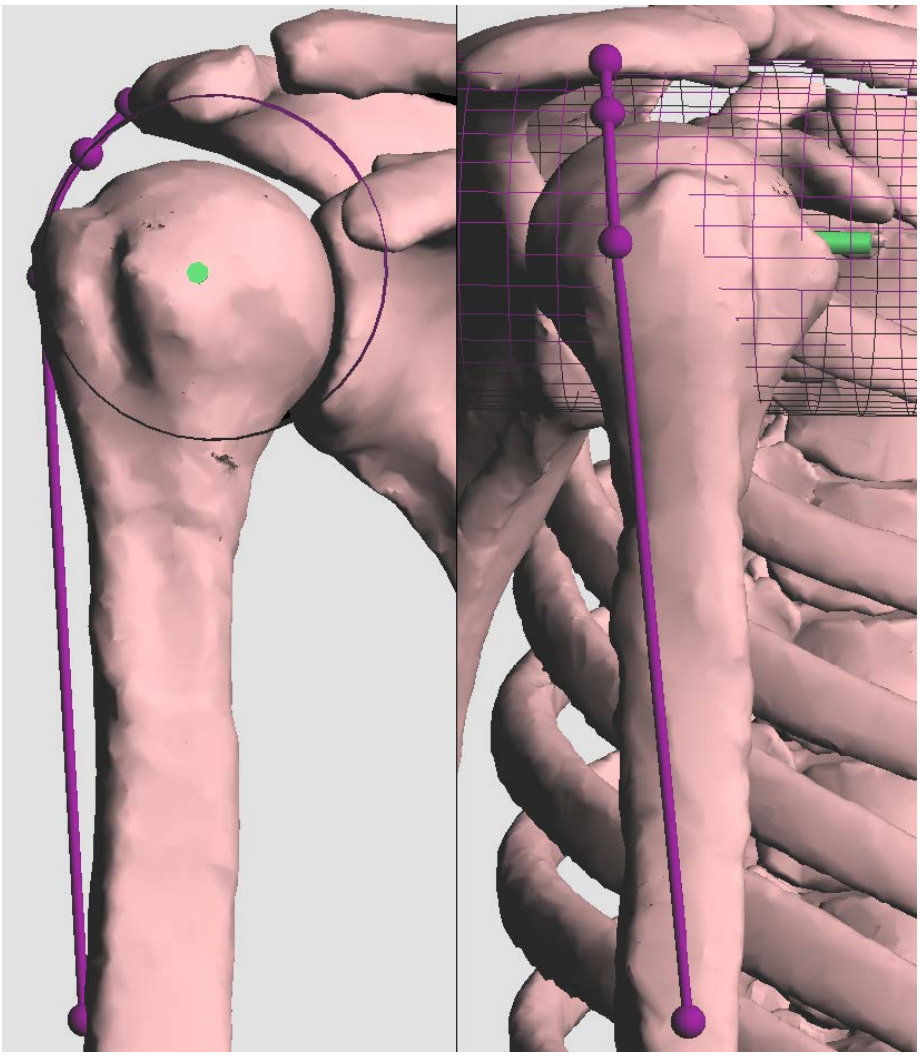

Figure 30: Depiction of physiology when the origin is placed laterally on the acromion. The joint center in green is positioned to best fit the model to the ALOK data while the muscle parameters are defined for anatomical correctness. Corresponding model results depicted in Figure 29

The lateralized-origin iteration of Sub-Study 2.2.1 required a different joint center in order to achieve a similar fit to the superior-origin iteration. However, it can be seen in Figure 29 that this change in position of the joint center was able to mitigate the effects of the change in origin position, such that the model predicted curves in Figures 27 and 29 have a very similar fit. The required position of the joint center was 3 mm lateral and

2 mm inferior to the expected anatomical joint center for a total deviation of approximately 3.4 mm.

The third iteration of Sub-Study 2.2.1 fixed the origin of the middle deltoid on the inferior portion of the acromion. This configuration can be seen in Figure 31.

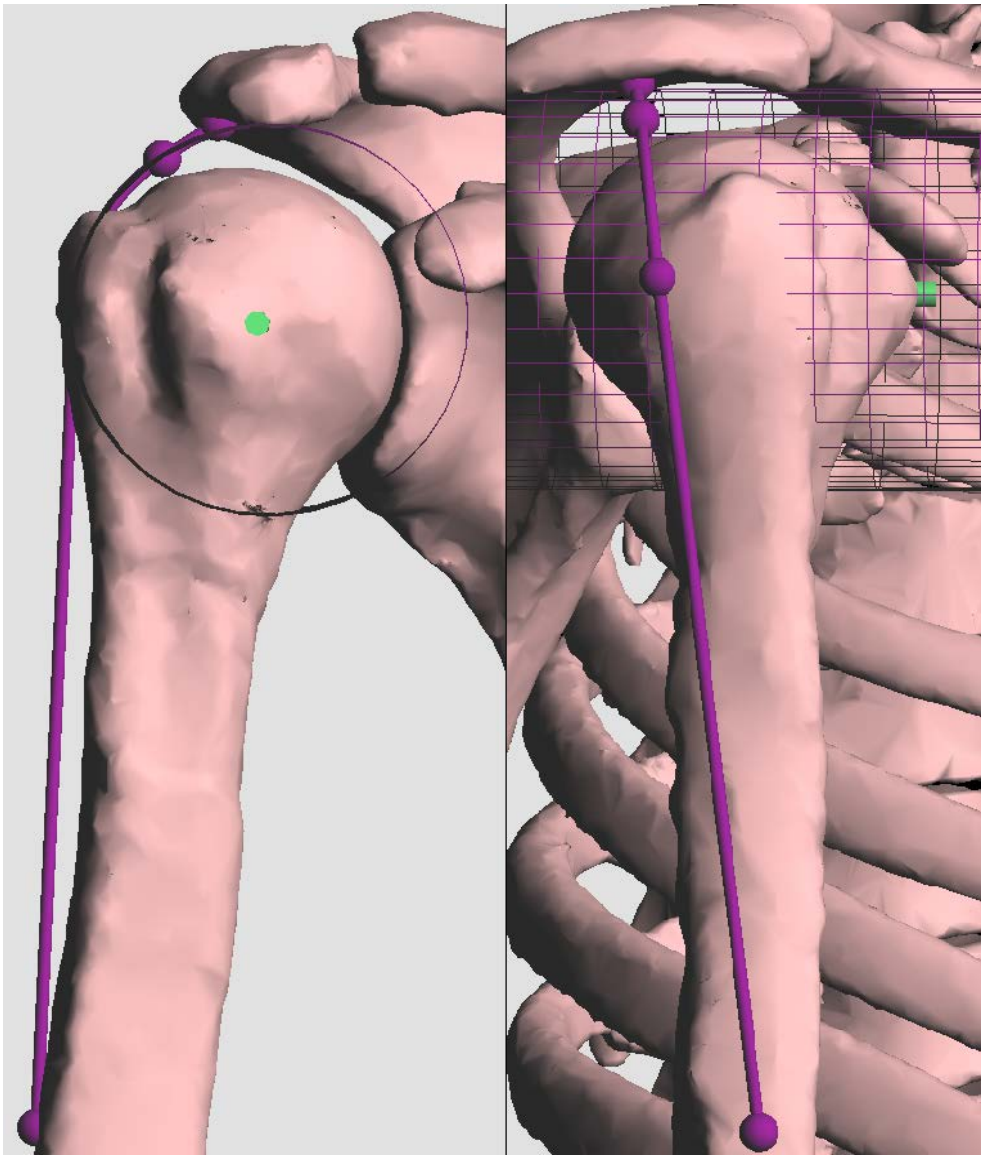

Figure 31: Inferior placement of the muscle origin (superior purple sphere) and placement of the via-cylinder and joint center (green) that allow this physiology to match the ALOK data, as shown in Figure 32.

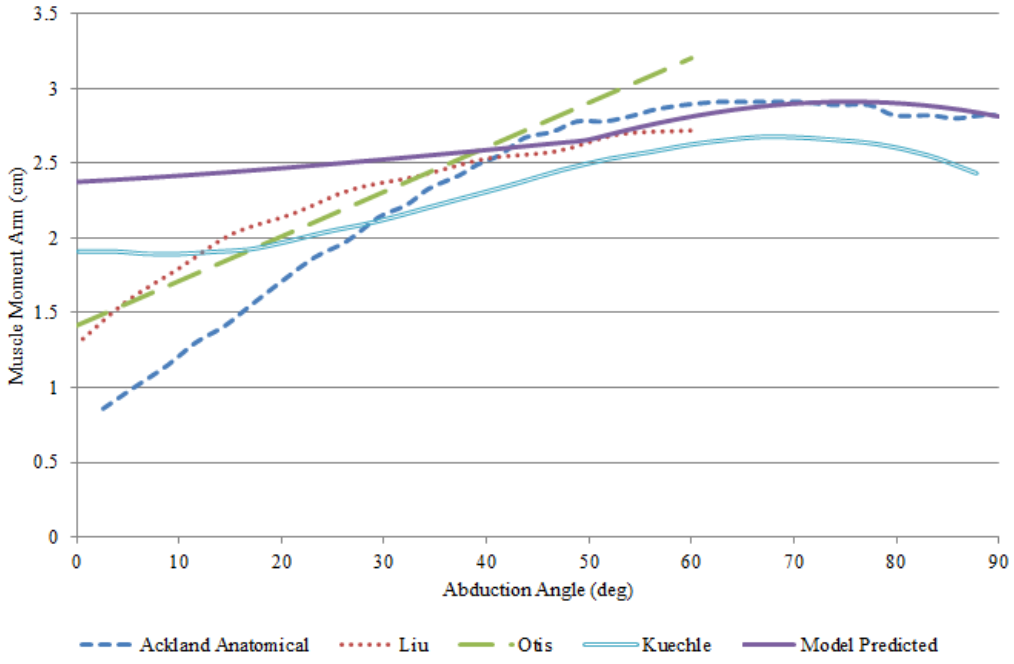

Figure 32: Comparison of model predicted moment-arm curve with inferior origin placement, as shown in Figure 31, to the data from the ALOK studies.

Again, Figure 32 shows that the movement of the joint center was able to offset almost all of the effect of the change in position of the origin, even though Sub-Study 1 showed that the placement of the origin can have a significant effect on the curve of the moment arms. The required position of the joint center was 2.3 mm medial and 4.8 mm inferior to the expected anatomical joint center for a total deviation of approximately 5.4 mm. The differences between the parameters of each of these three iterations are described in detail in Appendix A.

Sub-Study 2.2.2. The magnitude and the trends of the moment arm curve from Kuechle et al. [3] are more consistent with expectations and geometric muscle path than that of the other three ALOK studies, specifically in that Kuechle's moment arms are larger at the early abduction angles. Sub-Study 2.2.2 was designed to test how the model

prediction would fit the Kuechle data when provided with anatomically correct parameters. This sub-study was done with the superior positioning of the muscle origin, as depicted in Figure 27.

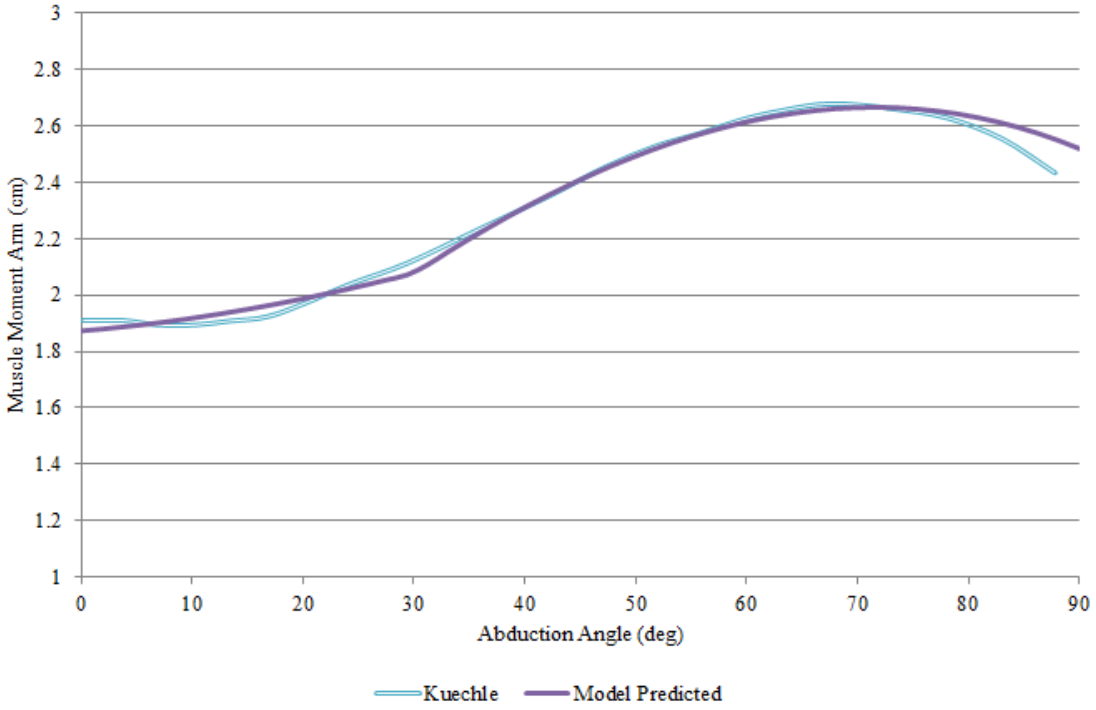

Figure 33: With physiologically correct parameters (as given in Appendix B) the model was able to accurately represent the Kuechle data [3]

As with the previous simulations, there was a range of parameter combinations that brought the model prediction into solid agreement with the Kuechle data. The model prediction that is shown in Figure 33 is a result of a superiorly placed origin, and a joint center that is nearly 11 mm superior to the anatomical joint center. Full parameters can be found in Appendix A. With alternate placement of the middle deltoid origin, it was possible to bring the predicted joint center within approximately 6 mm of the expected anatomical center. None of these configurations provided a muscle path that was

completely free of interference with the humeral head, however there was significantly less humeral head interference in this instance than there was in simulating the other anatomical data sets.

Sub-Study 2.3: Migrating Center of Rotation

In this sub-study the author attempted to justify the trends of the experimental data by simulating a center of rotation that migrates as abduction angle increases. Data was taken over five degree intervals and the model's center of rotation was adjusted to match each experimental dataset at the corresponding abduction angle. Figure 34 shows that iterative adjustment of the joint center allowed for the model to individually match the data for the Ackland anatomical and RSA studies as well as the Kuechle data [3,6,12].

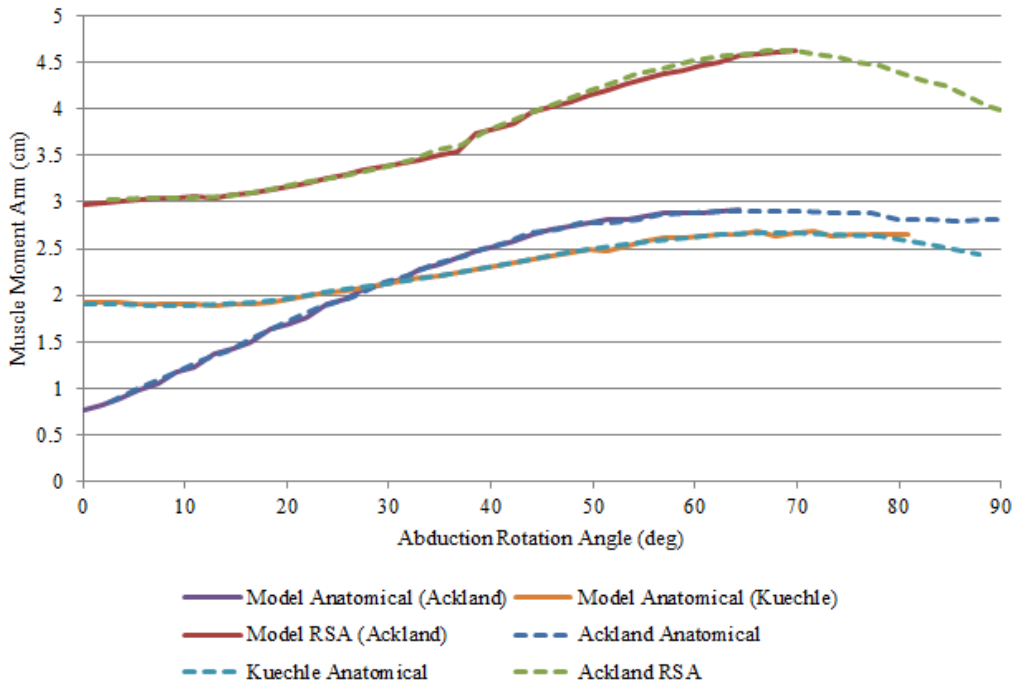

Figure 34: The center of rotation was adjusted every 5° to fit to fit the data from each of the three studies. The success of the fit is shown here. The migration of the joint center is shown in Figure 35.

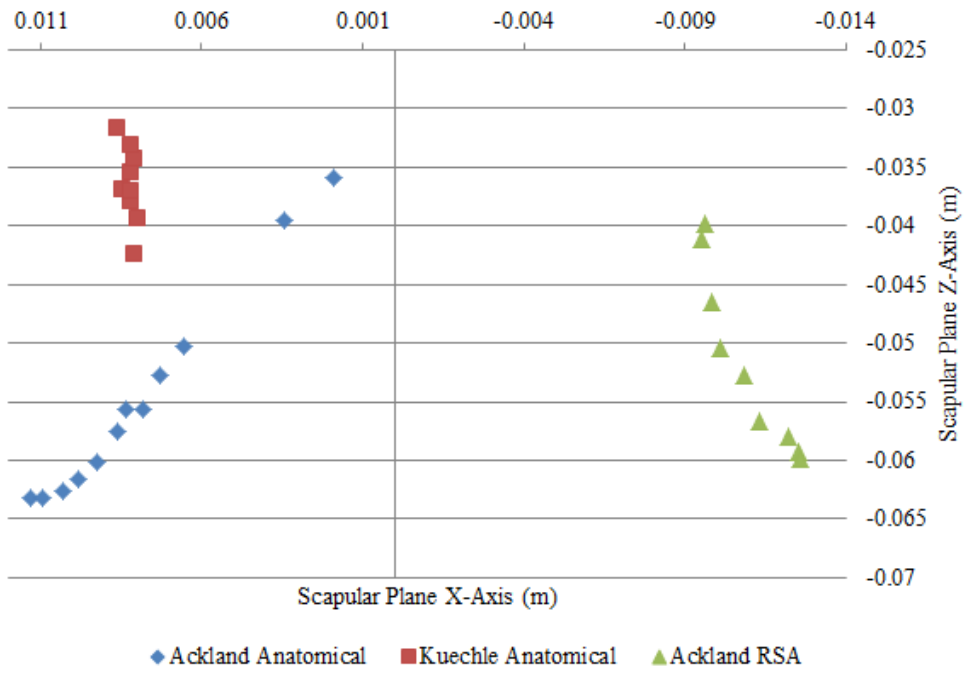

Figure 35: This data represents the migration of the model's joint center of rotation as it was necessary to match the moment arms of the middle deltoid from the model to the anatomical data from Kuechle [3] and Ackland [6], as well as the RSA data from Ackland [12]. Chart axes represent coordinates in the scapular reference frame, in meters with the X-axis reversed according to the model's convention.

Figure 35 shows the X and Y migration necessary to match the model to each data set. In order to match the model to the anatomical Ackland data for middle deltoid moment arms, there was a significant migration of the model's joint center. It required nearly 10 mm of translation in the scapular X-direction, and over 25 mm in Z-direction. To match the data from the anatomical Ackland data, the modeled joint center was migrated from the lower left blue diamond, corresponding to 0° of abduction, to upper right, at the upper limits of abduction. The large gap seen in the progression of the blue-diamonds is where the slope of the model-predicted curve changed drastically. This required further migration to create the fit, but it is interesting to note that the linear trendline was maintained.

In order to match the model to the anatomical data from Kuechle et al., there was almost no migration in the X-direction, and a little more than 10 mm of total migration in the vertical direction. Although the order is not shown Figure 35, the red square representing the position of the glenohumeral center at maximum abduction is adjacent to the square representing the zero position. The model's joint center started at the upper-left-most red square and migrated downward before returning to a similar elevation. This bobbing motion is similar to the motion of the joint center that is described in literature, except that it has been reported to start low and move superiorly before dropping again [41,42].

In order to match the model to the RSA Ackland data for middle deltoid moment arms, there was 3 mm of medial migration, and 20 mm of inferior migration. This means that the model's joint center moved from the top-left green triangle to the bottom-right triangle. The final elevation of the joint center was similar to the experimental RSA joint center, but in the X-direction the final joint center was still approximately 6 mm lateral of the experimental center.

Sub-Study 2.4: Reverse Shoulder Data Comparison

After calibration with the anatomical data, the model was also compared with the RSA data found in literature [12,45,46] to ensure that the physiological parameters for the anatomical shoulder translated to the RSA shoulder. The muscle path parameters used in Sub-Study 2.2.1 that placed the middle deltoid origin in a superior position were used in this sub-study, while the center of location was defined according to the center defined by the Ackland RSA study (see Figure 27). As seen in Figure 36, the model-

predicted data stayed within the range of values given by the three different data sets from literature, showing good agreement in trends and in magnitude.

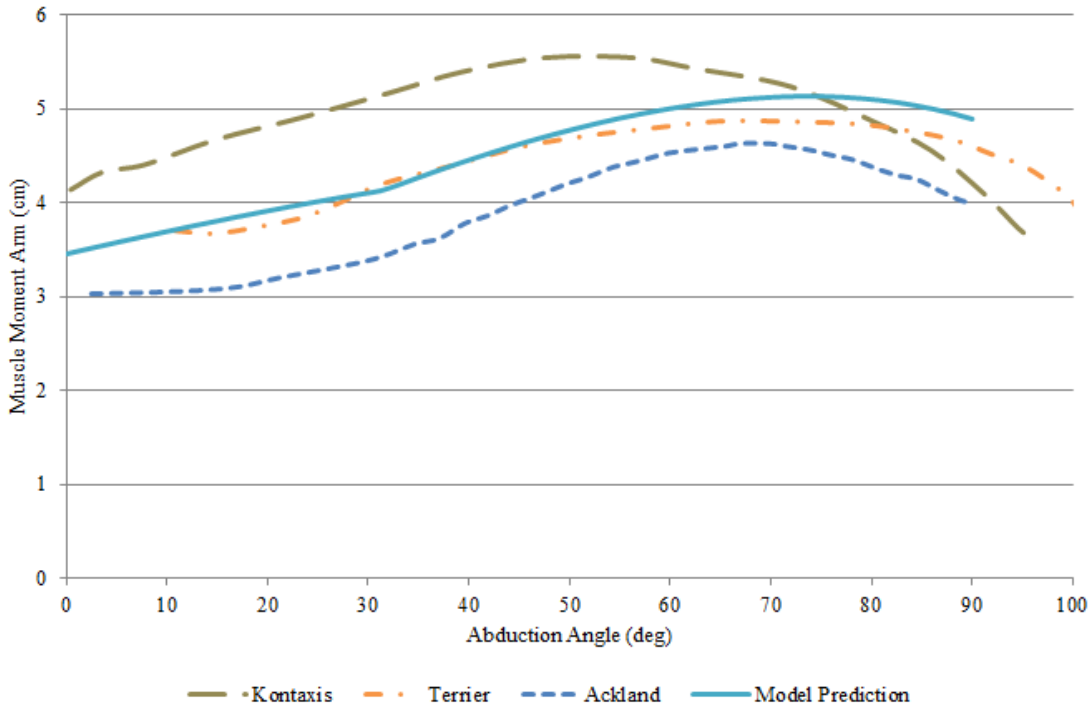

Figure 36: Plot of the experimental and model predicted data from literature compared to the predictions of this model for reverse shoulders

Sub-Study 3: Joint Center Simulations

Understanding the trends of the data as the joint center shifts will allow surgeons to position the joint center according to the individual needs of the patient. This set of simulations is designed to create a comprehensive description of these trends within a specified geometric range. Figure 37 depicts the grid of joint centers that were tested for this analysis, as it was described in Chapter 3.

Trends resulting from the manipulation of the other parameters (muscle origin and insertion, via-cylinder location and radius) have already been presented and hold value that applies largely to this model. The trends in mechanical advantage as a function of

the location of the joint center of rotation are presented separately here to illustrate greater detail for this impartant parameter that may be adjusted via implant design or surgical technique.

In general, the following trends were observed: lateral movement of the joint center changes the magnitude of the moment arms at low angles, while vertical translation changes the moment arms at high angles. Figure 37 is for reference in understanding the geometric significance of Figures 38-42.

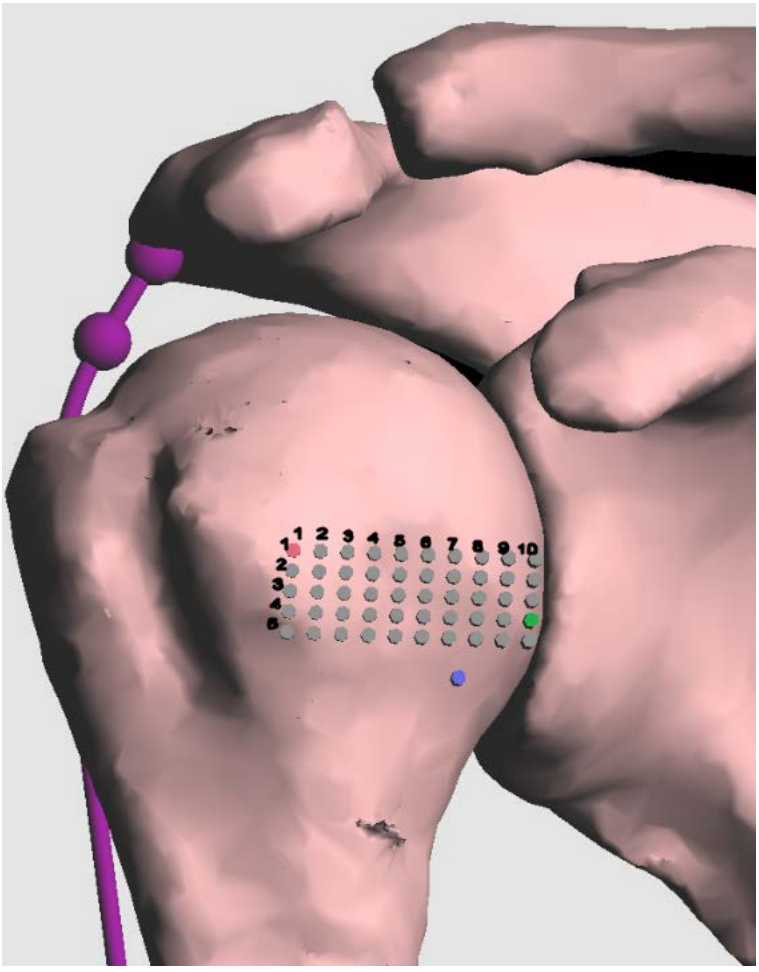

Figure 37: Grid of points used for the various joint center simulations. For use in positional reference for Figures 38 – 42. The red, green, and blue centers respectively mark the centers of rotation found by using the geometric center (anatomical), the 12 mm rule (RSA) and the center defined in the RSA study by Ackland et al. [12].

Sub-Study 3.1: Medial-Lateral Movement of the Joint Center

Figures 38 and 39 depict how the data trends when the center of rotation is shifted medially. Both Figures illustrate that moment arms for the middle deltoid do increase with medial translation of the joint center. As the rotation center moves medially, the moment arms at low angles increase significantly while those at higher angles remain more and more static, and even decrease at the upper limits of abduction. The distance between each column of test locations, or from (m, n) to (m, n+1), is 3 mm. There are a total of 10 columns within a total medial-lateral range of 27 mm.

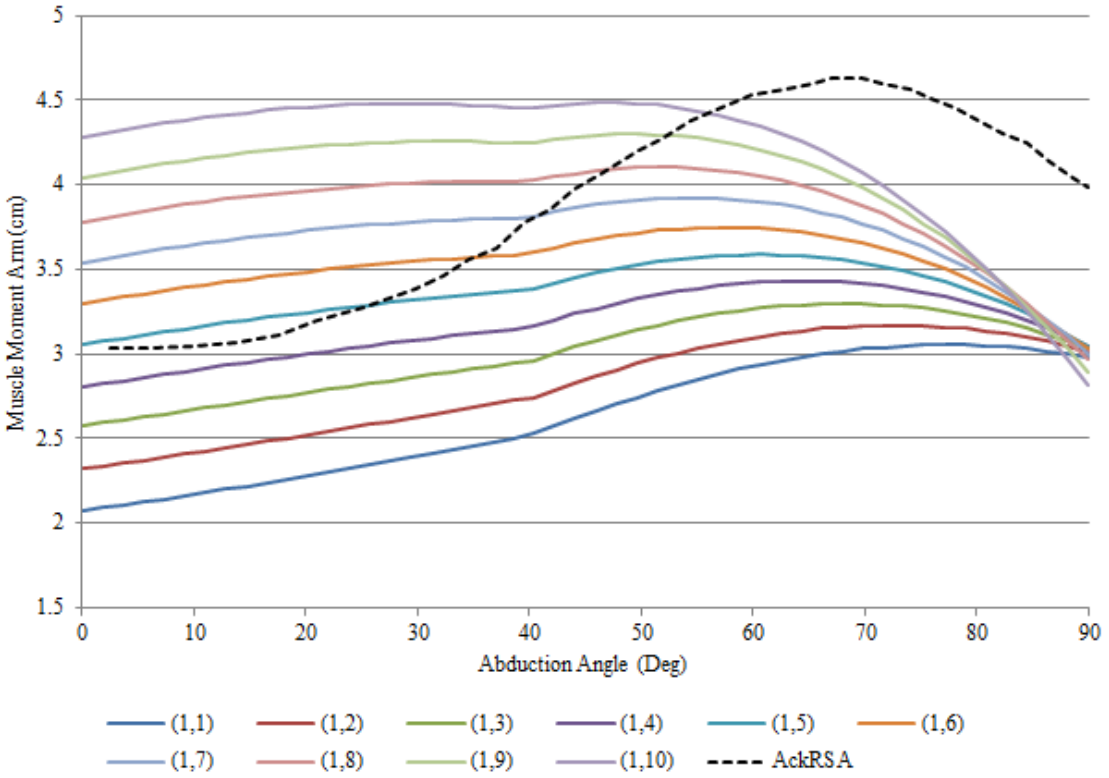

Figure 38: Trends in moment arm data for the middle deltoid as the center of rotation shifts medially along the superior border of the viable joint center range, as it is depicted in Figure 37. The Ackland RSA data for the middle deltoid is shown, for reference, as a dashed black line.

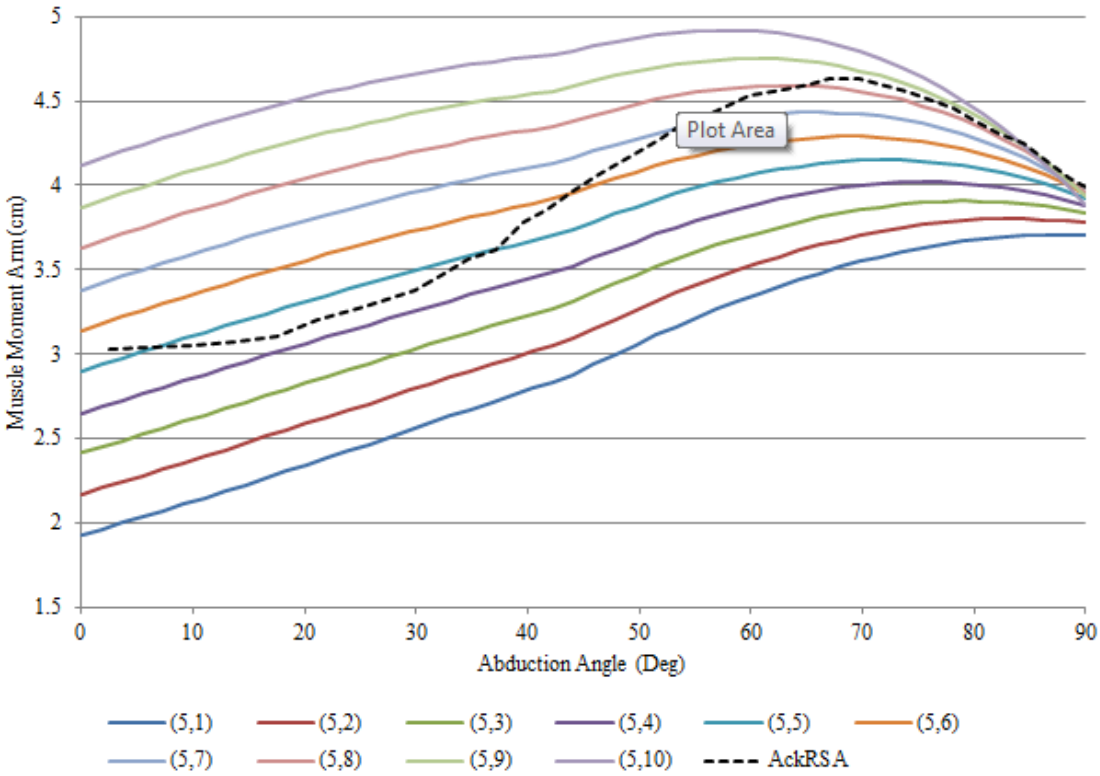

Figure 39: Trends in moment arm data for the middle deltoid as the center of rotation shifts medially along the bottom border of the viable joint center range, as it is depicted in Figure 37. The Ackland RSA data for the middle deltoid is shown, for reference, as a dashed black line.

By comparing Figures 38 and 39, a handful of interesting results are made clear. First, the medial-lateral positioning of the joint center has a pronounced effect on the magnitude of the moment arms at low angles of abduction. For each three millimeter medial shift in the joint center there is an 11.5% increase in the moment arm at zero degrees of abduction. This means that over the entire 27 mm range, there is a total percent increase of 106% over the resting position moment arm at the anatomical position. At the maximum abduction of 90° there is a much smaller effect: a maximum 2% increase in moment arm magnitude at 10 mm of medial movement, and a minimum -5% increase in magnitude at the full 27 mm of medialization.

For translation along the inferior row of joint centers, the trends are largely the same. At the resting position (0° of abduction) the same 11.5% increase in moment arm magnitude is seen between each successively medialized joint center. At maximum abduction (90°), a similarly small effect is also seen. The percent increase over the anatomical position ranges from 24.5% at zero millimeters of joint center medialization to 33% at 18 mm of medialization. The base increase of 25.5% is due to the effects of the inferior shift, as will be seen in the next section.

Another interesting result is that at the low angles of abduction, where the effects of medial-lateral translation are most noticeable, the moment arms relating to positions along the inferior row (shown in Figure 38) have lower moment arms than do the joint center positions along the superior border (shown in Figure 39). This trend is illustrated by comparing the moment arm curves of positions (1,1) and (5,1), or the positions (1,10) and (5,10). Generally, the moment arm is thought to be maximized by moving inferiorly. Apparently, this assumption holds only for angles of glenohumeral abduction under approximately 40°.

Sub-Study 3.2: Superior-Inferior Movement of the Joint Center

Other trends that result from superior-inferior movement of the joint center can be viewed in Figures 40-41. As distal translation occurs, the moment arms at high angles are increased while the moment arms at lower angles display a much smaller and slightly opposite effect. The distance between each row of test locations, or from (m, n) to (m+1, n), is 2.06 mm. There is a total of 5 rows within a total superior-inferior range of 8.25 mm.

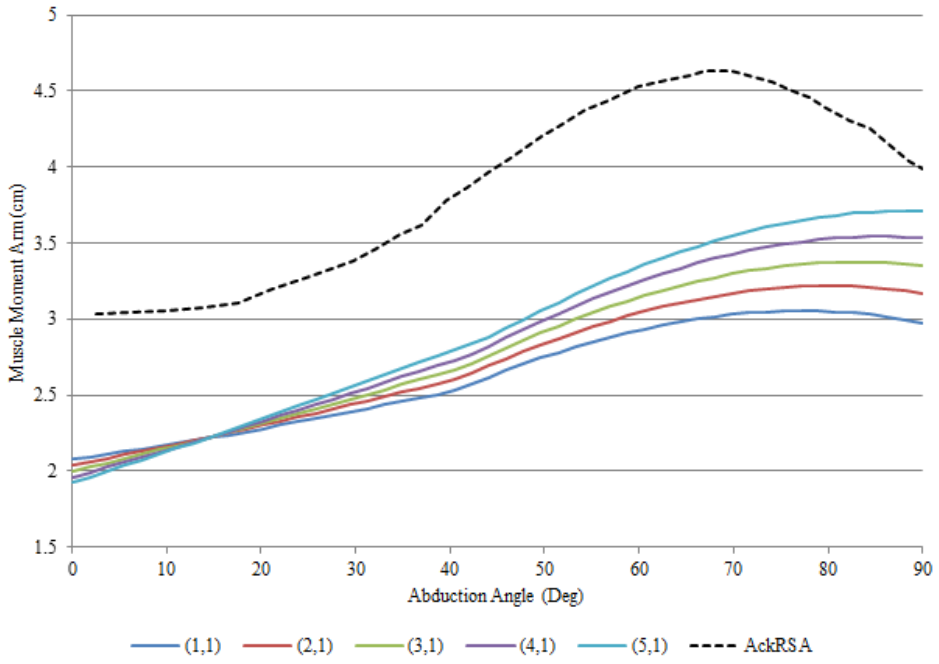

Figure 40: Trends in moment arm data for the middle deltoid as the center of rotation shifts inferiorly along the most lateral column of the viable joint center range, depicted in Figure 37. The Ackland RSA data is shown, for reference, as a dashed black line.

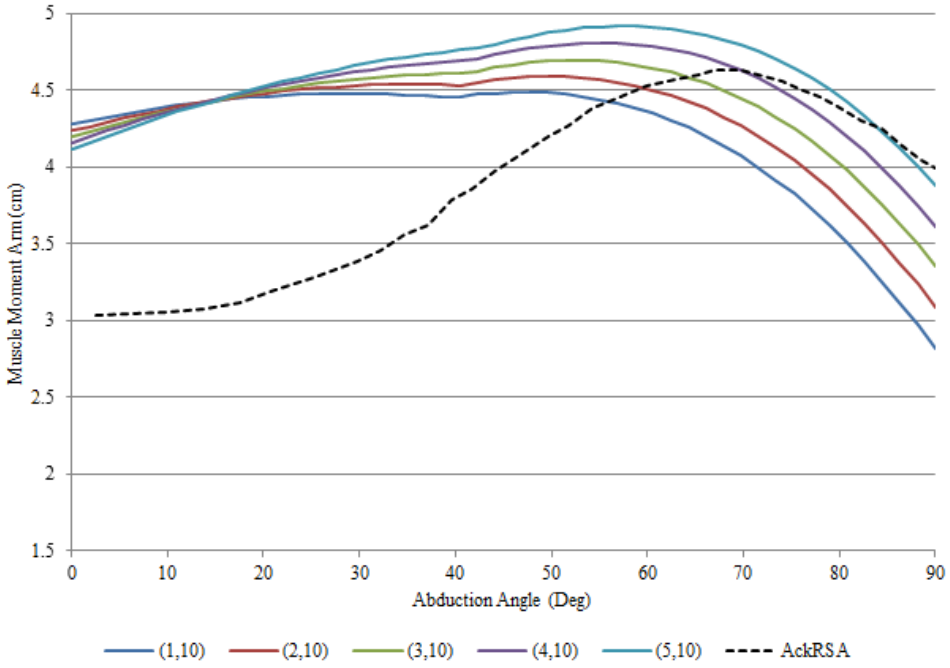

Figure 41: Trends in moment arm data for the middle deltoid as the center of rotation shifts inferiorly along the most medial column of the joint center range, as it is depicted in Figure 37. The Ackland RSA data is shown, for reference, as a dashed black line.

Figures 40-41 confirm that superior-inferior translation greatly affects both the magnitude and the profile of the moment arms at high abduction angles. Again we see the swap effect, where the most inferior positions create the lowest moment arms at resting position. Then as the arm moves through the range of abduction, these inferior centers of rotation outperform the superior positions in terms of mechanical advantage.

It is again shown that the low angles of abduction are negatively affected by inferior translation of the glenohumeral center. We also see confirmation that inferior translation of the joint center increases moment arms at the upper end of the range of motion. For the lateral border of the range (Figure 40), at 90° of abduction, the percent increase in moment arm magnitude per two millimeters of inferior shift is 6%. The percent change for the same interval on the medial end (Figure 41) is 9%. When these percentages are normalized to the same three millimeter interval that is taken in the medial-lateral translations, then the percent increases become 9% and 12.9%, respectively.

The combination of Figures 38-41 shows that mechanical advantage increases with distal and medial translation, both of which are possible directions of movement from the anatomical joint center (test location [1,1] in Figure 37). Furthermore, the increase in moment arm magnitude is roughly equal for medial and inferior translation. It is then possible to move the joint center in a direction that will adjust the magnitude of the moment arms across the entire range of motion and will essentially maintain the anatomical moment-arm profile. Increasing magnitude of the anatomical profile can be seen in Figure 42.

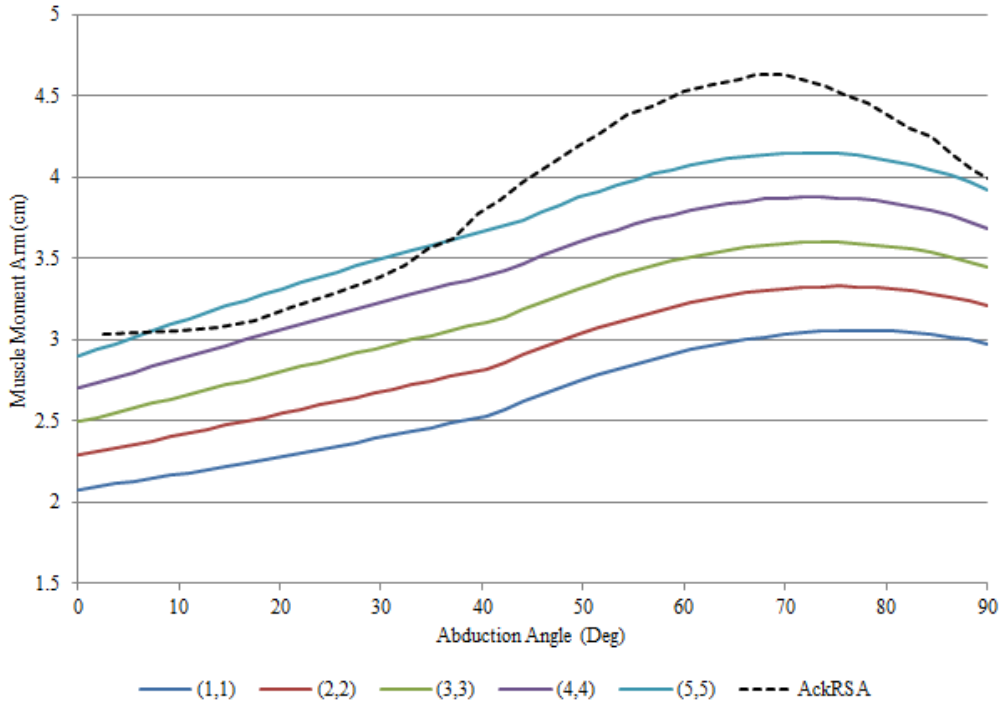

Figure 42: The anatomical profile of the curve may be increased in magnitude by positioning the joint center along an inferior-medial diagonal from the anatomical center

The position with the largest moment arm over the largest range of motion is the most inferior and medial position available, as was expected. Surprisingly, it did not create the largest moment arm at every angle of abduction. Physiological implications of this and other trends will be discussed in Chapter 5.

Sub-Study 3.3: Muscle Excursion

The excursion of the middle deltoid is the total change in muscle length between the extremes of the range of abduction. Figures 43 and 44 depict the total excursion of the deltoid as a function of the location of the joint center of rotation. As the center is moved medially, the excursion tends to increase in a fairly linear fashion with 5 mm of increase in total excursion for every 4.5 mm of medial translation of the anatomical

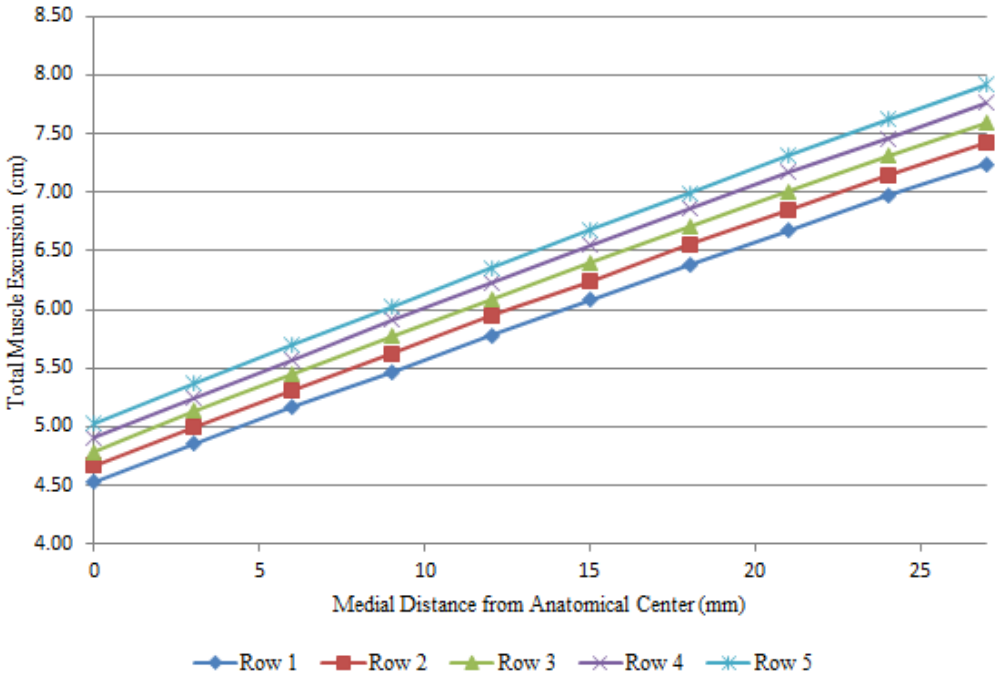

Figure 43: Total excursion of the middle deltoid as a function of the position of the joint center. Each curve represents the change in total excursion of the middle deltoid as the joint center is shifted medially along one of the rows depicted in Figure 37.

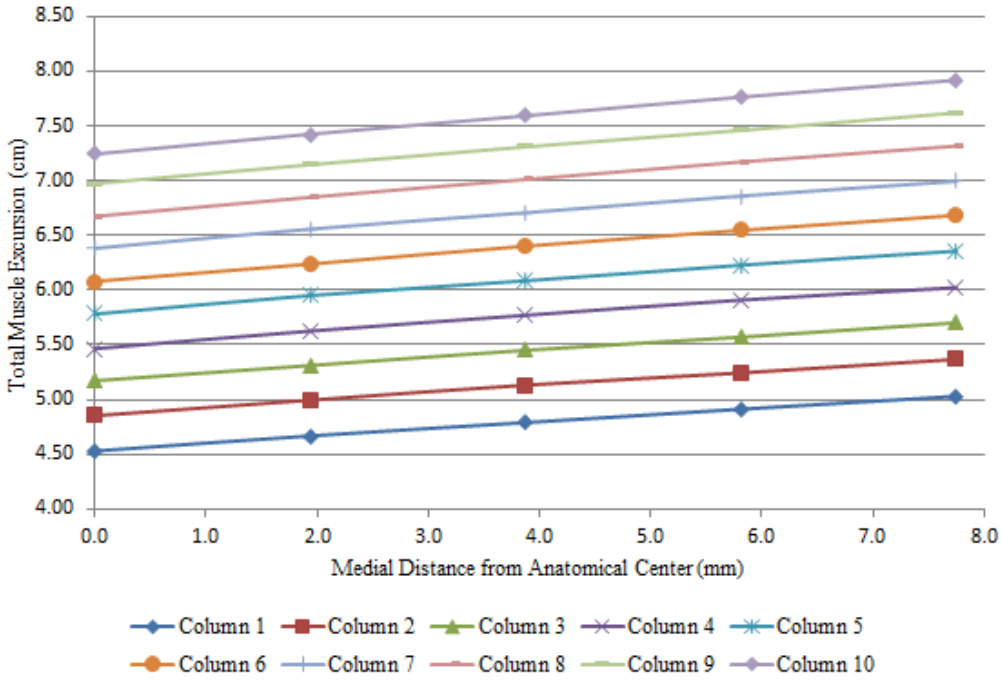

Figure 44: Total excursion of the middle deltoid as the joint center is moved inferiorly. Each curve represents a different column from Figure 37.

center. As seen in Figures 43 and 44, there is approximately 5 mm of increase in total excursion for every 7.75 mm that the joint center is moved inferiorly.

The increase is nearly linear. This is because the total muscle excursion is the integral of the moment arm function, or the area under the moment arm curve. There is also constant increases in moment arm magnitudes, at a given degree of abduction as the joint center is moved medially and inferiorly.

CHAPTER FIVE

Discussion

Experimental Data Trends

The model results compare well with the data trends reported in the literature of Ackland et al. [6,12], Kuechle et al. [3], Lui et al. [4], and Otis et al. [5]. Magnitude and general trends of the experimental data were duplicable by manipulation of our model parameters. This process created an important understanding of the viable locations and shapes of the various model parameters. It was this understanding that was used to create reliable data on a large range of shoulder models.

Replication of Unexpected Anatomical Data

As stated in Chapter 2, the experimental moment arm studies on the anatomical shoulder by Ackland et al. [6,12], Lui et al. [4], and Otis et al. [5] each report abduction moment arms for the middle deltoid that have unexpectedly low magnitudes for the early abduction angles. For example, at 0° of abduction (2.5° for the Ackland study) the moment arm magnitudes range from 8.5 mm to 14 mm for these three studies. The moment arm is related to the distance from the center of joint rotation to the muscle path. These are unexpected values because these magnitudes are substantially less than the radius of the humeral head, which ranges from 25 to 28 mm. Therefore, if abduction occurs about the geometric center of the humeral head, the implication of these studies is that the muscle path must pass inside the bone surface of the humeral head. For reference, the experimental moment arms for the anatomical middle deltoid are compared

in Figure 7 and the migration of the model's joint center in order to match the model to the experimental data (for each middle deltoid data set from the anatomical and RSA Ackland studies [6,12], and the anatomical Kuechle study [3]) was previously depicted in Figure 35.

An unexpected trend that is consistent across three separate studies is unlikely to be caused by experimental error and is much more likely to be a true result of an unanticipated interaction. It is possible that this interaction was identified by Ackland et al. when they stated that a potential limitation of the study was the inability to control "…glenohumeral joint translation during the tendon excursion experiments." *In vivo,* a healthy shoulder will experience some glenohumeral translation during rotation [4,41,43,44]. It is possible that this translation is magnified *ex vivo,* in the absence of the complex coordination of forces that stabilize the joint.

Each portion of Sub-Study 2 represents a separate attempt to use our model to elucidate the cause of the unexpected low-angle data. Sub-Study 2.1 was an attempt to find a way to explain the experimental data while using the *in vivo* position of the anatomical joint center. As expected, the results (Figures 25-26) showed that no anatomically justifiable configuration of the muscle parameters would mirror the experimental data trends while the joint center was locked at the anatomical position.

Sub-Study 2.2 was a reversal of Sub-Study 2.1. If the joint center could not be fixed in the anatomical position, then the muscle parameters would be fixed in an anatomical configuration and the joint center would be the variable. This method seemed more likely to explain the experimental data because the joint center implied by the experimental moment arm data might deviate from the actual joint center because of an

unanticipated interaction. This method was marginally successful (Figures 27-32) in that the data at the upper ranges of abduction matched well with the experimental data. However, Sub-Study 2.2 was ultimately unable to duplicate the data trends at the low angles of abduction, which were the trends in question.

Sub-Study 2.3 is similar to Sub-Study 2.2 in that the model's joint center of glenohumeral rotation is the variable parameter used to bring the model into agreement with the experimental data. The difference between the two procedures was that in Sub-Study 2.3 numerous joint centers were used through the range of abduction in order to explain the trends in the experimental data by using a migrating center of rotation in the model. As seen in Figure 34, the model was able to replicate the middle deltoid moment arms for each of the three experimental data sets, but this was achieved by adjusting the joint center to obtain agreement over intervals of 5°. Figure 35 is the depiction of how the model's joint center had to migrate in order to create this agreement between the model and each data set, which is the important result. For the anatomical Ackland study, the model's center of rotation was required to migrate significantly in both the X and Y directions (approximately 10 and 27 mm, respectively) in order to match the experimental results. For the RSA Ackland data, the migration was also significant, but much less than the anatomical data (approximately 3 mm horizontally, and 20 mm vertically).

Some translation is expected in a healthy shoulder, and actual translation of the humeral head with respect to the scapula may be exacerbated *ex vivo,* as discussed above. However, joint translation would not physically account for all of the migration of the joint center that resulted from Sub-Study 2.3. As long as the humerus was in constant

contact with the scapula, the translations in the X-direction should not occur. This implies that the at least some of the migration for the Ackland data, shown in Figure 35, is not a reflection of a physical translation in the *ex vivo* experiments, but rather is a result of some other interaction with the moment arm computation.

Reconciliation of Unexpected Anatomical Data

Sub-Study 2.3 may be able to provide further insight into the causes of the large migration of the joint center required in order to match our model to the Ackland anatomical data. Sub-Study 2.3 also tracked the migration of the joint center in matching the model to the data of Kuechle et al. [3]. The Kuechle data did not require the model's joint center to migrate in the X-direction. Rather, the migration takes a vertical path, moving down and then back up over a range of about 10 mm. While the magnitude of the migration is greater than what is reported *in vivo* in the literature, the migration of the Kuechle center is much closer to the *in vivo* trends than the Ackland data [41,42].

Because the migration of the Kuechle center does not deviate from the vertical, the greater magnitude of migration may be explained by the lack of coordinated muscular control in an *ex vivo* experiment and greater shifting of the humeral head. The migration of the Kuechle joint center is in line with the expected anatomical migration, which correlates directly to the moment arm data being more in line with the expected anatomical moment arm trends.

This correlation and the agreement between the Kuechle moment arm data and the expected *in vivo* moment arms indicates that the anomalies in the migration of the Ackland joint center are likely related to the unexpectedly low moment arms at low angles of abduction for Ackland [6], Liu [4], and Otis [5].

Comparing the Ackland RSA and Anatomical Studies.

The reverse shoulder implant is designed to stabilize the glenohumeral joint and increase torque capabilities of the glenohumeral muscles. The design of this implant attaches the glenohumeral center of rotation directly to the scapula. Because the glenosphere is mechanically secured to the scapula, any physical translation of the joint center should be extremely limited with respect to the scapular frame. Fixation of the glenohumeral joint center in an unanatomical position in the RSA study is the only significant differences between the methodologies of the anatomical and RSA studies by Ackland et al. [6,12]. Because this is the main difference between the two studies, it should account for the differences in the trends of the moment arm data and the migrations of the joint center between the anatomical and RSA studies.

In Figure 8 we see that the RSA study [12] reports consistently greater magnitudes of moment arms than does the anatomical study. This is an expected trend. However, we also see a difference in the trends of the data at low angles. The anatomical Ackland study reports increasingly small moment arms at low angles while the moment arms for the Ackland RSA study remain high at low angles. Having no physical translation of the joint center made a difference in moment arm trends at those low angles of abduction.

The lack of physical translation of the joint center also makes a difference in the migration required to match the model to the experimental data. However, the model's center of rotation still had to migrate in order to match the RSA data, which confirms that something other than humeral head translation is contributing to the migration of the joint center that is implied by the reported data. The total vertical migration required to match

the model to the Ackland RSA data is approximately 8 mm less than the total vertical migration for the anatomical Ackland data. This 8 mm difference is similar to the total vertical migration seen in matching our model to the Kuechle data. Finding serves to confirm that the main difference in migration of the model's joint center between matching with the anatomical and RSA data sets is that the RSA data set has no physical translation of the humeral head. Therefore, all of the migration seen in the RSA portion of Sub-Study 2.3 is a reflection of some other interaction that is influencing the values of the moment arms in the experimental studies, but is not reflected in the model predictions. In other words, the model was compensated by iterative adjustment of the joint center in a manner that would not physically occur.

Causes of Joint Center Migration in the Model's Fit to Experimental Data

The data from Kuechle et al. [3] does not reflect any changes in the joint center that would not occur *in vivo.* As shown in Table 2, the main difference between the methodology of Kuechle and the studies by Ackland et al. and Liu et al. is in the treatment of the muscle paths. Liu and Ackland cut away the muscle bellies and ran lines from the insertion to the origin. Kuechle left the muscles intact and threaded the line through the muscle itself. In each study, these lines were then used to track the change in muscle length as the humerus was abducted.

If the experimental treatment of the muscle path is the cause of the differences in moment arms between Kuechle and the other ALOK studies, then there are two possible implications for the movement of the model's joint center when it is used to mimic these experimental data sets. The first is that cutting the muscles away increases joint instability and allows for lateral and superior-inferior translation of the joint center. The

second is that passing the line through the muscle belly may ensure better stability of the experimental muscle path. The free lines in the other three studies could conceivably shift around obstacles as the humerus is passively abducted. Both of these possibilities would affect the instantaneous change in length for the tendon excursion method. As described by Equation 3, this change in length has a direct effect on the computed moment arms.

For example, during an experiment, if the humerus was abducted by 1° and the abduction caused the humeral head to slip inferiorly, then the change in length caused by the rotation would be mitigated by the opposing change in length caused by the inferior translation of the humeral head. Thus the change in length would be recorded as a value that is less than what it would have been with a fixed center of rotation, while the angle of abduction is accurately reported as 1°. The computed moment arm is then proportionally smaller than what it should have been, and the model must utilize a lateralized center of rotation in order to mimic the moment arm data.

This scenario is a possible explanation for the unexpectedly small moment arms at low angles, as well as the large migration of our modeled joint center when it is made to mimic the data of the Ackland studies.

Model Validation Against Literature

Comparing the current model against models and data previously described in the literature provides a measure of validation. It is this validation which allows for the use of this model to collect further data regarding the influence of the glenohumeral center of rotation.

The data sets from the experimental Ackland studies [6,12] and the data sets from the models used in the studies of Terrier et al., and Kontaxis et al., [45,46] were not

perfectly comparable to the current model. Both computational studies simulated scapular rotation, giving their data a total humerothoracic range of approximately 150°. This difference in abduction range was compensated for by scaling each data set to eliminate the effects of scapular rotation. This is a valid modification for the middle deltoid because the entire muscle operates within the scapular frame.

In comparing the current model to the data from the ALOK studies, the scaled data from the Ackland RSA study, and the Kontaxis and Terrier models, our model represents well the trends and magnitudes of the muscle moment arms.

For the reverse shoulder configurations, the model fit well with the data from Ackland, Terrier, and Kontaxis. Using the RSA center of rotation defined by Ackland et al., the model predicted a moment arm curve that fit within the magnitudes of the other studies and mimicked the trends of the other studies – specifically a fairly level slope at early angles of abduction followed by a rising and falling action, with peak moment arms occurring between 50° and 75°.

For the anatomical configurations, the model was able to fit the Kuechle data with an R^2 value of 0.95. For the other ALOK studies, our model fit well for the higher angles of abduction but diverged for low angles of abduction. However, the divergence between the low-angle moment arm predictions of this model and the low angle experimental data might be because of anomalies in the experimental studies caused by instability in the glenohumeral joint, as discussed previously.

Effect of Center of Rotation Location

The validated model was used to study the effects on middle deltoid moment arms caused by variations in the location of the glenohumeral center of rotation. The results of

this study have application in the design and use of the reverse shoulder prosthesis, which alters the joint center location in order to increase joint stability and increase the torque potential of the joint by increasing the moment arms of the deltoid and surrounding muscles. The results of Sub-Study 3 show that the location of the glenohumeral center of rotation has a sizeable effect on the magnitude and shape of the moment arm profile as a function of glenohumeral abduction angle.

Implications for Moment Arm Magnitude

It is a common belief that moving the joint center medially and inferiorly will increase the moment arms and the potential torque at the joint. This belief is substantiated by the results displayed in Figures 8, and 37-42. As the center of rotation is shifted medially or inferiorly the magnitude of the moment arms is increased. Moving the joint center in either direction will have a roughly equivalent effect on the magnitude of the muscle moment arms but will affect opposite ends of the curve.

Medial movement was found to affect the left section of the moment arm curve, which corresponds to the low angles of abduction (approximately 0-50°). It is within this range of abduction that the muscle path wraps around the underlying anatomy (e.g. the humeral head). I

Inferior movement of the joint center was found to affect the moment arms at higher angles of abduction (approximately 40-90°), where the muscle tends to lift free of the underlying anatomy. In this range of abduction the middle deltoid has a nearly direct path from the acromion to the deltoid tuberosity.

Implications for Joint Range of Motion

Another topic that might be considered when designing a total shoulder implant or arthroplasty procedure is what range of motion is going to be most important to the patient. It may not always be possible to get the center of rotation to reside at both the most medial and most inferior position possible. In such a case the designer would need to know if the patient needed more assistance with low or high-angle rotations due to musculoskeletal deficiencies or because of habitual motions. The data provided by the current model would then provide guidance on selecting an appropriate position for the joint center.

When considering how far to medialize a patient's joint center, one thing that could be considered is the decrease in moment arm magnitude that occurs at the highest angles of elevation. If a patient struggles with that range of motion, as was reported by Bergmann et al. [38], then it may be worthwhile to set the center of rotation inferior of the glenoid center and slightly lateral to the glenoid face by selecting an RSA device with a lateral offset and placing the center bore for the glenoid component inferior to the center of the glenoid. This would sacrifice some amount of mechanical advantage at lower angles but would provide an increased mechanical advantage at the upper limit of the range of motion. This orientation would also minimize the risk of impingement, as the rim of the humeral component would be distanced from the glenoid. For reference, see results at the upper limit of rotation in Figures 38-42.

Also shown in Figure 42, it was surprising to note that the profile of the moment arms for the anatomical joint center can be preserved as the moment arm magnitude is

preserved. For reference, see the uniform increase in mechanical advantage across the range of motion in Figure 42.

Because medial and inferior translations have roughly equivalent effects, the moment arm profile of the anatomical joint can be preserved over the full range of motion by moving the joint center medially and inferiorly at an angle 30-45° below the horizontal. Maximum moment arms will obviously occur at fully medialized positions. However, the more natural mechanics of the shoulder could be maintained while still increasing the mechanical advantage over the entire range of motion. This would allow the muscles to operate at their naturally effective lengths, with greater effect. However, staying within the defined range of viable locations for the joint center would limit the increase in moment arms to 35-50%, as opposed to possible gains of over 100% albeit in a more limited range.

Muscle Excursion

The muscle excursion is the integral of the moment arm, or area under the moment arm curve, as a function of abduction angle. It was initially surprising how linear the increase of the muscle excursion was when the glenohumeral joint center was moved medially or inferiorly (see Figures 43 and 44). However, consideration of the results of Sub-Study 2.3 revealed that the moment arms at each angle of abduction increased by a constant percentage for each medial or inferior shift of the joint center. The linear increase in the muscle excursion curves is a reflection of the constant increase in moment arm magnitude as the joint center is shifted medially and inferiorly.

The muscle excursion data permits a broader consideration of the physiology of the muscle. As the total excursion of the muscle is changed by the location of the joint

center, then the muscle must operate over a different range of lengths over the range of motion. For example, if total excursion increases, then the force potential of the muscle, as governed by its force-length curve, will be affected. Thus there is a trade-off. As the joint center is moved to provide greater moment arms to the glenohumeral muscles, the force capabiulities of those muscles is compromised by the change in excursion. This trade-off could be optimized by relating muscle excursion to the force-length curve. Further work could then relate the position of the joint center to the potential torque output of the joint by combining knowledge of the moment arms and the muscle force potential as a function of the muscle length.

Limitations

While this paper makes several important contributions, it also is subject to several limitations. The foremost among them is the limitation of the scope of the research to the middle deltoid. The middle deltoid was chosen for being the most influential abductor as well as the most affected of all the glenohumeral muscles in abduction. However, for a complete understanding of the implications for a patient's outcome after RSA, the effect on all affected muscles must be understood. Otherwise, efforts to optimize the mechanical advantage for the middle deltoid may come at the detriment of other muscles.

A second limitation is the focus on abduction in the coronal plane. Other muscles become important in other motions such as flexion or axial rotation. No shoulder surgery would be considered successful if the outcome only allowed the patient to effectively move their arm in a single plane. Daily motions often require combinations of flexion, abduction, and rotation. Having data for the effects the joint center location on each

muscle and for each rotational degree of freedom, would further help to optimize implant design and surgical procedure.

A third limitation is one that affects every attempt at musculoskeletal modeling. Our understanding and representation of muscle physiology, and even muscular geometry, is not complete. In this study the middle deltoid was separated from the anterior and posterior sub-regions in order to narrow the site of the origin and maintain a more accurate line of action. Even though the middle deltoid represented a third of the muscle and the possible area of attachment, a single line of action does not necessarily represent all of the area from which the middle deltoid originates. During simulations it was made clear that the attachment area was large enough to have many viable locations for the model's origin point. It was also made clear that the choice of origin location within the anatomic area had a significant effect on moment arm data. When a specific point is chosen to represent the entire origin there is a risk of giving great weight to a single line of action out of hundreds of significantly different lines of action.

Contributions

This study contributes to the field of knowledge in several ways. The first contribution is the musculoskeletal model that was developed and validated. The model should be adaptable for future research into the moment arms of the other glenohumeral muscles or into the joint kinematics of the shoulder. It may also be used to provide input data for other types of modeling such as finite element analysis for optimization, stress analysis, or fatigue over time.

The second contribution of this study was somewhat unexpected. Through model simulations and research into previous studies from literature, this study has developed

insights into the effects of glenohumeral joint translation on experimentally-determined moment arms. As stated in the literature, there is a natural translation of the humeral head, and thus the glenohumeral joint center, during abduction. In *ex vivo* experiments, this natural translation seems to be exacerbated by the lack of a coordinated muscular effort to stabilize the joint. The result is reported moment arm data that is too low at early angles of abduction. The effects of this lack of coordinated musculature may also be seen *in vivo* with massive rotator cuff damage.

Finally, the main purpose of this study was to quantify the advantages gained by the middle deltoid when the joint center is manipulated during Reverse Shoulder Arthroplasty. Previous work looked at specific glenohumeral joint center locations, but this study presents consideration of a broad range of angles. Surgical procedures necessitated a comprehensive look at the results of altering the shoulders kinematics. The data presented in this paper and in its Appendices will facilitate further musculoskeletal modeling and will also facilitate design and personalization of the implants and procedures that affect the lives of those who seek relief from joint damage and pain.

Future Research

The most immediate area for future work is to expand this model to include the rest of the glenohumeral muscles. Ideally a similar process would be repeated for flexion and axial rotation. The groundwork and literature research for this has been done during the course of this study, including data extraction from the experimental studies on all muscles and in all types of rotation.

The next step is to develop and run optimization simulations to achieve an understanding of the global effects of joint center location. Adding 15 or more distinct

muscle subdivisions would greatly increase the complexity of the model, but the computational power already exists to handle such simulations. This study would be able to identify specific zones for placing the joint center that will optimize the increase in mechanical advantage such that the most influential muscles collectively gain as much advantage as possible.

A further layer of complexity that would be of some benefit would be to model the entire spread of the muscle origin. This could be done by employing multiple lines of action. By spreading them over the origin the resultant forces and moment arms values could be averaged by the respective weight of the area that each individual line represents. This layer of complexity would also multiply the required computational power but is still not beyond the computational capabilities that are already available.

Finally, this research will be most useful to surgeons and medical implant designers once the position of the glenohumeral joint center can be directly related to the potential torque of the joint. Moment arms provide a good indication of what kind of benefit a patient may receive from a movement in their joint center, but precise customization for every patient will be difficult until physiological variables are accounted for. This will require modeling the changes in the moment arms, muscle excursion, and potential force in the muscle as it relates to the muscle force-length relationship.

APPENDICES

APPENDIX A

Detail of Sub-Study Parameters

Table A.1: Final model parameters used for Sub-Study 2.1. This sub-study used a fixed center of rotation at the anatomical position. The origin and insertion of the middle deltoid, respectively on the acromion and the deltoid tuberosity, were adjusted for best fit of the model prediction to the ALOK [3–6] experimental data. A via-cylinder was used as an obstacle to manipulate the muscle path between the origin and insertion. Its center, size, and orientation (R-Matrix) are also listed as they were used to achieve best fit with the experimental data. All numbers are in meters, in the scapular reference frame.

Parameter	Fixed Anatomical Joint Center
Origin Location	[0.012356, -0.020001, -0.017416]
Insertion Location	[0.017099, 0.010275, -0.127973]
Via-Cylinder Center	[-0.056768, 0.0, -0.046947]
Via-Cylinder Radius	-0.033
Via-Cylinder R-Matrix	[0.354121, -0.22379, 0.908288; -0.831068, 0.369829, 0.414841; 0.424191, 0.89845, 0.053351]
Center of Rotation	[0.0, 0.0, -0.04384]

Table A.2: Final model parameters for Sub-Study 2.2.1 – Three iterations of fixed muscle parameters with different origin locations. Joint center is varied to achieve best fit. All numbers are in meters in the scapular reference frame. See description of Table A.1 for further details and information.

Parameter	Superior Origin Placement	Lateral Origin Placement	Inferior Origin Placement
Origin Location	[0.013653, -0.020001, -0.008919]	[0.014819, -0.020001, -0.014279]	[0.008079, -0.020001, -0.016262]
Insertion Location	[0.017099, 0.010275, -.127973]	[0.017099, 0.010275, -.127973]	[0.017099, 0.010275, -.127973]
Via-Cylinder Center	[-0.001551, 0.0, -0.031432]	[-0.001667, 0.0, -0.035751]	[-0.004052, 0.0, -0.041149]
Via-Cylinder Radius	-0.0304	-0.0304	-0.0304
Via-Cylinder R-Matrix	[0.354121, -0.22379, 0.908288; -0.831068, 0.369829, 0.414841; 0.424191, 0.89845, 0.053351]	[0.354121, -0.22379, 0.908288; -0.831068, 0.369829, 0.414841; 0.424191, 0.89845, 0.053351]	[0.354121, -0.22379, 0.908288; -0.831068, 0.369829, 0.414841; 0.424191, 0.89845, 0.053351]
Center of Rotation	[0.000481, 0.0, -0.033399]	[0.001513, 0.0, -0.039036]	[-0.002717, 0.0, -0.041833]

Table A.3: Final model parameters used for Sub-Study 2.2.2 – Validation of the model against experimental data by Kuechle et al. [3]. All numbers are in meters, in the scapular frame. All parameters adjusted in order to achieve best fit. See description of Table A.1 for further information.

Parameter	Kuechle Comparison
Origin Location	[0.013653, -0.020001, -0.008919]
Insertion Location	[0.017099, 0.010275, -.127973]
Via-Cylinder Center	[-0.001967, 0.0, -0.0317]
Via-Cylinder Radius	-0.0304
Via-Cylinder R-Matrix	[0.354121, -0.22379, 0.908288; -0.831068, 0.369829, 0.414841; 0.424191, 0.89845, 0.053351]
Center of Rotation	[0.000821, 0.0, -0.03247]

Table A.4: Final model parameters used for Sub-Study 2.3. This substudy investigates migration of the instantaneous joint center during abduction, specifically in the anatomical data from Ackland et al [6]. All numbers are in meters, in scapular frame. See Table A.1 for further information.

Parameter	Migrating Joint Center
Origin Location	[0.013653, -0.020001, -0.008919]
Insertion Location	[0.017099, 0.010275, -.127973]
Via-Cylinder Center	[-0.001551, 0.0, -0.031432]
Via-Cylinder Radius	-0.033
Via-Cylinder R-Matrix	[0.354121, -0.22379, 0.908288; -0.831068, 0.369829, 0.414841; 0.424191, 0.89845, 0.053351]
Center of Rotation	Various, see Appendix B

APPENDIX B

Joint Centers of Rotation from Sub-Study 2.3

Table B.1: Sub-Study 2.3 tracked the migration of the model's center of rotation as it was made to fit experimental moment arm curves iteratively for small ranges of abduction. This table describes the joint centers used to replicate the anatomical Ackland data [6] through 65° of glenohumeral motion. Each row represents the location of the center of rotation for the given range of angles. All coordinates are in the scapular frame. Table A.3 lists the muscle path parameters used for all parts of Sub-Study 2.3.

Interval	Abduction Angle (deg)	Joint Center Location (m)
1	0.0 - 2.5	[0.011333, 0.0, -0.06317]
2	2.5 - 7.5	[0.010933, 0.0, -0.063253]
3	7.5 - 12.5	[0.01033, 0.0, -0.06267]
4	12.5 - 17.5	[0.00985, 0.0, -0.06157]
5	17.5 - 22.5	[0.00925, 0.0, -0.06007]
6	22.5 - 27.5	[0.008636, 0.0, -0.057485]
7	27.5 - 32.5	[0.008336, 0.0, -0.055619]
8	32.5 - 37.5	[0.007837, 0.0, -0.055619]
9	37.5 - 42.5	[0.007285, 0.0, -0.052802]
10	42.5 - 47.5	[0.006524, 0.0, -0.050202]
11	47.5 - 52.5	[0.003421, 0.0, -0.039574]
12	52.5 - 65.0	[0.001919, 0.0, -0.035842]

Table B.2: The joint centers used to replicate the anatomical Kuechle data [3] through 70° of glenohumeral motion. For further information See Table B.1.

Interval	Abduction Angle (deg)	Joint Center Location (m)
1	0.0 - 7.5	[-0.009629, 0.0, -0.039744]
2	7.5 - 12.5	[-0.009529, 0.0, -0.041127]
3	12.5 - 22.5	[-0.009829, 0.0, -0.046475]
4	22.5 - 32.5	[-0.010129, 0.0, -0.050458]
5	32.5 - 37.5	[-0.010829, 0.0, -0.052741]
6	37.5 - 42.5	[-0.011329, 0.0, -0.056707]
7	42.5 - 47.5	[-0.012212, 0.0, -0.05799]
8	47.5 - 52.5	[-0.012512, 0.0, -0.05929]
9	52.5 - 62.5	[-0.012612, 0.0, -0.05989]
10	62.5 - 70.0	[-0.015479, 0.0, -0.053382]

Table B.3: The joint centers used to replicate the Ackland RSA data [12] through 80° of glenohumeral motion. For further information see Table B.1.

Interval	Abduction Angle (deg)	Joint Center Location (m)
1	0.0 - 12.5	[0.008971, 0.0, -0.031738]
2	12.5 - 17.5	[0.008471, 0.0, -0.036938]
3	17.5 - 50.0	[0.008084, 0.0, -0.042469]
4	50.0 - 57.5	[0.007984, 0.0, -0.039387]
5	57.5 - 62.5	[0.008184, 0.0, -0.037905]
6	62.5 67.5	[0.008167, 0.0, -0.03700]
7	67.5 - 72.5	[0.008167, 0.0, -0.035479]
8	72.5 - 77.5	[0.008067, 0.0, -0.034264]
9	77.5 - 80.0	[0.008167, 0.0, -0.03309]

APPENDIX C

Joint Center Dependent Moment Arm Data

Table C.1: Set of moment arm data by location: Column headings identify the row and column in reference to the superior row in Figure 37. All values are in centimeters.

Abd (deg)	1 1	1 2	1 3	1 4	1 5	1 6	1 7	1 8	1 9	1 10
0.0	2.078	2.323	2.576	2.806	3.057	3.297	3.542	3.781	4.040	4.277
1.8	2.093	2.339	2.593	2.825	3.076	3.318	3.563	3.804	4.063	4.301
3.7	2.110	2.356	2.611	2.843	3.095	3.337	3.583	3.825	4.085	4.323
5.5	2.127	2.374	2.628	2.861	3.113	3.356	3.603	3.845	4.106	4.344
7.3	2.144	2.392	2.646	2.879	3.131	3.375	3.621	3.864	4.125	4.364
9.2	2.162	2.410	2.664	2.896	3.149	3.392	3.640	3.882	4.143	4.382
11.0	2.181	2.428	2.682	2.914	3.167	3.410	3.657	3.900	4.160	4.399
12.9	2.200	2.446	2.700	2.932	3.184	3.426	3.673	3.916	4.176	4.415
14.7	2.219	2.465	2.718	2.949	3.201	3.442	3.689	3.931	4.190	4.428
16.5	2.239	2.484	2.736	2.966	3.217	3.458	3.703	3.945	4.203	4.441
18.4	2.259	2.503	2.753	2.983	3.233	3.473	3.717	3.958	4.215	4.451
20.2	2.280	2.523	2.771	2.999	3.248	3.487	3.730	3.969	4.225	4.460
22.0	2.301	2.543	2.789	3.016	3.263	3.500	3.742	3.980	4.234	4.467
23.9	2.322	2.562	2.807	3.032	3.277	3.513	3.753	3.989	4.242	4.473
25.7	2.344	2.582	2.825	3.048	3.291	3.524	3.763	3.997	4.247	4.477
27.6	2.366	2.602	2.842	3.063	3.304	3.536	3.772	4.004	4.252	4.479
29.4	2.389	2.622	2.860	3.079	3.317	3.546	3.780	4.010	4.255	4.479
31.2	2.411	2.643	2.877	3.094	3.329	3.556	3.787	4.014	4.256	4.478
33.1	2.434	2.663	2.895	3.108	3.341	3.564	3.793	4.017	4.256	4.474
34.9	2.457	2.683	2.912	3.122	3.352	3.572	3.798	4.019	4.254	4.469
36.7	2.481	2.704	2.929	3.136	3.363	3.580	3.801	4.019	4.250	4.462
38.6	2.505	2.724	2.945	3.150	3.373	3.586	3.804	4.018	4.245	4.453
40.4	2.528	2.744	2.963	3.166	3.387	3.599	3.815	4.027	4.252	4.457
42.2	2.573	2.787	3.004	3.203	3.420	3.628	3.841	4.049	4.269	4.471
44.1	2.618	2.829	3.042	3.237	3.451	3.655	3.863	4.068	4.283	4.480
45.9	2.662	2.869	3.077	3.269	3.478	3.678	3.882	4.082	4.293	4.485
47.8	2.704	2.907	3.110	3.298	3.503	3.698	3.898	4.093	4.299	4.486
49.6	2.743	2.942	3.141	3.325	3.525	3.715	3.910	4.101	4.300	4.482
51.4	2.781	2.975	3.170	3.349	3.544	3.729	3.919	4.104	4.297	4.473
53.3	2.816	3.006	3.195	3.370	3.560	3.739	3.923	4.103	4.289	4.458
55.1	2.850	3.035	3.218	3.388	3.572	3.746	3.924	4.097	4.277	4.439
56.9	2.881	3.061	3.239	3.403	3.581	3.749	3.921	4.088	4.259	4.414
58.8	2.909	3.084	3.256	3.415	3.587	3.748	3.913	4.073	4.237	4.384
60.6	2.936	3.105	3.271	3.423	3.588	3.743	3.901	4.054	4.209	4.348
62.4	2.960	3.123	3.282	3.428	3.587	3.735	3.885	4.030	4.175	4.305
64.3	2.981	3.138	3.291	3.430	3.581	3.722	3.864	4.000	4.136	4.257
66.1	3.000	3.151	3.296	3.429	3.572	3.704	3.838	3.966	4.091	4.202
68.0	3.016	3.160	3.298	3.424	3.559	3.682	3.807	3.926	4.040	4.140
69.8	3.030	3.167	3.296	3.415	3.541	3.656	3.772	3.880	3.983	4.071
71.6	3.041	3.170	3.291	3.402	3.519	3.625	3.731	3.829	3.920	3.996
73.5	3.048	3.170	3.283	3.385	3.493	3.589	3.684	3.771	3.849	3.913
75.3	3.053	3.167	3.271	3.364	3.463	3.548	3.633	3.708	3.772	3.822
77.1	3.055	3.160	3.255	3.340	3.427	3.503	3.575	3.638	3.688	3.724
79.0	3.054	3.150	3.235	3.310	3.388	3.452	3.512	3.562	3.597	3.618
80.8	3.049	3.137	3.211	3.277	3.343	3.395	3.443	3.480	3.499	3.504
82.7	3.041	3.120	3.184	3.239	3.293	3.333	3.368	3.391	3.393	3.382
84.5	3.030	3.099	3.152	3.197	3.239	3.266	3.287	3.295	3.280	3.251
86.3	3.015	3.074	3.116	3.150	3.179	3.193	3.200	3.193	3.160	3.113
88.2	2.997	3.046	3.076	3.098	3.114	3.115	3.106	3.083	3.031	2.967
90.0	2.976	3.013	3.031	3.042	3.044	3.031	3.006	2.967	2.896	2.812

Table C.2: Second set of moment arm data by location. Column headings identify the row and column in reference to second row in Figure 37. All values are in centimeters.

Abd (deg)	2 1	2 2	2 3	2 4	2 5	2 6	2 7	2 8	2 9	2 10
0.0	2.042	2.287	2.528	2.770	3.021	3.259	3.507	3.746	3.995	4.235
1.8	2.063	2.309	2.551	2.794	3.046	3.284	3.533	3.773	4.023	4.264
3.7	2.085	2.331	2.574	2.817	3.070	3.308	3.559	3.800	4.050	4.292
5.5	2.107	2.354	2.597	2.841	3.094	3.333	3.584	3.825	4.076	4.318
7.3	2.130	2.377	2.620	2.864	3.118	3.356	3.608	3.850	4.101	4.343
9.2	2.153	2.400	2.643	2.888	3.142	3.380	3.632	3.873	4.124	4.367
11.0	2.177	2.424	2.667	2.911	3.165	3.402	3.655	3.896	4.147	4.389
12.9	2.201	2.447	2.690	2.934	3.187	3.424	3.677	3.918	4.168	4.410
14.7	2.225	2.471	2.713	2.957	3.210	3.446	3.698	3.938	4.188	4.430
16.5	2.250	2.496	2.737	2.979	3.232	3.467	3.718	3.958	4.207	4.448
18.4	2.276	2.520	2.760	3.002	3.253	3.487	3.738	3.976	4.224	4.464
20.2	2.301	2.545	2.784	3.024	3.274	3.506	3.756	3.993	4.240	4.479
22.0	2.328	2.569	2.807	3.046	3.295	3.525	3.774	4.010	4.255	4.492
23.9	2.354	2.594	2.830	3.068	3.315	3.543	3.790	4.025	4.268	4.504
25.7	2.381	2.619	2.854	3.089	3.334	3.561	3.806	4.039	4.280	4.513
27.6	2.408	2.644	2.877	3.110	3.353	3.577	3.821	4.051	4.291	4.522
29.4	2.435	2.669	2.900	3.131	3.372	3.593	3.835	4.063	4.299	4.528
31.2	2.463	2.695	2.922	3.151	3.389	3.608	3.847	4.073	4.307	4.533
33.1	2.490	2.720	2.945	3.171	3.407	3.623	3.859	4.081	4.313	4.536
34.9	2.518	2.745	2.967	3.191	3.423	3.636	3.870	4.089	4.317	4.537
36.7	2.546	2.770	2.990	3.210	3.439	3.649	3.879	4.095	4.320	4.536
38.6	2.574	2.795	3.012	3.229	3.455	3.661	3.888	4.100	4.321	4.533
40.4	2.603	2.820	3.033	3.247	3.469	3.671	3.895	4.104	4.322	4.532
42.2	2.642	2.858	3.070	3.282	3.502	3.703	3.925	4.131	4.346	4.552
44.1	2.692	2.905	3.113	3.321	3.538	3.735	3.953	4.156	4.366	4.568
45.9	2.740	2.949	3.154	3.359	3.571	3.764	3.978	4.176	4.382	4.580
47.8	2.786	2.992	3.192	3.393	3.602	3.790	4.000	4.194	4.395	4.587
49.6	2.831	3.032	3.229	3.425	3.629	3.813	4.018	4.207	4.403	4.590
51.4	2.873	3.070	3.262	3.455	3.654	3.832	4.033	4.216	4.407	4.588
53.3	2.913	3.106	3.294	3.481	3.675	3.849	4.044	4.222	4.406	4.581
55.1	2.951	3.139	3.322	3.505	3.694	3.861	4.051	4.223	4.401	4.569
56.9	2.987	3.170	3.348	3.526	3.709	3.870	4.054	4.220	4.391	4.552
58.8	3.021	3.199	3.371	3.543	3.720	3.876	4.053	4.212	4.376	4.530
60.6	3.052	3.224	3.392	3.558	3.728	3.877	4.048	4.200	4.355	4.501
62.4	3.081	3.248	3.409	3.569	3.733	3.875	4.038	4.183	4.330	4.467
64.3	3.107	3.268	3.423	3.577	3.734	3.868	4.024	4.160	4.299	4.427
66.1	3.131	3.286	3.434	3.581	3.730	3.857	4.005	4.133	4.262	4.380
68.0	3.152	3.300	3.442	3.582	3.723	3.842	3.981	4.100	4.219	4.326
69.8	3.170	3.312	3.447	3.579	3.712	3.822	3.952	4.061	4.169	4.266
71.6	3.185	3.320	3.448	3.572	3.697	3.797	3.918	4.017	4.114	4.198
73.5	3.198	3.325	3.445	3.561	3.677	3.768	3.878	3.967	4.052	4.123
75.3	3.208	3.327	3.439	3.546	3.652	3.734	3.833	3.910	3.982	4.041
77.1	3.214	3.326	3.429	3.527	3.623	3.694	3.783	3.848	3.906	3.951
79.0	3.217	3.321	3.415	3.504	3.590	3.649	3.726	3.778	3.823	3.852
80.8	3.218	3.312	3.398	3.476	3.551	3.599	3.664	3.703	3.732	3.746
82.7	3.214	3.300	3.376	3.444	3.507	3.544	3.595	3.620	3.634	3.631
84.5	3.208	3.284	3.350	3.407	3.458	3.482	3.520	3.530	3.528	3.508
86.3	3.198	3.264	3.319	3.366	3.404	3.415	3.438	3.434	3.414	3.376
88.2	3.184	3.240	3.285	3.319	3.345	3.342	3.350	3.330	3.292	3.235
90.0	3.167	3.212	3.245	3.268	3.280	3.263	3.256	3.218	3.162	3.086

Table C.3: Third set of moment arm data by location. Column headings identify the row and column in reference to third row in Figure 37. All values are in centimeters.

Abd (deg)	3 1	3 2	3 3	3 4	3 5	3 6	3 7	3 8	3 9	3 10
0.0	2.002	2.249	2.494	2.736	2.978	3.224	3.466	3.711	3.955	4.193
1.8	2.028	2.276	2.522	2.765	3.007	3.254	3.497	3.743	3.988	4.226
3.7	2.055	2.304	2.550	2.793	3.037	3.284	3.527	3.774	4.020	4.259
5.5	2.082	2.332	2.578	2.822	3.066	3.314	3.557	3.804	4.051	4.290
7.3	2.109	2.360	2.606	2.850	3.094	3.343	3.587	3.834	4.080	4.320
9.2	2.138	2.388	2.634	2.879	3.123	3.371	3.615	3.862	4.109	4.349
11.0	2.166	2.417	2.663	2.907	3.151	3.399	3.643	3.890	4.137	4.377
12.9	2.195	2.446	2.691	2.935	3.179	3.426	3.670	3.917	4.163	4.403
14.7	2.225	2.475	2.719	2.963	3.206	3.453	3.696	3.942	4.188	4.427
16.5	2.254	2.504	2.748	2.990	3.233	3.479	3.722	3.967	4.212	4.451
18.4	2.285	2.534	2.776	3.018	3.259	3.505	3.747	3.991	4.235	4.473
20.2	2.315	2.564	2.805	3.045	3.285	3.530	3.770	4.014	4.257	4.493
22.0	2.346	2.593	2.833	3.072	3.311	3.554	3.793	4.035	4.277	4.512
23.9	2.377	2.623	2.861	3.099	3.336	3.578	3.815	4.055	4.295	4.529
25.7	2.409	2.653	2.889	3.125	3.361	3.601	3.836	4.075	4.313	4.544
27.6	2.440	2.683	2.917	3.151	3.385	3.623	3.856	4.093	4.329	4.558
29.4	2.472	2.713	2.945	3.177	3.408	3.644	3.875	4.110	4.343	4.571
31.2	2.504	2.743	2.972	3.202	3.431	3.665	3.894	4.125	4.356	4.581
33.1	2.537	2.773	2.999	3.227	3.454	3.684	3.911	4.139	4.368	4.590
34.9	2.569	2.803	3.027	3.251	3.475	3.703	3.926	4.152	4.378	4.597
36.7	2.601	2.833	3.053	3.275	3.496	3.721	3.941	4.164	4.386	4.602
38.6	2.634	2.863	3.080	3.299	3.517	3.738	3.955	4.174	4.393	4.605
40.4	2.667	2.893	3.106	3.322	3.536	3.754	3.968	4.183	4.398	4.606
42.2	2.701	2.925	3.138	3.351	3.564	3.780	3.992	4.206	4.419	4.625
44.1	2.755	2.977	3.185	3.396	3.605	3.818	4.026	4.236	4.445	4.647
45.9	2.808	3.026	3.231	3.438	3.643	3.852	4.056	4.262	4.467	4.665
47.8	2.858	3.073	3.274	3.477	3.679	3.884	4.084	4.285	4.485	4.679
49.6	2.907	3.118	3.315	3.514	3.712	3.912	4.108	4.304	4.500	4.688
51.4	2.954	3.161	3.354	3.548	3.742	3.938	4.128	4.320	4.510	4.693
53.3	2.998	3.202	3.390	3.580	3.769	3.960	4.145	4.332	4.516	4.693
55.1	3.041	3.240	3.423	3.609	3.793	3.978	4.158	4.339	4.517	4.689
56.9	3.081	3.276	3.454	3.635	3.813	3.993	4.168	4.342	4.514	4.679
58.8	3.120	3.309	3.482	3.658	3.831	4.005	4.173	4.341	4.506	4.664
60.6	3.156	3.340	3.508	3.677	3.845	4.012	4.174	4.335	4.493	4.643
62.4	3.189	3.369	3.530	3.694	3.855	4.016	4.171	4.325	4.474	4.617
64.3	3.220	3.394	3.549	3.707	3.862	4.016	4.163	4.309	4.451	4.584
66.1	3.248	3.417	3.566	3.717	3.864	4.011	4.151	4.289	4.421	4.545
68.0	3.274	3.437	3.579	3.723	3.863	4.002	4.134	4.263	4.386	4.500
69.8	3.297	3.453	3.588	3.725	3.858	3.989	4.112	4.231	4.344	4.448
71.6	3.318	3.467	3.595	3.724	3.849	3.971	4.085	4.194	4.296	4.388
73.5	3.335	3.478	3.597	3.719	3.835	3.948	4.052	4.151	4.241	4.322
75.3	3.350	3.485	3.597	3.710	3.817	3.920	4.014	4.101	4.180	4.248
77.1	3.361	3.488	3.592	3.696	3.794	3.887	3.970	4.046	4.111	4.166
79.0	3.369	3.489	3.583	3.679	3.767	3.849	3.920	3.983	4.036	4.076
80.8	3.374	3.485	3.571	3.656	3.734	3.805	3.865	3.914	3.952	3.977
82.7	3.376	3.478	3.554	3.630	3.697	3.756	3.803	3.838	3.861	3.870
84.5	3.374	3.467	3.533	3.598	3.654	3.700	3.734	3.755	3.762	3.754
86.3	3.368	3.452	3.508	3.562	3.606	3.639	3.659	3.665	3.655	3.629
88.2	3.359	3.434	3.478	3.521	3.552	3.572	3.577	3.567	3.539	3.495
90.0	3.347	3.410	3.443	3.474	3.493	3.498	3.488	3.461	3.415	3.351

Table C.4: Fourth set of moment arm data by location. Column headings identify the row and column in reference to fourth row in Figure 37. All values are in centimeters.

Abd (deg)	4 1	4 2	4 3	4 4	4 5	4 6	4 7	4 8	4 9	4 10
0.0	1.962	2.204	2.451	2.698	2.939	3.181	3.424	3.670	3.911	4.161
1.8	1.993	2.235	2.484	2.732	2.973	3.217	3.460	3.707	3.949	4.199
3.7	2.024	2.268	2.516	2.765	3.007	3.251	3.496	3.743	3.985	4.236
5.5	2.056	2.300	2.549	2.799	3.041	3.286	3.531	3.779	4.021	4.272
7.3	2.089	2.333	2.582	2.832	3.075	3.320	3.565	3.813	4.055	4.307
9.2	2.122	2.366	2.615	2.866	3.108	3.353	3.599	3.847	4.089	4.341
11.0	2.156	2.400	2.648	2.899	3.141	3.386	3.631	3.880	4.121	4.373
12.9	2.190	2.433	2.681	2.932	3.174	3.419	3.664	3.912	4.153	4.404
14.7	2.224	2.467	2.714	2.965	3.206	3.451	3.695	3.943	4.183	4.434
16.5	2.259	2.501	2.748	2.997	3.238	3.482	3.726	3.973	4.212	4.462
18.4	2.294	2.535	2.781	3.030	3.270	3.513	3.756	4.002	4.240	4.489
20.2	2.329	2.570	2.814	3.062	3.301	3.543	3.785	4.030	4.266	4.515
22.0	2.365	2.604	2.847	3.094	3.332	3.573	3.813	4.057	4.292	4.539
23.9	2.401	2.639	2.880	3.126	3.362	3.601	3.840	4.082	4.316	4.561
25.7	2.437	2.673	2.912	3.157	3.392	3.629	3.867	4.107	4.339	4.582
27.6	2.473	2.708	2.945	3.188	3.421	3.657	3.892	4.131	4.360	4.602
29.4	2.510	2.743	2.977	3.219	3.450	3.683	3.917	4.153	4.380	4.619
31.2	2.547	2.777	3.010	3.249	3.478	3.709	3.940	4.174	4.398	4.635
33.1	2.583	2.812	3.042	3.279	3.505	3.734	3.963	4.194	4.415	4.650
34.9	2.620	2.846	3.073	3.308	3.532	3.758	3.984	4.213	4.431	4.662
36.7	2.657	2.881	3.105	3.337	3.558	3.781	4.004	4.230	4.445	4.673
38.6	2.694	2.915	3.136	3.365	3.583	3.804	4.024	4.246	4.457	4.682
40.4	2.731	2.949	3.167	3.393	3.608	3.825	4.042	4.260	4.468	4.688
42.2	2.768	2.983	3.197	3.420	3.632	3.846	4.060	4.277	4.483	4.702
44.1	2.819	3.032	3.245	3.466	3.676	3.888	4.099	4.313	4.515	4.729
45.9	2.876	3.086	3.295	3.513	3.719	3.928	4.136	4.345	4.543	4.753
47.8	2.931	3.137	3.343	3.557	3.760	3.965	4.169	4.374	4.567	4.773
49.6	2.984	3.187	3.389	3.599	3.798	3.999	4.198	4.399	4.588	4.789
51.4	3.035	3.235	3.432	3.639	3.834	4.030	4.225	4.421	4.604	4.800
53.3	3.085	3.280	3.473	3.676	3.866	4.058	4.248	4.439	4.617	4.807
55.1	3.132	3.323	3.512	3.710	3.895	4.083	4.267	4.453	4.625	4.809
56.9	3.177	3.364	3.547	3.741	3.922	4.104	4.283	4.462	4.628	4.806
58.8	3.220	3.402	3.581	3.769	3.945	4.121	4.295	4.468	4.627	4.797
60.6	3.260	3.438	3.611	3.794	3.964	4.135	4.302	4.469	4.621	4.784
62.4	3.299	3.471	3.639	3.816	3.981	4.145	4.306	4.466	4.610	4.765
64.3	3.335	3.501	3.663	3.835	3.993	4.151	4.305	4.457	4.593	4.739
66.1	3.368	3.529	3.685	3.851	4.002	4.153	4.300	4.444	4.571	4.708
68.0	3.399	3.554	3.703	3.863	4.007	4.151	4.289	4.425	4.543	4.670
69.8	3.427	3.576	3.718	3.871	4.008	4.144	4.274	4.401	4.510	4.626
71.6	3.452	3.595	3.730	3.875	4.005	4.133	4.254	4.372	4.470	4.575
73.5	3.474	3.611	3.738	3.876	3.998	4.117	4.229	4.336	4.423	4.516
75.3	3.494	3.623	3.743	3.873	3.986	4.096	4.198	4.294	4.369	4.450
77.1	3.510	3.632	3.744	3.865	3.970	4.070	4.162	4.246	4.309	4.375
79.0	3.524	3.638	3.741	3.854	3.948	4.039	4.119	4.192	4.241	4.293
80.8	3.534	3.640	3.734	3.837	3.922	4.002	4.071	4.130	4.166	4.202
82.7	3.540	3.638	3.723	3.816	3.891	3.959	4.016	4.062	4.082	4.102
84.5	3.544	3.632	3.707	3.791	3.854	3.911	3.954	3.986	3.991	3.993
86.3	3.543	3.623	3.687	3.760	3.812	3.856	3.886	3.903	3.891	3.875
88.2	3.539	3.609	3.663	3.725	3.765	3.796	3.811	3.812	3.783	3.747
90.0	3.531	3.591	3.634	3.684	3.712	3.728	3.729	3.713	3.666	3.610

Table C.5: Fifth set of moment arm data by location. Column headings identify the row and column in reference to bottom row in Figure 37. All values are in centimeters.

Abd (deg)	5 1	5 2	5 3	5 4	5 5	5 6	5 7	5 8	5 9	5 10
0.0	1.926	2.170	2.413	2.650	2.897	3.143	3.381	3.630	3.869	4.117
1.8	1.962	2.207	2.451	2.688	2.936	3.182	3.421	3.671	3.911	4.160
3.7	1.998	2.244	2.488	2.726	2.975	3.222	3.461	3.712	3.952	4.202
5.5	2.035	2.281	2.526	2.764	3.014	3.261	3.501	3.752	3.993	4.242
7.3	2.072	2.319	2.564	2.802	3.052	3.300	3.540	3.791	4.032	4.282
9.2	2.110	2.356	2.602	2.840	3.090	3.338	3.578	3.830	4.071	4.320
11.0	2.148	2.395	2.640	2.878	3.128	3.376	3.616	3.867	4.108	4.358
12.9	2.187	2.433	2.678	2.916	3.166	3.413	3.653	3.904	4.145	4.394
14.7	2.226	2.472	2.716	2.954	3.203	3.450	3.689	3.940	4.180	4.429
16.5	2.265	2.510	2.754	2.992	3.240	3.486	3.725	3.975	4.215	4.462
18.4	2.305	2.549	2.792	3.029	3.276	3.522	3.760	4.009	4.248	4.494
20.2	2.345	2.588	2.830	3.066	3.313	3.557	3.794	4.042	4.280	4.525
22.0	2.385	2.627	2.868	3.103	3.348	3.591	3.827	4.074	4.311	4.554
23.9	2.426	2.667	2.906	3.139	3.383	3.625	3.859	4.105	4.341	4.582
25.7	2.466	2.706	2.944	3.175	3.418	3.658	3.891	4.135	4.369	4.609
27.6	2.507	2.745	2.981	3.211	3.452	3.691	3.921	4.164	4.396	4.633
29.4	2.548	2.784	3.019	3.247	3.485	3.722	3.951	4.192	4.421	4.657
31.2	2.589	2.823	3.056	3.282	3.518	3.753	3.980	4.218	4.445	4.678
33.1	2.631	2.862	3.093	3.316	3.551	3.783	4.007	4.243	4.468	4.698
34.9	2.672	2.901	3.129	3.350	3.582	3.812	4.034	4.267	4.489	4.716
36.7	2.713	2.940	3.165	3.384	3.613	3.840	4.059	4.290	4.509	4.733
38.6	2.754	2.978	3.201	3.417	3.644	3.868	4.084	4.311	4.527	4.747
40.4	2.795	3.017	3.237	3.450	3.673	3.894	4.107	4.331	4.544	4.760
42.2	2.836	3.055	3.272	3.482	3.702	3.919	4.129	4.349	4.559	4.771
44.1	2.877	3.094	3.309	3.518	3.736	3.952	4.160	4.378	4.585	4.796
45.9	2.938	3.152	3.364	3.569	3.784	3.996	4.201	4.416	4.619	4.826
47.8	2.997	3.208	3.417	3.619	3.830	4.039	4.239	4.450	4.650	4.852
49.6	3.055	3.262	3.467	3.665	3.873	4.078	4.275	4.481	4.677	4.874
51.4	3.110	3.314	3.515	3.710	3.914	4.114	4.307	4.509	4.700	4.891
53.3	3.164	3.364	3.561	3.752	3.951	4.148	4.336	4.533	4.719	4.905
55.1	3.215	3.411	3.605	3.791	3.986	4.178	4.361	4.553	4.734	4.914
56.9	3.265	3.457	3.646	3.828	4.018	4.204	4.383	4.569	4.744	4.918
58.8	3.312	3.500	3.684	3.862	4.047	4.228	4.401	4.581	4.750	4.917
60.6	3.358	3.540	3.720	3.892	4.072	4.248	4.415	4.589	4.752	4.911
62.4	3.400	3.578	3.753	3.920	4.094	4.264	4.425	4.592	4.748	4.900
64.3	3.441	3.613	3.783	3.945	4.113	4.276	4.431	4.591	4.740	4.883
66.1	3.479	3.646	3.810	3.966	4.128	4.284	4.432	4.585	4.726	4.860
68.0	3.514	3.676	3.834	3.984	4.139	4.289	4.429	4.573	4.706	4.830
69.8	3.547	3.703	3.855	3.998	4.146	4.288	4.421	4.557	4.680	4.794
71.6	3.577	3.727	3.872	4.009	4.149	4.284	4.408	4.535	4.649	4.752
73.5	3.605	3.748	3.886	4.016	4.148	4.274	4.390	4.507	4.610	4.702
75.3	3.629	3.765	3.897	4.019	4.143	4.260	4.367	4.473	4.566	4.644
77.1	3.651	3.780	3.903	4.018	4.133	4.241	4.338	4.433	4.514	4.579
79.0	3.669	3.790	3.906	4.012	4.119	4.217	4.303	4.386	4.455	4.506
80.8	3.684	3.798	3.905	4.003	4.099	4.187	4.262	4.333	4.388	4.424
82.7	3.696	3.801	3.900	3.988	4.075	4.151	4.215	4.272	4.314	4.333
84.5	3.704	3.801	3.891	3.969	4.045	4.110	4.161	4.204	4.231	4.233
86.3	3.708	3.797	3.877	3.945	4.010	4.062	4.100	4.129	4.140	4.124
88.2	3.709	3.788	3.858	3.916	3.969	4.008	4.033	4.045	4.040	4.004
90.0	3.706	3.776	3.835	3.882	3.922	3.948	3.958	3.954	3.931	3.875

APPENDIX D

Excursion Data

Table D.1: Length and total excursion of the middle deltoid in abduction.

Grid Position	Muscle Length (cm)		Total Excursion (cm)
	0°	90°	
1,1	16.43	11.90	4.53
1,2	16.43	11.58	4.85
1,3	16.42	11.25	5.17
1,4	16.42	10.95	5.47
1,5	16.42	10.63	5.78
1,6	16.41	10.33	6.08
1,7	16.41	10.02	6.38
1,8	16.40	9.73	6.67
1,9	16.40	9.42	6.98
1,10	16.40	9.15	7.24
2,1	16.45	11.78	4.67
2,2	16.44	11.45	5.00
2,3	16.44	11.13	5.31
2,4	16.44	10.81	5.63
2,5	16.43	10.48	5.95
2,6	16.43	10.19	6.24
2,7	16.42	9.86	6.56
2,8	16.42	9.57	6.85
2,9	16.42	9.27	7.15
2,10	16.41	8.98	7.43
3,1	16.46	11.67	4.79
3,2	16.46	11.33	5.13
3,3	16.46	11.00	5.45
3,4	16.45	10.68	5.77
3,5	16.45	10.36	6.09
3,6	16.44	10.04	6.40
3,7	16.44	9.73	6.71
3,8	16.43	9.42	7.01
3,9	16.43	9.12	7.31
3,10	16.43	8.83	7.59
4,1	16.48	11.57	4.91
4,2	16.47	11.23	5.24
4,3	16.47	10.90	5.57
4,4	16.47	10.56	5.91
4,5	16.46	10.23	6.23
4,6	16.46	9.91	6.55
4,7	16.45	9.59	6.86
4,8	16.45	9.28	7.17
4,9	16.45	8.98	7.46
4,10	16.44	8.68	7.77
5,1	16.50	11.47	5.03
5,2	16.50	11.13	5.37
5,3	16.49	10.79	5.70
5,4	16.49	10.47	6.02
5,5	16.49	10.13	6.36
5,6	16.48	9.80	6.68
5,7	16.48	9.48	6.99
5,8	16.47	9.16	7.32
5,9	16.47	8.85	7.62
5,10	16.46	8.54	7.92

REFERENCES

[1] Hootman J. M., and Helmick C. G., 2006, "Projections of US prevalence of arthritis and associated activity limitations," Arthritis Rheum., **54**(1), pp. 226–229.

[2] Kuechle D. K., Newman S. R., Itoi E., Niebur G. L., Morrey B. F., and An K. N., 2000, "The relevance of the moment arm of shoulder muscles with respect to axial rotation of the glenohumeral joint in four positions," Clin. Biomech. Bristol Avon, **15**(5), pp. 322–329.

[3] Kuechle D. K., Newman S. R., Itoi E., Morrey B. F., and An K.-N., 1997, "Shoulder muscle moment arms during horizontal flexion and elevation," J. Shoulder Elbow Surg., **6**(5), pp. 429–439.

[4] Liu J., Hughes R., Smutz W., Niebur G., and Nan-An K., 1997, "Roles of deltoid and rotator cuff muscles in shoulder elevation," Clin. Biomech., **12**(1), pp. 32–38.

[5] Otis J. C., Jiang C. C., Wickiewicz T. L., Peterson M. G., Warren R. F., and Santner T. J., 1994, "Changes in the moment arms of the rotator cuff and deltoid muscles with abduction and rotation," J. Bone Joint Surg. Am., **76**(5), pp. 667–676.

[6] Ackland D. C., Pak P., Richardson M., and Pandy M. G., 2008, "Moment arms of the muscles crossing the anatomical shoulder," J. Anat., **213**(4), pp. 383–390.

[7] "Rotator cuff strengthening - treating and preventing shoulder injury" [Online]. Available: http://www.pponline.co.uk/encyc/rotator-cuff-strengthening-treating-and-preventing-shoulder-injury-40881. [Accessed: 14-May-2013].

[8] Petersen S. A., and Hawkins R. J., 1998, "REVISION OF FAILED TOTAL SHOULDER ARTHROPLASTY," Orthop. Clin. North Am., **29**(3), pp. 519–533.

[9] Bohsali K. I., Wirth M. A., and RockwoodJr. C. A., 2006, "Complications of Total Shoulder Arthroplasty," J. Bone Jt. Surg., **88**(10), pp. 2279–2292.

[10] Sirveaux F., Favard L., Oudet D., Huquet D., Walch G., and Mole D., 2004, "Grammont inverted total shoulder arthroplasty in the treatment of glenohumeral osteoarthritis with massive rupture of the cuff RESULTS OF A MULTICENTRE STUDY OF 80 SHOULDERS," J. Bone Joint Surg. Br., **86-B**(3), pp. 388–395.

[11] Ackland D. C., Richardson M., and Pandy M. G., 2012, "Axial rotation moment arms of the shoulder musculature after reverse total shoulder arthroplasty," J. Bone Joint Surg. Am., **94**(20), pp. 1886–1895.

[12] Ackland D. C., Roshan-Zamir S., Richardson M., and Pandy M. G., 2010, "Moment arms of the shoulder musculature after reverse total shoulder arthroplasty," J. Bone Joint Surg. Am., **92**(5), pp. 1221–1230.

[13]Flatow E. L., and Harrison A. K., 2011, “A history of reverse total shoulder arthroplasty,” Clin. Orthop., **469**(9), pp. 2432–2439.

[14]Gallinet D., Clappaz P., Garbuio P., Tropet Y., and Obert L., 2009, “Three or four parts complex proximal humerus fractures: Hemiarthroplasty versus reverse prosthesis: A comparative study of 40 cases,” Orthop. Traumatol. Surg. Res., **95**(1), pp. 48–55.

[15]Wall B., 2007, “Reverse Total Shoulder Arthroplasty: A Review of Results According to Etiology,” J. Bone Jt. Surg. Am., **89**(7), p. 1476.

[16]Walker M., Willis M. P., Brooks J. P., Pupello D., Mulieri P. J., and Frankle M. A., 2012, “The use of the reverse shoulder arthroplasty for treatment of failed total shoulder arthroplasty,” J. Should. Elb. Surg. Am. Should. Elb. Surg. Al, **21**(4), pp. 514–522.

[17]Austin L., Zmistowski B., Chang E. S., and Williams G. R., 2011, “Is reverse shoulder arthroplasty a reasonable alternative for revision arthroplasty?,” Clin. Orthop., **469**(9), pp. 2531–2537.

[18]Nyffeler R. W., Werner C. M. L., and Gerber C., 2005, “Biomechanical relevance of glenoid component positioning in the reverse Delta III total shoulder prosthesis,” J. Should. Elb. Surg. Am. Should. Elb. Surg. Al, **14**(5), pp. 524–528.

[19]Levy J., Frankle M., Mighell M., and Pupello D., 2007, “The Use of the Reverse Shoulder Prosthesis for the Treatment of Failed Hemiarthroplasty for Proximal Humeral Fracture,” J. Bone Jt. Surg., **89**(2), pp. 292–300.

[20]Walker M., Brooks J., Willis M., and Frankle M., 2011, “How reverse shoulder arthroplasty works,” Clin. Orthop., **469**(9), pp. 2440–2451.

[21]Frankle M., Siegal S., Pupello D., Saleem A., Mighell M., and Vasey M., 2005, “The Reverse Shoulder Prosthesis for Glenohumeral Arthritis Associated with Severe Rotator Cuff DeficiencyA Minimum Two-Year Follow-up Study of Sixty Patients,” J. Bone Jt. Surg., **87**(8), pp. 1697–1705.

[22]Ackland D. C., and Pandy M. G., 2011, “Moment arms of the shoulder muscles during axial rotation,” J. Orthop. Res. Off. Publ. Orthop. Res. Soc., **29**(5), pp. 658–667.

[23]Ackland D. C., Lin Y.-C., and Pandy M. G., 2012, “Sensitivity of model predictions of muscle function to changes in moment arms and muscle-tendon properties: a Monte-Carlo analysis,” J. Biomech., **45**(8), pp. 1463–1471.

[24]Kohout J., Kellnhofer P., and Martelli S., 2012, “Fast deformation for modelling of musculoskeletal system.”

[25]Gatti C. J., Dickerson C. R., Chadwick E. K., Mell A. G., and Hughes R. E., 2007, “Comparison of model-predicted and measured moment arms for the rotator cuff muscles,” Clin. Biomech., **22**(6), pp. 639–644.

[26]Favre P., Sheikh R., Fucentese S. F., and Jacob H. A. C., 2005, "An algorithm for estimation of shoulder muscle forces for clinical use," Clin. Biomech., **20**(8), pp. 822–833.

[27]Audenaert A., and Audenaert E., 2008, "Global optimization method for combined spherical–cylindrical wrapping in musculoskeletal upper limb modelling," Comput. Methods Programs Biomed., **92**(1), pp. 8–19.

[28]Gatti C. J., and Hughes R. E., 2009, "Optimization of Muscle Wrapping Objects Using Simulated Annealing," Ann. Biomed. Eng., **37**(7), pp. 1342–1347.

[29]Alta T. D., Bergmann J. H., Veeger D. J., Janssen T. W., Burger B. J., Scholtes V. A., and Willems W. J., 2011, "Kinematic and clinical evaluation of shoulder function after primary and revision reverse shoulder prostheses," J. Shoulder Elbow Surg., **20**(4), pp. 564–570.

[30]Nolan B. M., Ankerson E., and Wiater J. M., 2011, "Reverse total shoulder arthroplasty improves function in cuff tear arthropathy," Clin. Orthop., **469**(9), pp. 2476–2482.

[31]Kalouche I., Sevivas N., Wahegaonker A., Sauzieres P., Katz D., and Valenti P., 2009, "Reverse shoulder arthroplasty: does reduced medialisation improve radiological and clinical results?," Acta Orthop. Belg., **75**(2), pp. 158–166.

[32]Gutiérrez S., Comiskey C. A., Luo Z.-P., Pupello D. R., and Frankle M. A., 2008, "Range of impingement-free abduction and adduction deficit after reverse shoulder arthroplasty. Hierarchy of surgical and implant-design-related factors," J. Bone Joint Surg. Am., **90**(12), pp. 2606–2615.

[33]Farshad M., and Gerber C., 2010, "Reverse total shoulder arthroplasty-from the most to the least common complication," Int. Orthop., **34**(8), pp. 1075–1082.

[34]Valenti P., Sauzières P., Katz D., Kalouche I., and Kilinc A. S., 2011, "Do less medialized reverse shoulder prostheses increase motion and reduce notching?," Clin. Orthop., **469**(9), pp. 2550–2557.

[35]Kelly II J. D., Humphrey C. S., and Norris T. R., 2008, "Optimizing glenosphere position and fixation in reverse shoulder arthroplasty, Part One: The twelve-mm rule," J. Shoulder Elbow Surg., **17**(4), pp. 589–594.

[36]Lévigne C., Boileau P., Favard L., Garaud P., Molé D., Sirveaux F., and Walch G., 2008, "Scapular notching in reverse shoulder arthroplasty," J. Shoulder Elbow Surg., **17**(6), pp. 925–935.

[37]Virani N. A., Cabezas A., Gutiérrez S., Santoni B. G., Otto R., and Frankle M., "Reverse shoulder arthroplasty components and surgical techniques that restore glenohumeral motion," J. Shoulder Elbow Surg.

[38]Bergmann J. H. M., de Leeuw M., Janssen T. W. J., Veeger D. H. E. J., and Willems W. J., 2008, "Contribution of the reverse endoprosthesis to glenohumeral kinematics," Clin. Orthop., **466**(3), pp. 594–598.

[39]Kwon Y. W., Pinto V. J., Yoon J., Frankle M. A., Dunning P. E., and Sheikhzadeh A., 2012, "Kinematic analysis of dynamic shoulder motion in patients with reverse total shoulder arthroplasty," J. Should. Elb. Surg. Am. Should. Elb. Surg. Al, **21**(9), pp. 1184–1190.

[40]De Toledo J. M., Loss J. F., Janssen T. W., van der Scheer J. W., Alta T. D., Willems W. J., and Veeger D. H. E. J., 2012, "Kinematic evaluation of patients with total and reverse shoulder arthroplasty during rehabilitation exercises with different loads," Clin. Biomech. Bristol Avon, **27**(8), pp. 793–800.

[41]Poppen N. K., and Walker P. S., 1976, "Normal and abnormal motion of the shoulder," J. Bone Joint Surg. Am., **58**(2), pp. 195–201.

[42]Terrier A., Reist A., Vogel A., and Farron A., 2007, "Effect of supraspinatus deficiency on humerus translation and glenohumeral contact force during abduction," Clin. Biomech., **22**(6), pp. 645–651.

[43]Meskers C. G., van der Helm F. C., Rozendaal L. A., and Rozing P. M., 1998, "In vivo estimation of the glenohumeral joint rotation center from scapular bony landmarks by linear regression," J. Biomech., **31**(1), pp. 93–96.

[44]Veeger H. E., 2000, "The position of the rotation center of the glenohumeral joint," J. Biomech., **33**(12), pp. 1711–1715.

[45]Terrier A., Reist A., Merlini F., and Farron A., 2008, "Simulated joint and muscle forces in reversed and anatomic shoulder prostheses," J. Bone Joint Surg. Br., **90-B**(6), pp. 751–756.

[46]Kontaxis A., and Johnson G. R., 2009, "The biomechanics of reverse anatomy shoulder replacement – A modelling study," Clin. Biomech., **24**(3), pp. 254–260.

[47]Garner B. A., and Pandy M. G., 2001, "Musculoskeletal Model of the Upper Limb Based on the Visible Human Male Dataset," Comput. Methods Biomech. Biomed. Engin., **4**(2), pp. 93–126.

[48]Spitzer V. M., and Whitlock D. G., 1998, "The visible human dataset: The anatomical platform for human simulation," Anat. Rec., **253**(2), pp. 49–57.

[49]Garner B. A., and Pandy M. G., 2000, "The Obstacle-Set Method for Representing Muscle Paths in Musculoskeletal Models," Comput. Methods Biomech. Biomed. Engin., **3**(1), pp. 1–30.

[50]Ackland D. C., Roshan-Zamir S., Richardson M., and Pandy M. G., 2011, "Muscle and joint-contact loading at the glenohumeral joint after reverse total shoulder arthroplasty," J. Orthop. Res. Off. Publ. Orthop. Res. Soc., **29**(12), pp. 1850–1858.